DESIGN, SIMULATION AND OPTIMIZATION OF A 4×4 MICROSTRIP PATCH ANTENNA ARRAY FOR 5G COMMUNICATION

OCTOBER, 2025

DESIGN, SIMULATION AND OPTIMIZATION OF A 4×4

MICROSTRIP PATCH ANTENNA ARRAY

FOR 5G COMMUNICATION

BY

OKOLI ARINZECHUKWU MIRACLE	ENG2002292
ADIBOR LYDIA EGUONO	ENG2002195
ONIYEMOFE MELODY URINRIN	ENG2002308
ONYELA UDOCHUKWUKA	ENG2002311

A PROJECT SUBMITTED TO THE DEPARTMENT OF ELECTRICAL/ELECTRONIC ENGINEERING, FACULTY OF ENGINEERING, UNIVERSITY OF BENIN, BENIN CITY.

OCTOBER, 2025

CERTIFICATION

This is to certify that this project work was carried out by **Okoli Arinzechukwu Miracle**, **Adibor Lydia Eguono**, **Oniyemofe Melody Urinrin**, and **Onyela Udochukwuka**, in partial fulfillment of the requirements for the award of the degree of Bachelor of Electrical/Electronic Engineering in the Department of Electrical/Electronic Engineering, Faculty of Engineering, University of Benin, Benin City, Edo State.

Dr. N. Bello	Date
(Project Supervisor)	
Engr. Dr. O.S Omorogiuwa	Date
(Head of Department)	

CERTIFICATION OF THESIS ON PLAGIARISM

We the undersigned declare that this project report by, **Okoli Arinzechukwu Miracle**, **Adibor Lydia Eguono**, **Oniyemofe Melody Urinrin**, and **Onyela Udochukwuka**, on Design, Simulation and Optimization of a 4×4 Microstrip Patch Antenna Array for 5G Communication has successfully passed the anti-plagiarism test and does not violate any copyright regulations

Dr. N. Bello	Date
(Project Supervisor)	
Engr. Dr. O.S Omorogiuwa	Date
(Head of Department)	

DEDICATION

This work is dedicated to God almighty and also to the Oniyemofe family, the Adibor family, the Okoli family and Onyela family, for their unending support, and love, throughout our study in the University of Benin.

ACKNOWLEDGEMENT

We give thanks to Almighty God for His love, grace, mercy, and protection throughout our stay at the University of Benin. Our heartfelt appreciation also goes to the families of Oniyemofe, Onyela, Adibor, and Okoli, as well as our friends, for their financial, moral, and spiritual support during our years in the university. Finally, we sincerely thank Dr. N. Bello, our project supervisor, for his time, guidance, and dedication in reviewing this work and for teaching us the importance of discipline and striving for excellence.

ABSTRACT

The rapid expansion of fifth-generation (5G) wireless networks demands antenna arrays with wide bandwidth, high gain, and efficient beamforming capabilities to facilitate ultra-high-definition video streaming, extensive Internet of Things (IoT) connectivity, and communications with minimal latency. Nevertheless, traditional microstrip patch antennas continue to face fundamental challenges, including limited bandwidth, strong mutual coupling in array configurations, and reduced radiation efficiency caused by dielectric and surface wave losses. These challenges hinder their suitability for high-performance 5G applications.

This project presents the design and simulation of a 4×4 microstrip patch antenna array optimized for sub-6 GHz 5G applications. The Rogers 4350B substrate is utilized because of its low-loss characteristics and stable dielectric properties. To improve performance, U-shaped slots are added to the radiating elements, and a Defected Ground Structure (DGS) is incorporated into the ground plane. The design, analysis, and optimization of the antenna are carried out using ANSYS HFSS, focusing on achieving wide impedance bandwidth, high gain, and improved inter-element isolation without physical fabrication. The selection of materials, substrate parameters, and design dimensions are carefully chosen to facilitate future fabrication and experimental validation.

Simulation results show that the proposed antenna achieves a gain of 10.64 dB, a bandwidth of 180 MHz, radiation efficiency of 72.3%, and a return loss (S_{11}) of –19.96 dB at 3.5 GHz. In comparison, the conventional 4×4 array of the same dimensions without slots and DGS recorded a gain of 10.31 dB, no substantial bandwidth as the return loss at the resonance frequency, 3.5 GHz, is above the -10 dB line, efficiency of 64.39%. The observed improvements are primarily attributed to the DGS, which effectively suppresses surface waves, minimizes mutual coupling, and enhances current distribution uniformity across the array. Overall, the optimized DGS-based antenna demonstrates superior performance in terms of gain, bandwidth, and element isolation, making it a strong candidate for compact and efficient sub-6 GHz 5G base station and user terminal applications. The findings of this study provide a useful framework for further research and practical realization of high-performance antenna arrays for next-generation wireless communication systems.

Table of Contents

CERTIFICATION iii

CERTIFICATION OF THESIS ON PLAGIARISM iv

DEDICATION v

ACKNOWLEDGEMENT vi

ABSTRACT vi

LIST OF FIGURES x

LIST OF TABLES xiii

LIST OF ABBREVATIONS xiv

1 INTRODUCTION 1

1.1 Background of the Study . . . 1
1.2 Problem Statement . . . 2
1.3 Aim and Objectives of the Study . . . 2
1.3.1 Aim . . . 2
1.3.2 Objectives . . . 3
1.4 Significance of the Study . . . 3
1.5 Scope of the Study . . . 3

2 LITERATURE REVIEW 5

2.1 Overview . . . 5
2.1.1 5G Communication . . . 5
2.1.1.1 5G Frequency Bands . . . 7
2.1.2 Antennas: Theory, Design, and Modern Applications . . . 10
2.1.2.1 Wire Antennas . . . 10
2.1.2.2 Patch Antennas . . . 10
2.1.2.3 Patch(Radiating element) . . . 11
2.1.2.4 Feed Line . . . 11
2.1.2.5 Contacting Methods . . . 12
2.1.2.6 Inset Feed . . . 12
2.1.2.7 Coaxial Probe Feed . . . 13
2.1.2.8 Non-contact Feeding . . . 13
2.1.2.9 Aperture coupled Feed . . . 14
2.1.2.10 Proximity coupled Feed . . . 15

2.1.2.11 Feed Division Techniques . . . 15
2.1.2.12 Dielectric Substrate . . . 17
2.1.2.13 Ground Plane . . . 19
2.1.3 DGS . . . 20
2.1.3.1 Cavity Modeling . . . 21
2.1.3.2 Transmission-line Modeling . . . 21
2.1.3.3 Full-wave Numerical Method . . . 21
2.1.4 Antenna Arrays . . . 22
2.1.5 Key Parameters In Antenna Design . . . 23
2.1.6 Practical Considerations . . . 26
2.1.7 Ansys HFSS . . . 27
2.1.8 Available Resources . . . 28
2.1.9 Review of Related Works . . . 29
2.1.10 Research Gap . . . 40

3 METHODOLOGY 43
3.1 Introduction to Methodology . . . 43
3.2 Research Design . . . 43
3.2.1 Overview . . . 43
3.2.2 Design and Analysis Methods . . . 43
3.3 Design Methodology . . . 50
3.3.1 Flowchart of Methodology . . . 50
3.3.2 Single Patch Antenna Design and Optimization . . . 51
3.3.3 Performance Enhancement: Adding Slots and DGS . . . 75
3.3.4 Array Construction and Final Simulation . . . 88

4 OUTCOMES AND DISCUSSION 98
4.1 Introduction . . . 98
4.2 Simulation Results Overview . . . 98
4.3 Return Loss (S_{11}) . . . 98
4.4 Voltage Standing Wave Ratio (VSWR) . . . 99
4.5 Radiation Pattern and Gain . . . 99
4.6 Surface Current Distribution . . . 99
4.7 Discussion . . . 100
4.8 Comparative Performance Evaluation . . . 101
4.9 Discussion of Results . . . 103
4.9.1 Conventional 4×4 Array without U-Slots and DGS . . . 103
4.9.2 4×4 Array with U-Slots Only . . . 104
4.9.3 4×4 Array with Combined U-Slots and DGS . . . 104

4.9.4 Performance Analysis and Key Observations 105
4.10 Overview 106

5 CONCLUSION AND RECOMMENDATIONS 108
5.1 Project Overview 108
5.2 Conclusion 108
5.3 Impact of the Research 108
5.4 Limitations 109
5.5 Recommendations for Future Study 109
5.6 Closing Remarks 110

LIST OF FIGURES

2.1 5G frequency spectrum (Alsaif et al. 2021) 7
2.2 5G spectrum allocation in different bands (Mahmood et al. 2021) 9
2.3 A microstrip patch antenna (Chowdhury et al. 2019) 11
2.4 An inset feed used in a 2×2 patch antenna array 13
2.5 A patch antenna with a coaxial probe feed mechanism (M. Rahman 2017) 14
2.6 A patch antenna with an aperture-coupled feed mechanism (Naji et al. 2012) 15
2.7 A patch antenna with a proximity coupled feed mechanism (Rowe et al. 2006) 16
2.8 Radiation pattern of a $\frac{\lambda}{2}$ dipole compared with an isotropic antenna (Balanis 2016). 24

3.1 Single Patch Layout 46
3.2 Flow Chart of Methodology 51
3.3 Open Ansys 52
3.4 Select the HFSS module 52
3.5 Navigate to Design Properties 53
3.6 Add Variables 53
3.7 A list of all necessary parameters 54
3.8 A list of all necessary parameters 54
3.9 Parameters have been added successfully 55
3.10 Click on the Draw box icon 55
3.11 Create a cuboid in the modeler space 56
3.12 Select CreateBox 56
3.13 Set the dimensions according to your defined parameters 57
3.14 Rename the object to substrate 57
3.15 Assign the material to **RO4350B** and choose a desired transparency and color 58
3.16 Create a ground plane and rename it GND 59
3.17 Create the patch and set its dimensions 59
3.18 Create the feedline and set its parameters 60
3.19 Created feedline 60
3.20 Feedline Dimensions 61
3.21 Draw a thin rectangle on the feedline 61
3.22 Select the newly created rectangle 62
3.23 Duplicate the gap 62
3.24 Select both the feedline and patch 63
3.25 Unite the feedline and patch 63
3.26 Subtract the gaps from the patch 64

3.27 Select the edge faces of the feedline and select create object from edge . . 64
3.28 Sweep along path 65
3.29 The created port 65
3.30 Rename the object as port 66
3.31 Assign finite conductivity boundary to patch and GND 66
3.32 Assign port excitation 67
3.33 Click Next 67
3.34 Click New Line 68
3.35 Draw the integration line 68
3.36 Click Next 69
3.37 Click Finish 69
3.38 Port with assigned excitation 70
3.39 Setting up analysis 71
3.40 Analysis Setup 71
3.41 Set operating frequency 72
3.42 Analysis has been setup 72
3.43 Creating Open Region 73
3.44 Click OK 73
3.45 Generating Results 74
3.46 Select Solution type 75
3.47 Select HFSS with Hybrid Arrays and Modal 75
3.48 U-slot parameters 76
3.49 Complete U-slot parameters 76
3.50 Set a vertical height for the U-slot 77
3.51 Rectangular arm of the U-slot 77
3.52 Creating object from face 78
3.53 Thicken the created object 78
3.54 Moving faces along normal 79
3.55 Properties window 79
3.56 Unite U-slot arms 80
3.57 Subtracting U-slots from patch 80
3.58 Dimensions of polygons 81
3.59 Polygons 81
3.60 Subtracted Polygons from ground plane 82
3.61 Additional Rectangle 82
3.62 Dimensions and position of first polygon 83
3.63 Dimensions and position of second polygon 83
3.64 Dimensions and position of third polygon 84
3.65 Dimensions and position of fourth polygon 84

3.66 Dimensions and position of first rectangle 85
3.67 Dimensions and position of second rectangle 85
3.68 Dimensions and position of third rectangle 86
3.69 Dimensions and position of fourth rectangle 86
3.70 Dimensions and position of fifth rectangle 87
3.71 Complete DGS 87
3.72 Duplicate and mirror the single patch 88
3.73 Dimensions and position of feedlines 89
3.74 Dimensions and position of feedlines 89
3.75 2×1 array with feedlines 90
3.76 Duplicate and mirror the 2×1 array 90
3.77 Dimensions and position of feedlines 91
3.78 Feedlines 91
3.79 Duplicate and mirror the 2×2 array 92
3.80 4×2 array 92
3.81 Duplicate and mirror the 4×2 array 93
3.82 4×4 array 93
3.83 Join the feedlines 94
3.84 Unite all patches and ground planes 94
3.85 Create a new port 95
3.86 Create open region 95
3.87 Click OK 96
3.88 Final Array 97

4.1 Modeled return loss (S_{11}) for the single MPA. 99
4.2 Simulated return loss (S_{11}) for the 4×4 MPA array with U-slots and DGS. 100
4.3 VSWR plot for the 4×4 MPA array with U-slots and DGS. 101
4.4 (a) 2D radiation pattern of the single MPA. 102
4.5 (b) 3D radiation pattern of the single MPA. 102
4.6 (a) 2D radiation pattern of the 4×4 MPA array. 102
4.7 (b) 3D radiation pattern of the 4×4 MPA array. 102
4.8 Surface current distribution on the 4×4 MPA array with U-slots and DGS. 103
4.9 4×4 array without U-slots and DGS. 104
4.10 Simulated S_{11} parameter of 4×4 array without U-slots and DGS. 104
4.11 4×4 array with U-slots only. 105
4.12 Simulated S_{11} parameter of 4×4 array with U-slots only. 105
4.13 4×4 array with U-slots and DGS. 106
4.14 Simulated S_{11} parameter of 4×4 array with U-slots and DGS. 106

LIST OF TABLES

2.1 Comparison of Common Feed Mechanisms for Microstrip Patch Antennas 17
2.2 Comparison of common antenna substrates at 3.5 GHz 26
2.3 Comparison of common SMA connectors at 3.5 GHz 27

3.1 Overview of the performance metrics for the simulated antenna. 46

4.1 Overview of modeled antenna performance metrics 98
4.2 Comparison of the suggested antenna with existing 5G array configurations 101

LIST OF ABBREVATIONS

1G first generation. ii, 5, 6

2G second generation. ii, 5, 6

3G third generation. ii, 5, 6

3GPP 3rd Generation Partnership Project. ii, 6, 7

4G fourth generation. ii, 5, 9, 28

5G fifth-generation. ii, 1, 3, 5, 6, 8–11, 20, 22, 26, 28, 34, 37, 40

6G sixth generation. ii, 10

ADS Advanced Design System. ii, 35, 36

ANN Artificial Neural Network. ii, 44

CAD Computer Aided Design. ii

CDMA Code Division Multiple Access. ii, 43

DGS Defected Ground Structure. ii, 2, 21, 23, 29, 34, 40

DPF Driving Point Impedance Function. ii, 35, 36

EBG Electromagnetic BandGap. ii, 2, 35

FEM Finite Element Method. ii, 32, 35, 36

FFBP-ANN Feedforward Back Propagation Network. ii

FPD Filtering Power Divider. ii, 46

GGW Groove-Gap Waveguide. ii, 41

GSM Global System for Mobile Communication. ii, 6, 43

HFSS High Frequency Structure Simulator. ii, 3, 4, 32, 43

IoT Internet of Things. ii, 5, 28, 40

ISM Industrial, Scientific, and Medical. ii, 42

LTE Long Term Evolution. ii, 1, 5, 6, 43

MIMO Multiple Inputs Multiple Outputs. ii, 1, 6, 32, 37, 40

MoM Method of Moments. ii, 35, 36

MPAs Microstrip Patch Antennas. ii, 1, 2, 12, 34, 36

MSPAA Microstrip Patch Antenna Array. ii, 35

NTT Nippon Telegraph and Telephone. ii, 5

OFDMA Orthogonal Frequency Division Multiple Access. ii, 6

PBG Photonic Band Gap. ii, 35

PCB Printed Circuit Board. ii, 1, 13, 35

PEC Perfect Electric Conductor. ii, 32

RF Radio Frequency. ii, 30, 31

SMA SubMiniature version A. ii, 30, 31

UWB Ultra Wide Band. ii, 41

VNAs Vector Network Analyzers. ii, 2

VSWR Voltage Standing Wave Ratio. ii, 3, 14, 28, 34, 38

WiMAX Worldwide Interoperability for Microwave Access. ii, 43

WLANs Wide Local Area Networks. ii, 42, 43

WPD Wilkinson Power Divider. ii, 45

Chapter ONE

INTRODUCTION

1.1 Background of the Study

The demand for faster data rates, more connectivity, and lower latency communication has led to the deployment of fifth-generation (5G) wireless networks. The 5G network utilizes the same mid-frequency band as the 4G Long Term Evolution (LTE), known as the sub-6 GHz band (3.3–5.0 GHz). This frequency band offers a good balance between large-area coverage and data speed within the 5G spectrum. Although the low-frequency band (below 1 GHz) offers better building penetration, it cannot provide the high data speeds of the sub-6 GHz band. Likewise, while the high-frequency band (millimeter wave) enables high-speed data rates, its poor penetration and shorter range of coverage are its significant disadvantages.

An important aspect of implementing 5G networks is the choice of antenna, which should offer high gain, low propagation loss, high bandwidth, cost-efficiency, and miniaturization. This project focuses on Microstrip Patch Antennas (MPAs),which are preferred because of their small dimensions, lightweight construction, simple manufacturing process, affordability, and compatibility with Printed Circuit Board (PCB) technology. Arrays of multiple patch antennas can be configured to increase gain, widen coverage, and improved the overall antenna performance. This makes them ideal for Multiple Inputs Multiple Outputs (MIMO) systems used in 5G. Their adaptability enables comparison of different substrate materials and structural techniques based on desired electrical properties and cost considerations.

Material and structural advantages and limitations also play a crucial role in the fabrication process. Each decision presents trade-offs, and the selection must overcome limitations such as narrow bandwidth, impedance mismatch, and mutual coupling that degrade antenna efficiency.

Microstrip patch antennas typically exhibit bandwidths of less than 500 MHz, limiting their data transmission capacity and the number of simultaneous users. This can be improved in various ways; however, this project focuses on integrating patch slots and Defected Ground Structures (DGS) into the antenna design. The slots are patterns etched on the conducting surface (patch) of the antenna and Defected Ground Structure (DGS) are etched patterns on the ground plane that increase the fringing electromagnetic field, which enhances parasitic capacitance (which is constructive in this instance) and coupling between the patch and the ground plane. This improves bandwidth performance. The shape and placement of slots and DGS elements significantly influence their effectiveness.

In summary, MPAs offer a compact, cost-effective solution for sub-6 GHz 5G applications. Although they have bandwidth limitations, integrating DGS into their design

increases parasitic capacitance and mutual coupling constructively, thus significantly enhancing bandwidth. Optimizing this integration is essential to developing efficient antennas for 5G high-speed and high-connectivity requirements.

1.2 Problem Statement

Despite their numerous advantages, conventional microstrip patch antennas (MPAs) still face key challenges that limit their suitability for high-performance 5G applications, particularly within the sub-6 GHz band. These challenges include narrow bandwidth (typically less than 500 MHz), mutual coupling in array configurations, and reduced radiation efficiency resulting from dielectric and surface wave losses.

While several enhancement techniques, such as Electromagnetic Bandgap (EBG) structures, metamaterial loading, and multilayer stacking, have been proposed, these methods often lead to complex geometries, higher design costs, and increased computational demands.

In this study, the focus is shifted away from physical fabrication toward simulation-based design and optimization. Using ANSYS HFSS, a 4×4 microstrip patch antenna array incorporating Defected Ground Structures (DGS) and slot modifications is modeled, analyzed, and optimized to achieve enhanced bandwidth, gain, and isolation between elements.

Furthermore, most existing studies and journal publications provide only the final results of antenna array designs without presenting detailed, step-by-step procedures for the design and simulation processes, making it difficult for researchers and students to replicate or build upon their work.

This approach enables detailed parametric investigation and performance evaluation under various configurations without the constraints of material costs, measurement errors, or laboratory limitations. Therefore, the key problem addressed is how to numerically optimize a 4×4 microstrip patch antenna array design for 5G sub-6 GHz operation using RO4350B substrate to achieve high gain, wide bandwidth, and minimal mutual coupling, utilizing simulation tools as the sole research method.

1.3 Aim and Objectives of the Study

1.3.1 Aim

This study aims to design and simulate a 4×4 microstrip patch antenna array incorporating U-slots and defected ground structures (DGS) to enhance bandwidth, gain, and overall performance for sub-6 GHz 5G applications.

1.3.2 Objectives

- To design a 4×4 microstrip patch antenna array using Rogers 4350B substrate to minimize dielectric loss.
- To integrate U-slots and Defected Ground Structures (DGS) into the antenna design for improved bandwidth and reduced mutual coupling.
- To simulate the antenna structure and optimize its performance parameters using ANSYS High Frequency Structure Simulator (HFSS).
- To demonstrate a step-by-step ANSYS HFSS procedure for implementing, simulating, and validating the proposed antenna design.
- To perform a parametric study to analyze the effects of U-slot dimensions and DGS geometry on antenna performance metrics.
- To evaluate key antenna parameters such as return loss (S_{11}), Voltage Standing Wave Ratio (VSWR), bandwidth, gain, and efficiency to verify suitability for sub-6 GHz 5G operation.

1.4 Significance of the Study

This project contributes to the ongoing advancement of efficient antenna systems for 5G wireless communication. It puts forward a practical antenna design that combines beneficial substrate material characteristics with U-slot and defected ground structure (DGS) techniques to overcome the limitations of conventional microstrip antenna arrays. The use of ANSYS HFSS for design and simulation enables researchers and students to perform detailed antenna analysis and performance optimization without the need for expensive laboratory equipment. This approach enhances accessibility for academic institutions and research environments with limited technical or financial resources, thereby promoting broader participation in antenna design and innovation.

1.5 Scope of the Study

This study focuses on the design and simulation of a 4×4 rectangular microstrip patch antenna array operating within the sub-6 GHz frequency range such as bands n77 (3.3–4.2 GHz) and n78 (3.3–3.8 GHz) for 5G wireless communication applications. The antenna is designed using the Rogers 4350B substrate to minimize dielectric losses and integrates U-slot and defected ground structure (DGS) techniques to enhance bandwidth and reduce mutual coupling between array elements. The entire design process is implemented and

analyzed using ANSYS HFSS, which serves as a virtual prototyping tool for performance evaluation.

The scope of this work is limited to simulation-based design and analysis; fabrication and physical measurements are not included. Key performance parameters such as return loss (S_{11}), bandwidth, gain, radiation pattern, and mutual coupling are evaluated to validate the proposed design's suitability for sub-6 GHz 5G applications. The study follows established antenna theory and array design methodologies as outlined by (Balanis 2016).

Chapter TWO

LITERATURE REVIEW

2.1 Overview

2.1.1 5G Communication

5G is the fifth generation of mobile communication technology. It succeeds the fourth generation (4G/LTE) technology. The emergence of 5G networks was influenced by the growing demand for higher data speeds, greater reliability, and more efficient wireless communication. 5G represents a significant advancement over its predecessors, including the fourth generation (4G), third generation (3G), and second generation (2G). It incorporates many technologies that enable higher data rates, ultra-low latency, reliability, and increased connectivity (Huseien et al. 2021), thereby paving the way for Internet of Things (IoT) applications.

The mobile wireless industry began its journey of technological innovation, revolution, and evolution in the early 1970s. Over the years, it has undergone four to five generational shifts, each marked by significant advancements. In recent years, the global telecommunications sector has experienced remarkable growth and transformation (Dange et al. 2021).

Nippon Telegraph and Telephone (NTT) developed the first generation of mobile networks (1G), popularly known as a cell phone, in 1979. It uses analog signal transmission and supports only voice communication. The first generation (1G) lacked data services, including basic text messaging, restricting its functionality to simple call operations. Additionally, this technology suffered from significant drawbacks, such as poor voice clarity, high susceptibility to electromagnetic interference, and inadequate security, making it vulnerable to eavesdropping (Ganatra 2017).

The second generation of cellular network 2G was developed in Finland in 1991 under the Global System for Mobile Communication (GSM) standard. The 2G introduced a significant shift from analog to digital signal transmission, thereby overcoming the limitations of 1G communication by improving voice quality and introducing data services, which facilitated SMS (S. A. Patil et al. 2021). It has a maximum data rate of 64kbps and operates within a bandwidth of 30-200 kHz. A better iteration, called the 2.5G, was later introduced and combines both packet-switched and circuit-switched technologies to facilitate data rates of up to 144 kbps (Ganatra 2017).

The third-generation (3G) wireless technology introduced significant improvements over previous cellular networks. It provided improved network capabilities, with a minimum data transmission rate of 2 Mbps and higher data transfer speeds than earlier generations. The implementation of the 3G technology was facilitated by the 3rd Generation Partnership Project (3GPP). The introduction of 3G networks enabled higher band-

width and significantly increased data transfer rates, making them capable of handling web-based applications, audio streaming, etc. Under optimal conditions, 3G networks can achieve data rates of 100-300 Mbps (Salih et al. 2020).

The commercial deployment of 4G networks commenced in 2009, with initial rollouts occurring in Stockholm, Sweden, and Oslo, Norway. This advanced wireless standard is conceptually encapsulated by the acronym "MAGIC," representing its core capabilities: Mobile multimedia, Anywhere access, Global mobility solutions, Integrated wireless architecture, and Customized services (Dange et al. 2021). A key technological innovation enabling 4G's enhanced performance is Orthogonal Frequency Division Multiple Access (OFDMA), implemented through Long-Term Evolution (LTE) standards (Andrews et al. 2016). This modulation scheme, when combined with multiple-input multiple-output (MIMO) antenna configurations (specifically 2×2 MIMO), facilitates theoretical peak download speeds of up to 150 Mbps for high-performance user equipment (Dange et al. 2021).

The fifth generation (5G) cellular technology ushered in a new era of wireless communications, introducing significant improvements over previous generations. The conceptual foundation for 5G emerged in academic and industry circles during the early 2000s, with standardization efforts commencing around 2010 through organizations like 3GPP. However, it was first commercially deployed in South Korea in 2018, then in the United States in 2019.

2.1.1.1 5G Frequency Bands

5G wireless networks use a wide range of frequency bands with each having its own unique characteristics, hence making them suitable for different applications. These frequency bands have their distinct advantages and disadvantages in terms of bandwidth, coverage, and applications. The 5G spectrum is broadly categorized into three leading bands as shown in figure 2.1, which are:

1. Low-band (sub-1 GHz)
2. Mid-band (1-6GHz)
3. High-band millimeter wave (24-100 GHz)

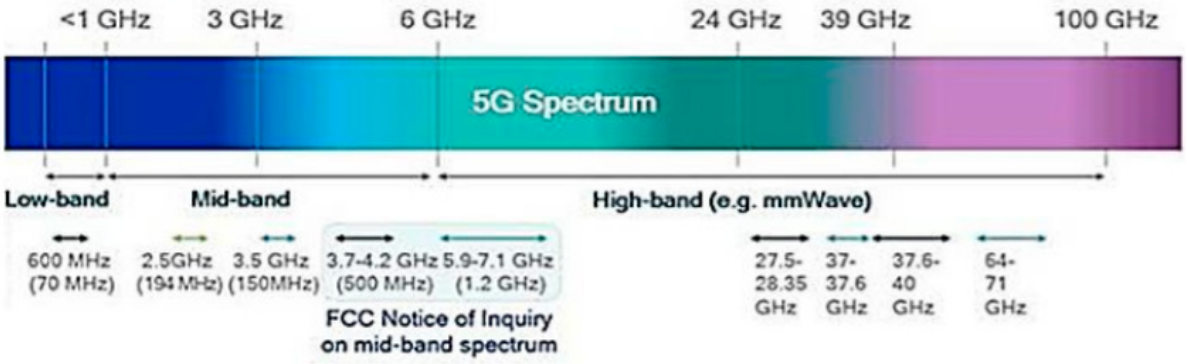

Figure 2.1: 5G frequency spectrum (Alsaif et al. 2021)

1. **Low Band Spectrum (Sub-1 GHz)**
   The low-band frequency spectrum operates below 1 GHz (typically 600-900 MHz) and serves as the backbone of 5G coverage across a nation due to its excellent propagation characteristics. These frequencies can penetrate through buildings and cover a wide geographical range with fewer base stations. The 600 MHz (n71) and 700 MHz (n28) bands are extremely valuable to mobile operators seeking to extend 5G coverage beyond urban centers. The low-band spectrum has some limitations, with the major limitation being that it has a very narrow bandwidth, hence constraining the maximum attainable data rates to 100-200 Mbps, which is extremely low compared to the data rates of the mid-band and high-band spectrum (Shafi et al. 2017).

2. **Mid-band (1-6GHz)**
   The mid-band spectrum lies between the low-band and high-band (mmWave) and thus provides an optimal balance between coverage and high speed, making it suitable for most 5G applications (Mahmood et al. 2021). The C-band (3.3-4.2 GHz)

and the 2.5 GHz band have become significant globally, as they offer channel bandwidths up to 100 MHz that enable peak download speeds approaching 1 Gbps (Shafi et al. 2017), while maintaining reasonable coverage. The 3.5 GHz band (n78) in particular has become a global workhorse for 5G, as it has been adopted by numerous countries as their primary 5G frequency. Mid-band signals can cover several kilometers while still delivering substantial capacity improvements over 4G networks, making them ideal for urban and suburban areas. The major limitation of the mid-band spectrum is its unavailability in some areas; hence, efficient spectrum management and spectrum sharing techniques are employed to maximize utilization.

For this project, the sub-6 GHz band, particularly the n-78 band at 3.5 GHz (the center frequency of the n-78 band), is chosen due to its numerous practical advantages. Moreover, this band provides a balance between performance, coverage, speed, and ease of fabrication. It also makes up a significant portion of the current 5G deployment globally. Hence, it is an ideal target for academic research and prototyping.

3. **High-band millimeter wave (24-100GHz)**
   The millimeter-wave spectrum, which ranges from 24 to 100 GHz (Shafi et al. 2017), is the most advanced part of the 5G network. It includes the following high-frequency bands: 28 GHz (n257), 39 GHz (n260), and 60 GHz (unlicensed). It has a large channel bandwidth of up to 400 MHz, enabling multi-gigabit data rates and extremely low latency. Millimeter waves have the highest speed among the bands, with a peak theoretical speed of 5 Gbps. The major limitation of the millimeter wave spectrum is that it covers only a limited area, ranging from 200 to 300 meters. They also cannot penetrate through buildings and even foliage (Andrews et al. 2016). This necessitates extremely dense network deployments with small cells every few hundred meters, significantly increasing infrastructure costs. The high-band spectrum is primarily deployed in dense urban centers, stadiums, and other high-traffic locations where capacity demands justify the investment. Another unique advantage of millimeter waves is their support for precise beamforming, enabling highly directional communication that can improve spectral efficiency and reduce interference in crowded environments.

A critical analysis of these spectrum bands shows that each has a unique role in the 5G ecosystem. Low-band provides the coverage layer, mid-band delivers the performance layer, and high-band enables the ultra-capacity layer. Network providers employ carrier aggregation techniques to combine these frequency bands for improved performance. The spectrum allocation of the different bands in the 5G spectrum is shown in Figure 2.2. The 5G spectrum is actively being explored, with higher frequencies (even above 100 GHz)

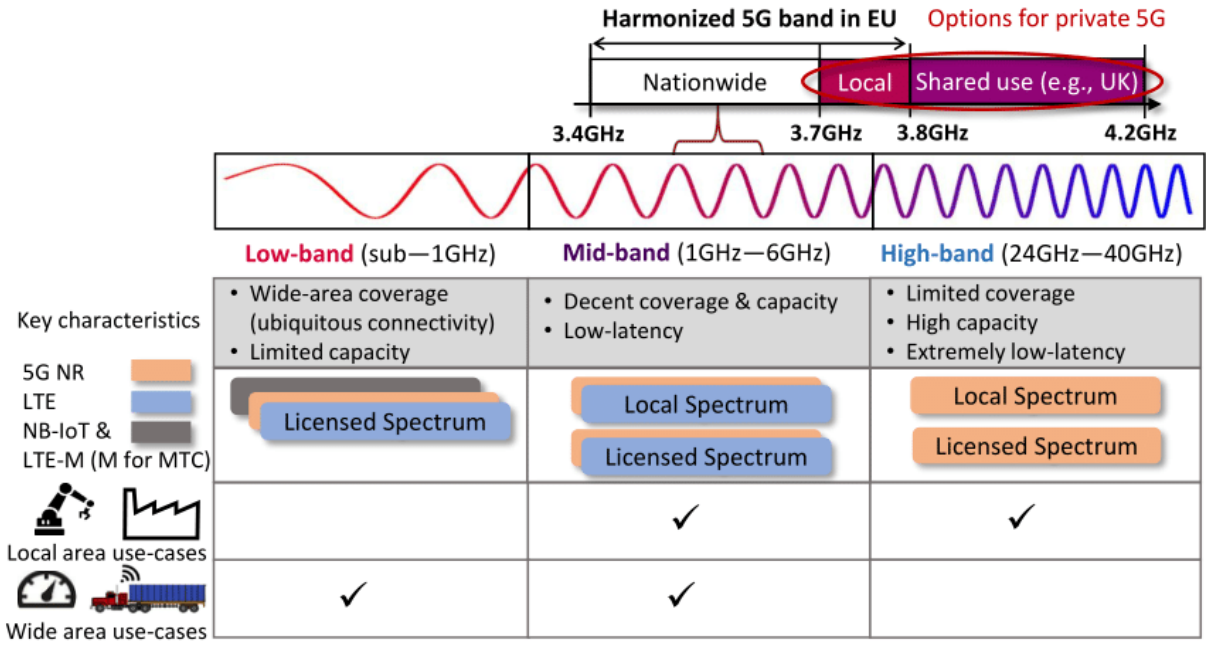

Figure 2.2: 5G spectrum allocation in different bands (Mahmood et al. 2021)

being considered for sixth generation (6G) communication, though molecular absorption poses challenges (Rappaport et al. 2019). Efficient management of the 5G spectrum is essential to meet the growing global demand for wireless connectivity.

2.1.2 Antennas: Theory, Design, and Modern Applications

An antenna is a device that radiates and receives electromagnetic waves, typically radio waves (Balanis 2016). It converts electronic signals into electromagnetic waves and vice versa. An antenna matches the impedance of the transmission line or wave guide in a way that maximizes power transfer and reduces losses. The operation of antennas is based on several principles, such as Maxwell's equations, field regions, radiation mechanisms, and impedance matching using Smith charts and other similar devices. An antenna is a very important device in wireless communication systems. Modern antennas are usually referred to as directional antennas because they focus radiation in a specific direction and dampen or limit radiation in other directions (Balanis 2016).

Antennas have their origins in the work of James Clerk Maxwell,, who combined various theories of electromagnetism to form what we now know as Maxwell's equations. This paved the way for others such as Hertz and Marconi to make significant advancement in electromagnetics. Cell phones, televisions, radios, and routers all use antennas for their functioning. An antenna may take various forms depending on the required application, working frequency range, polarization, and pattern of radiation. It may be in the form of a conducting wire, an aperture patch, an array, a reflector, a lens, and other non-traditional forms (Balanis 2016).

2.1.2.1 Wire Antennas

Wire antennas are the most common type of antenna. They are made up of conducting material, usually copper or aluminum. Wire antennas have different designs. A dipole antenna is one of the fundamental and foundational types of antennas. It forms the basis for more complex antennas. A dipole is made up of two conducting materials. It radiates maximum power in a perpendicular direction and zero power along the axis of the wire (Kraus et al. 2011).

The antennas used in 5G communication differ in design and structure, but are closely related in their electromagnetic operation. Both antennas and dipoles emit electromagnetic waves through resonance. These antennas are called patch antennas and they are a planar form of dipole antennas (Balanis 2016).

2.1.2.2 Patch Antennas

Recently, printed antennas have become more prominent due to their ease of integration into circuits. This is a result of its flat screen and compact physical structure. Patch antennas are the most commonly used type of printed antenna (M. U. Khan et al. 2015). A patch antenna can also be called a Microstrip antenna or Microstrip Patch Antennas (MPAs). MPAs have many advantages in that they are easy to fabricate, are cost-effective, have been studied extensively in their theory, making them relatively easy to

understand (M. U. Khan et al. 2015). Patch antennas can easily conform to curved shapes such as aircraft wings, bodies of cars, and headgear. This makes them preferred for military applications. Standard modeling techniques used in analyzing microstrip patch antennas are cavity model, transmission line model, and the full-wave method. A microstrip patch antenna is basically made up of 4 elements, which are: the ground plane, the dielectric substrate, the radiating patch, and the feed line. This is shown in figure 2.3. The metallic materials that form the patch may take different shapes, which include circular, rectangular, triangular, elliptical, trapezoidal, and several others. The shape dramatically affects the bandwidth, gain, and size of the antenna. The most common types of shape for Microstrip antennas are the circular and the rectangular shaped patch (Balanis 2016).

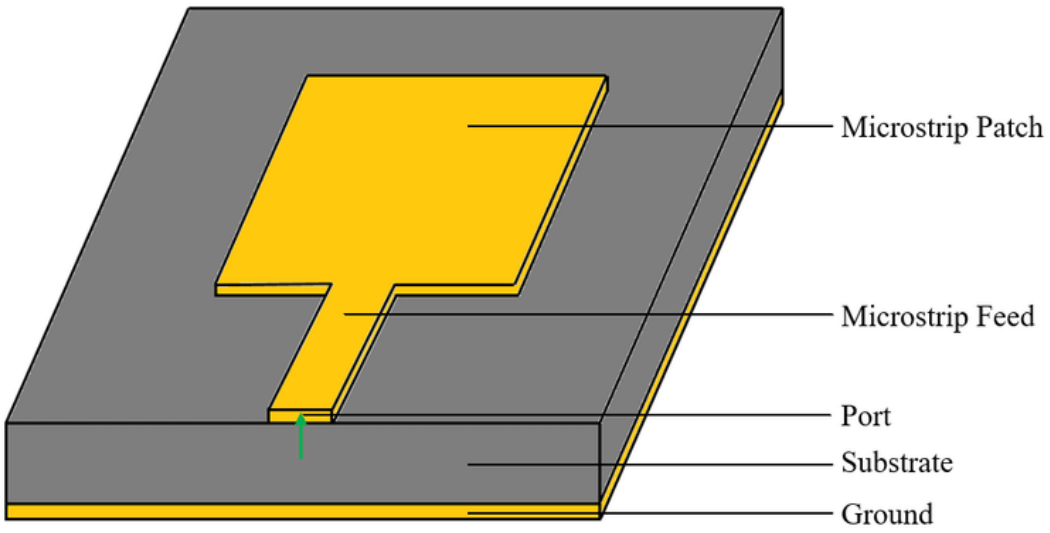

Figure 2.3: A microstrip patch antenna (Chowdhury et al. 2019)

2.1.2.3 Patch(Radiating element)

The patch is a metallic surface that is placed on top of the substrate (for a microstrip) and radiates the electromagnetic waves. It is made of highly conductive metal, e.g, Copper or Gold. The shape of the patch greatly affects the radiation characteristics.

For this project, a rectangular patch is used due to its simple geometry and ease of analysis, and copper is used as the metallic material due to its high conductivity, which is widely used in PCB design.

2.1.2.4 Feed Line

The feed line is the structure used to transmit power from the source (transmitter or VNA) to the patch. In choosing a feed mechanism, it is crucial to ensure that the input

impedance of the antenna is matched to the characteristic impedance of the transmission line or source in order to ensure maximum power transfer with minimal reflection, while still keeping the design compact and straightforward.

The technique of the microstrip line determines how the radio frequency or electromagnetic waves are passed from its source to the patch of the microstrip line on the antenna. This dramatically affects some parameters of the microstrip line, including its bandwidth, its efficiency, its fabrication complexity, and its thickness. Microstripline feeding can be broadly classified into two major categories, namely: the contacting and the non-contacting methods (Rashid et al. 2019).

2.1.2.5 Contacting Methods

In the contacting method, the patch is directly connected to the source of the electromagnetic wave. Examples of this method include microstripline feed, coaxial feed, inset feed, and notch feed. In a inset feed, we connect the strip, usually made of the same material as the substrate, directly to the microstrip line patch. This is advantageous because it is easy to fabricate, and the feed and patch can be grafted onto the same surface,, creating a flat, planar structure (Rashid et al. 2019). Inset feed is actually a variation of microstripline feed in which the feed is set into the patch to allow easy impedance matching (A. Kumar et al. 2017). In coaxial feed, also called probe feed, the inner conductor of the coaxial cable is drawn through the dielectric and connected directly to the patch, while the outer shield conductor is connected to the substrate ground plane. This connection allows flexible placement for easy impedance matching. A limitation of this method, however, is that it requires drilling and may have inductance issues for thick substrate (Thakur et al. 2018). Notch feed involves creating a notch or gap at the point of feed insertion. With this notch, we can improve the impedance by fine-tuning it to enhance the bandwidth, have multiple frequency operations, reduce size, and carry out resonance frequency tuning (Hossain et al. 2024). Varying the width of the notch affects the return loss, VSWR, and resonance frequency, while varying the gap of the notch affects the impedance matching and resonant frequency, and varying the notch angle affects resonant frequency and bandwidth.

The main feed mechanisms that employ the contacting methods are as follows:

2.1.2.6 Inset Feed

An inset feed is a method used to link the feed line to the patch to achieve better impedance matching. Rather than placing the feed line right at the patch's edge, where the input impedance is usually very high, the feed is inserted inward, into the patch itself. Moving away from the edge towards the center of the patch, the input impedance gradually decreases.

By adjusting the feed line to the proper depth, it is possible to identify a location along the patch's width where the impedance is either matched or closely approximated. This enables the antenna to function efficiently, facilitating the transfer of power from the feed to the antenna without the necessity for additional matching components. An image of an inset feed is shown in figure 2.4

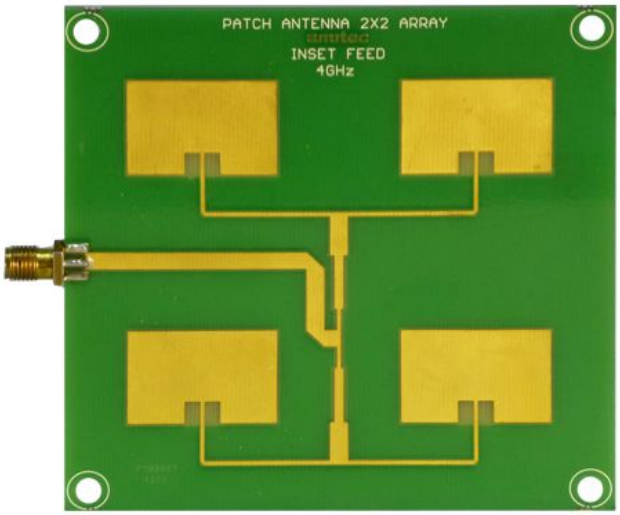

Figure 2.4: An inset feed used in a 2×2 patch antenna array

2.1.2.7 Coaxial Probe Feed

In coaxial probe feeding, a coaxial cable is used to connect the patch antenna. The center conductor of the coaxial cable is soldered to the patch from underneath the ground plane, while the outer conductor is connected to the ground. This allows the signal to be fed vertically into the patch. It is commonly used in prototyping because it is easy to adjust the probe to achieve impedance matching. Coaxial probe feeds provide low spurious radiation and reasonable control over the feed point. They, however, become difficult to implement and tune in very high-frequency or large-scale array designs. An image of a coaxial probe feed is shown in figure 2.5

2.1.2.8 Non-contact Feeding

In non-contact feeding, the source and patch are not directly connected. Instead, power transfer from the source is done by electromagnetic field coupling (Rashid et al. 2019). They are of two types, namely, the aperture coupled type and the proximity coupled type. The proximity-coupled type is also called the electromagnetic coupling scheme or apertureless coupling. This type of feeding uses two dielectric substrates, and the feed line is between these substrates. It uses an electromagnetic field to inductively couple the energy from a microstripline to the patch at the upper surface of the upper substrate

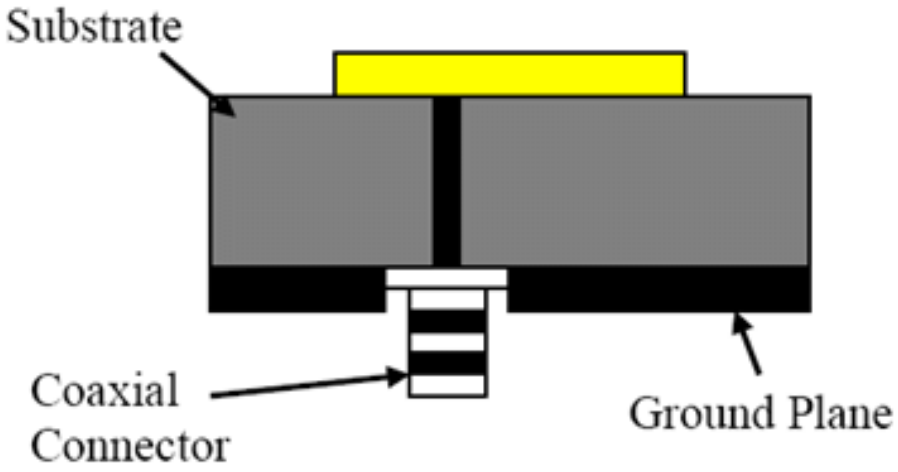

Figure 2.5: A patch antenna with a coaxial probe feed mechanism (M. Rahman 2017)

material. The inductive coupling is possible because the position of the patch on the microstripline overlaps (Kanniyappan 2017). The ground plane is located underneath the second dielectric substrate. The intensity and efficiency of the coupling depend on the area of overlap, the substrate thickness, and the dielectric constant (Fistum 2017). The result of this leads to high bandwidth, low spurious feed radiation, and good impedance matching. In aperture-coupled feeds, the radio frequency feed line is separated from the patch substrate by the ground plane. The ground plane has a slot or aperture, from which its field is coupled to the product of the patch. As a result of this, it has: enhanced bandwidth, greater than that of proximity coupled feeding; substantial reduction in spurious radiation and feed disturbances; high efficiency, and good return loss performance. Accuracy is obtained by tuning the aperture dimensions, such as overlapping area, dielectric constant, and substrate thickness. Although it has significant advantages, it has some disadvantages in that it is complex to fabricate, may lead to an increase in the overall thickness, and a reduction in efficiency due to energy leakage through the slot (V. Kumar 2020).

The common types of non-contact feed mechanisms are explained below:

2.1.2.9 Aperture coupled Feed

This approach utilizes a slot that is created in the ground plane situated between two dielectric layers. The patch antenna is located on the upper substrate, while the feed line is positioned on the lower substrate. The energy from the feed moves through the slot in the ground plane and couples with the patch above. This technique provides enhanced isolation between the feed and the radiating element. This helps reduce unwanted radiation and improves performance. Aperture coupling has a good bandwidth, primarily when different dielectric materials are used for the substrates. It is more complex to fabricate

since it involves multiple layers and precise alignment. An image of an aperture-coupled feed is shown in figure 2.6

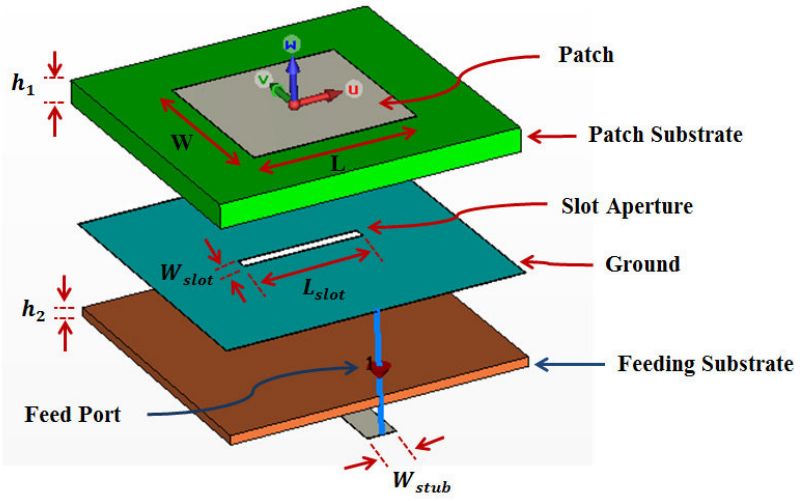

Figure 2.6: A patch antenna with an aperture-coupled feed mechanism (Naji et al. 2012)

2.1.2.10 Proximity coupled Feed

In proximity-coupled feeding, the feed line is put on one medium and the patch is put on another, but there is no direct electrical link between them. A dielectric layer is crossed via electromagnetic coupling to transport the energy from the feed to the patch. This technology offers excellent bandwidth and efficient power transfer owing to the extensive coupling area and the lack of direct contact. Since there is no slot or probe, this method avoids the mechanical weaknesses of coaxial feeds and the complexity of slot alignment in aperture coupling. However, it still requires two substrate layers and careful control of spacing, making it more challenging to fabricate than simpler feed methods. An image of a proximity coupled feed is shown in figure 2.7

The advantages and disadvantages of the feed mechanisms discussed are highlighted in table 2.1.

For this project, we shall be making use of the inset feed because it is fully planar and easy to integrate; it works well in arrays like 4×4.

2.1.2.11 Feed Division Techniques

In corporate feeding, it is a feed technique in which the power from the input signal is progressively divided into equal or controlled unequal paths, such that every antenna element receives power (Maharjan 2020). Within this technique exist different division techniques such as the T Junction dividers, Wilkinson power dividers, Quarter wave transformers, Hybrid couplers, and unequal power dividers.

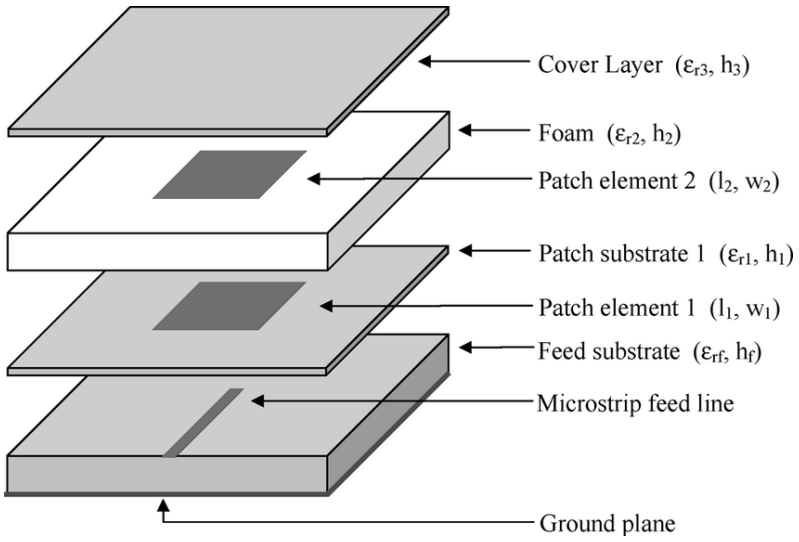

Figure 2.7: A patch antenna with a proximity coupled feed mechanism (Rowe et al. 2006)

Quarterwave transformer is a principle used in transforming impedances to allow equal power division. The impedance transformation is controlled by the width of the transformer. These transformers can be connected in cascade with dividers to enable wideband operations. This has a slight disadvantage of increasing the line length. Quarter-wave transformers are usually used with T-junction or Wilkinson dividers to maintain a matching impedance of 50Ω. In Hybrid couplers, we use coupled microstrip lines to divide power at a phase difference. This improves isolation but is more complex and causes a larger physical footprint. In unequal power dividers, the line impedance is adjusted in such a way to intentionally ensure that power is divided non-uniformly (Uddin et al. 2020). This is because of the advantages it may have in terms of amplitude tapering (Karimi et al. 2022)

Wilkinson feed divider technique is a passive microwave circuit used in antenna array designs. This method of power division divides the input signal into either equal or unequal output signals. It employs a quarter-wave transformer to create a two-way split divider. The design features two quarter-wavelength transmission lines with an impedance of $\sqrt{2Z_o}$ and includes a resistor linked between the outputs to ensure isolation between the input and the output. This configuration yields an equal distribution of power, excellent isolation, and minimal insertion loss. (Wilkinson 1960). There are different variations in the Wilkinson dividers; these include: Two-way Wilkinson divider, with one input and two outputs, Multi-Way Wilkinson divider, having one input and several outputs, and unequal Wilkinson divider, in which outputs have unequal power (Pozar 2012). It has high complexity in fabrication and is limited by the resistors' thermal capacity. Compared to T Junction, it has better isolation and matching(Pozar 2012)

The T-junction power divider is pivotal in microstrip and waveguide corporate-feed networks. It functions by ensuring equal or predetermined unequal power division among

Table 2.1: Comparison of Common Feed Mechanisms for Microstrip Patch Antennas

Feed Mechanism	**Advantages**	**Disadvantages**
Inset Feed	- Allows for better impedance matching by controlling the inset distance - Low profile, planar, and compact	- Slightly more complex to fabricate compared to edge feed - Limited bandwidth
Coaxial Probe Feed	- Excellent impedance matching - Reduced spurious radiation	- Non-planar; requires drilling through substrate - Harder to integrate in arrays
Aperture Coupling	- Offers wide bandwidth - Good isolation between feed and radiating element	- Difficult fabrication - Requires multilayer structure and alignment
Proximity Coupling	- Very wide bandwidth - No physical contact between feed and patch (reduces losses)	- Complex design - Requires precise alignment of stacked layers

antenna elements. For optimal performance, T-junction dividers are frequently paired with impedance transformers such as quarter-wavelength sections to maintain impedance matching and minimize signal reflections(Sahana 2024). In large arrays, cascaded T-junctions create multi-branch corporate feeds, which distribute power to numerous elements while maintaining control over amplitude and phase. T-junction power dividers are implemented across a variety of antenna array platforms. In microstrip patch antenna arrays, their integration with quarter-wave transformers has led to significant improvements in gain, directivity, and bandwidth, making them effective in wireless applications (Farahbakhsh et al. 2017). For millimeter-wave slot arrays, advanced T-junction designs within groove gap waveguides support wideband and low-loss operation, ensuring efficient feed networks in demanding frequency ranges (Ismam et al. 2023). T-junction dividers enhance array performance by achieving balanced power delivery and broadband impedance matching. They are key to deploying amplitude tapering schemes like the Chebyshev distribution, which is essential for sidelobe suppression in large linear arrays(Ismam et al. 2023). High-frequency and ultrawideband implementations of T-junction dividers have demonstrated efficient bandwidth extension, practical for arrays operating from several gigahertz up to tens of gigahertz(Ghimire et al. 2021).

2.1.2.12 Dielectric Substrate

In the development of high-frequency antennas for 5G communication, selecting the appropriate substrate is vital for influencing the antenna's efficiency, bandwidth, and overall performance.

When designing microstrip line antennas, it is essential to pick the right substrate

material. This selection can affect the size, bandwidth, gain, and efficiency of surface wave loss, as well as the mechanical and environmental durability of the patch antenna. There are several substrate parameters that can be considered, they include dielectric constant, substrate thickness, loss tangent, surface-wave effect, and mechanical and environmental properties (Hemalatha et al. 2023).

The dielectric constant is an important parameter that affects the choice of substrate material used as the dielectric. The dielectric constant is also called relative permittivity. It compares how much electric field can be stored in a material relative to air. Most dielectric materials used as substrates have a relative permeability within the range of 2.2 to 12. Specifically, the size, performance, and bandwidth of the microstripline antenna are affected by the dielectric constant of the substrate. The greater the value of the permittivity, the lesser the wavelength inside the antenna and the smaller the antenna size. High permittivity leads to greater confinement of the electric field, reducing fringing effect and leading to a narrower bandwidth. High permittivity leads to an energy loss, as the dielectric traps some of the energy; this leads to an overall reduction in efficiency. The greater the permittivity of the dielectric substrate, the less the interference and coupling of some systems (Hemalatha et al. 2023). For 5G applications, substrates such as Rogers RT5880 and Taconic RF-35, with dielectric constants ranging from 2.2 to 3.5, are preferred due to their low permittivity and low loss tangent, which help achieve high efficiency and wide bandwidth.

Loss tangent is another important factor that determines the selection of a dielectric material. It is also called the dissipation Factor or dielectric loss tangent. The dielectric loss tangent indicates the amount of energy dissipated as heat when electromagnetic waves travel through a dielectric material within the antenna structure. Mathematically, it is the ratio of the dielectric loss to the stored energy. The low loss tangent is good because it means that the dielectric material stores more energy than it loses. For frequency applications greater than 2 GHz, like those of a 5G network, Rogers RT5880 is usually used. A high loss tangent leads to a reduction in antenna efficiency because greater heat is generated by the antenna. This loss in efficiency due to the high permittivity leads to a reduction in available bandwidth. A substrate with a low loss tangent is capable of handling greater power without degrading (Joshi 2018).

The surface wave effect is an important characteristic of microstrip and printed antennas. A surface wave is an electromagnetic wave that propagates on the surface of a dielectric substrate instead of radiating out into free space. When a patch antenna radiates energy, not all its energy is radiated into free space. Some of it is trapped on the surface between the patch and the substrate material. This usually occurs when the dielectric constant of a substrate is high, or when the thickness is large relative to the wavelength of the electromagnetic wave. Surface wave effect is a significant disadvantage because energy that is not radiated is lost, reducing overall efficiency. The shape of the

radiation pattern of the electromagnetic waves can also be changed as a result of the surface wave effect. In addition, surface waves can magnetically couple to other nearby elements and degrade their performance. There are several ways of reducing surface wave effects, including using a dielectric substrate with low permittivity, using a thinner substrate, employing electromagnetic band gap structures, a defective ground plane, and air foams or foam substrates (Abdulhamed 2019).

Rogers 4350B was chosen over the commonly used **FR-4** substrate due to its superior electrical properties that are highly suitable for microwave and millimeter-wave applications. Specifically, Rogers 4350B has a very low dielectric constant ($\varepsilon_r \approx 3.48$) and an extremely low loss tangent ($\tan\delta \approx 0.0037$) compared to FR-4 ($\varepsilon_r \approx 4.4$, $\tan\delta \approx 0.02$). These characteristics result in reduced dielectric losses, improved impedance matching, and higher radiation efficiency, which are essential in 5G systems operating at sub-6 GHz and beyond. Additionally, Rogers 4350B offers excellent dimensional stability and low moisture absorption, making it ideal for precise fabrication and consistent performance under varying environmental conditions. Therefore, while FR-4 is more cost-effective, its lossy nature at high frequencies makes Rogers 4350B a more reliable and performance-optimized choice for this high-frequency antenna array design.

2.1.2.13 Ground Plane

The ground plane is made of copper, and it lies beneath the dielectric substrate. It provides a return path for current. Defective Ground Structure (DGS) is an advantageous technique in designing antennas.

A defective ground plane is an intentional pattern etched on the ground plane of a microstrip patch antenna. This is done in order to improve the performance of the antennas by changing the electromagnetic field distribution. Usually, the ground plane of an antenna is continuous and reflects the electromagnetic wave. However, by etching specific patterns on the ground plane, the electromagnetic field distribution can be modified. This helps us in band gap filtering, impedance matching, and radiation suppression to reduce phenomena like the surface wave effect. The overall effect of DGS is: an increase in efficiency, improved gain, miniaturization or reduction in size, improved bandwidth, and better impedance matching. The etches made on the ground plane may take different types or shapes depending on the purpose for which they are done. Due to their usefulness, DGS find application in 5G communication (Khandelwal et al. 2017).

These modifications change the current distribution and electromagnetic properties of the antenna, leading to the following improvements:

- **Impedance Matching**: DGS enhances impedance matching between the feed line and antenna. It introduces additional inductance and capacitance to help reduce signal reflection and improve power transfer efficiency.

- **Enhanced Bandwidth**: By changing the ground current path, DGS creates slow-wave effects and resonance behavior. This leads to a broader operational bandwidth, without a size increase.
- **Compact and Simple Design**: DGS structures are carried out by etching patterns into the ground plane. This simplicity allows for easy fabrication and compact antenna layouts.
- **Harmonic Suppression**: DGS suppresses unwanted higher-order harmonics, leading to better signal transmission and reduced interference.
- **Cost-Effective and Fabrication-Friendly**: DGS can be mass-produced because it can be done using PCB manufacturing processes.

2.1.3 DGS

The standard shapes used in defective ground structure are dumbbell-shaped, H-shaped, U-shaped, and circular or elliptical slots. Each of these shapes has its various advantages (Akbar et al. 2021).

The dumbbell-shaped Defected Ground Structure (DGS) is particularly effective in reducing mutual coupling between adjacent antenna elements. It also suppresses some specific surface wave modes and has a relatively good boundary compared to others. Its rectangular arms act like an inductor, and the narrow slot connecting them acts like a capacitor. Together, they create the effect of an LC band stop filter in the ground plane. The band-stop filter creates a frequency at which signals are attenuated, resulting in a notch in the antenna frequency. U-shaped slots are preferred when it comes to improving the boundary while maintaining good radiation efficiency. They do this by increasing the current path in the antenna. Circulars are used when compact designs are required due to the limited space between the patches. Rectangular slots are used when simplicity in design is the primary consideration. It achieves current disruption while still maintaining ease of fabrication.

H-shaped DGS is a defective ground plane in which a slot on the ground plane looks like an 'H'; a horizontal slot connecting two vertical slots. The horizontal slot forms a capacitive gap, and the two vertical legs form a large total inductance. This forces the current to divert between the central gap. The separation between the vertical slots affects the coupling strength. The overall effect of this H shape is that the capacitance and inductance result in a resonant stop band frequency lower than the working frequency of the patch. It is used in antenna size reduction, mutual coupling reduction, and suppression of harmonics. Although the H slot has several advantages, it also has some drawbacks, which include: distortions in radiation patterns in asymmetrical placement,

complexity in fabrication, and introduction of a narrow stop band. (A. Kumar et al. 2020)

2.1.3.1 Cavity Modeling

In cavity modeling, we treat the patch and substrate ground as a resonant cavity. That is, we assume the substrate and grounds are thin, making the field uniform across them (perfect electric conductors), and that the sides are perfect electric walls. This resonant cavity forms a close structure that confines the electromagnetic wave, leading to easy radiation of the patch (Pozar 2012). The cavity model is a simple analytical model that gives clarity into the resonance frequency and impedance. It is advantageous when it comes to circular and rectangular patches (Mehta 2015). This model has limitations in that it does not account for the losses at the edges due to fringing field, can only be used for thin patches, only works for simple shapes, assumes perfect conditions at the boundaries, and does not work appropriately for wideband antennas.

2.1.3.2 Transmission-line Modeling

The transmission-line modeling is another standard method of modeling microstrip line patch antennas. In transmission line modeling, the patch is taken as a transmission line of length l and with w. The conducting patch and the ground plane form a two-line system that is open at both ends. These openings cause electromagnetic waves to be reflected continuously until a resonant frequency is reached. The patch resonates when its length is approximately half a wavelength. This model helps us to easily estimate the resonant frequency, the impedance, the efficiency, and the bandwidth. It is straightforward, helpful for initial design and analysis, and a good fit for rectangular antennas. However, it has limitations in that it is not accurate for irregularly shaped objects and is not very precise at high frequencies (Mehta 2015).

2.1.3.3 Full-wave Numerical Method

When it comes to precision, the third standard method is used. This method is called the full-wave numerical method. Here, the wave behavior is not simplified, and both near-field and far-field effects are modeled accurately. It is also exact for patches with complex geometry. The full-wave numerical method is an advanced computer-based technique that uses simulations for the analysis of microstrip patch antennas. There are several types of full-wave numerical methods, the most common of which are: the method of moments, which is efficient for problems in the frequency domain; the finite difference time domain, which works properly for broadband analysis; and the finite elements method, which has high precision for inhomogeneous materials. This method helps us to simulate the actual performance of antennas, fine-tune shape sizes and material of choice, analyze losses,

impedance matching, and radiation pattern, and study the effect of mutual coupling. This high precision comes at high computational costs, takes a long time to simulate, requires significant expertise, and may not be necessary for simple tasks (E. A. Fubara et al. 2023).

2.1.4 Antenna Arrays

An antenna array is a combination of several antennas working as a single unit to transmit and receive electromagnetic waves. The individual antennas that combine to form the single antenna are called antenna array elements. By properly controlling the phase, amplitude, and geometry of each of these elements in the array, it is able to shape radiation patterns, carry out beam steering, and achieve capabilities not possible with a single antenna element (Nadar et al. 2023).

Antenna arrays can be fed in several ways, which include corporate feed, series feed, proximity feed, inset feed, and coaxial feed. We have previously discussed proximity feed, inset feed, and coaxial feed; these feeding techniques apply to both single antennas and antenna arrays. However, corporate feeding and series feeding apply only to multiple antenna arrays (Raza et al. 2019).

The series-fed antenna is also referred to as a traveling wave antenna. This is a technique of feeding antennas in which the radio frequency power travels sequentially from one patch element to another through a single feed line. Series-fed antennas are known for their simplicity. Each antenna element taps into the line, draws power, and radiates it as the signal flows through the line. The last element receives the lowest amount of power because of the power consumed by the preceding elements. Series-fed antennas are usually used in linear antenna arrays such as 1×4 or 1×8 arrays. They are well-known for their simplicity, compact layout, low weight, and low cost. However, they are not used for very high-frequency applications due to unequal power distribution, considerable phase shift accumulation, narrow bandwidth, and difficulty in beamforming (Rahim et al. 2008).

In corporate feeding, each array element is fed by branches from a single feed source. The power is distributed equally and remains in phase with each radiating element through a well-arranged branching network of transmission lines. It is referred to as a corporate feed because it is organized and has a central system, like a corporate structure in an organization. The fact that all of these antenna elements are in phase ensures that the radiation is coherent in the antenna array. Each individual branch of the corporate feed is carefully constructed to maintain constant input impedance. Impedance transformation is done with the aid of a quarter-wave transformer or by variation in the width of the branches. Corporate feed allows ease of beamforming by introducing controlled phase shifts in the network. It also provides high flexibility, as it can be used

for 2×2, 4×4, and 8×8 arrays. It is far more stable than a series feed in wideband and high-gain applications. However, in order to achieve accurate impedance transformation, a precise design is required as the array size increases. Feedlines may also occupy more surface area than necessary on the substrate. This increase in size results in high insertion loss, especially at high frequencies. Another challenge is the need for high precision in fabrication due to narrow line widths (Raza et al. 2019).

A 4×4 antenna is made up of 16 antennas arranged in a grid of four rows and four columns. This configuration provides several advantages over conventional single antennas. It finds applications in 5G communication, satellite systems, radar systems, and multiple-input output (MIMO) systems (Rahim et al. 2008).

2.1.5 Key Parameters In Antenna Design

The key parameters considered in the design of an antenna are discussed below:

1. **Directivity, D**

   Directivity is an essential characteristic of antennas. It quantifies the amount of power an antenna radiates in a specific direction per unit solid angle, compared to the power radiated per unit solid angle by an isotropic antenna that emits power uniformly in all directions. (Shaw 2013). It quantifies the extent of power directed towards a specific orientation. A greater directivity value indicates that the antenna is more directional, resulting in increased power transmission in the preferred direction.

   From a mathematical standpoint, directivity is defined as the ratio of the radiation intensity in the direction of maximum emission to the average radiation intensity across all directions. (Shaw 2013).

   $$D = \frac{U_{max}}{U_{avg}} \tag{2.1}$$

   where,
   U_{max} = Maximum radiation intensity (watts per steradian).
   U_{avg} = Average radiation intensity in all directions.

   The radiation pattern of an antenna provides an effective means to illustrate its directivity, serving as a graphical depiction of the antenna's power distribution across all directions. A highly directional antenna (high directivity value) will have a narrow main beam and smaller side lobes (Balanis 2016). Figure 2.8 shows the 2D and 3D plot of the radiation pattern of a $\frac{\lambda}{2}$ dipole compared with an isotropic antenna to illustrate the concept of directivity.

2. **Gain, G**

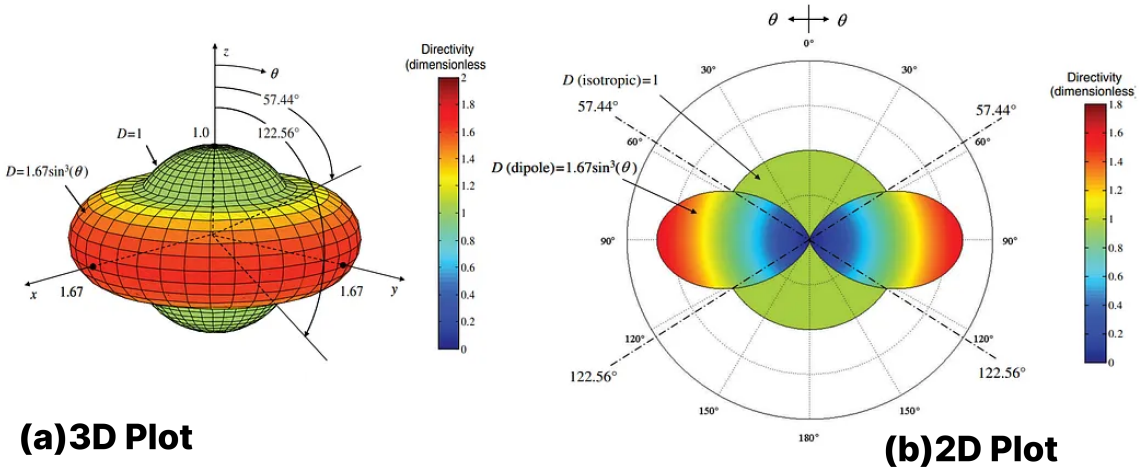

Figure 2.8: Radiation pattern of a $\frac{\lambda}{2}$ dipole compared with an isotropic antenna (Balanis 2016).

The gain of an antenna is a measure of how well it transmits and receives signals in a particular direction compared to an isotropic antenna (Balanis 2016). Antenna gain is a key factor evaluated during the design of antennas. It is commonly expressed in decibels (dB), either in relation to an isotropic radiator (dBi) or a dipole antenna (dBd).

Mathematically,

$$G(\theta, \phi) = \eta \cdot D(\theta, \phi) \tag{2.2}$$

where,
G = Gain
η = Radiation efficiency
D = Directivity

The gain and directivity of an antenna are closely related, as shown in equation 2.2. The directivity of an antenna is a theoretical indication of its ability to concentrate its beam in the intended direction, disregarding any losses. In contrast, the gain of an antenna takes into account ohmic losses, impedance mismatches, and surface waves.

3. **Bandwidth**
   Bandwidth refers to the range of frequencies over which an antenna maintains optimal performance (Balanis 2016). Modern wireless systems (5G, IoT) require antennas to support multiple frequency bands (e.g., 4G/5G dual-mode). The bandwidth of an antenna is proportional to its size, with smaller antennas having narrower bandwidths and larger antennas having wider bandwidths. Antenna bandwidth

is a significant parameter in antenna design. By carefully selecting antenna size, shape, and materials, and employing appropriate design techniques, engineers can optimize antennas for specific bandwidth requirements, balancing bandwidth with other performance characteristics.

4. **VSWR**

   It is a measure of how much power is transferred from the source to the antenna. It reflects how well the antenna is matched to the transmission line linking it to the source. A lower VSWR (nearer to 1:1) indicates a superior match and more effective power transfer, while a higher VSWR indicates a poorer match with increased signal reflection.

5. **Element Spacing**

   Element spacing (d) is the physical distance between adjacent antenna elements in an antenna array. It is measured in wavelengths (λ) of the operating frequency. In antenna arrays, element spacing is an important parameter that significantly impacts the array's radiation pattern and performance. Generally, spacing between elements is recommended to be around half the wavelength $\frac{\lambda}{2}$ of the operating frequency, but not greater than $\frac{\lambda}{2}$ to minimize unwanted coupling and reduce grating lobes (Ren et al. 2022). Grating lobes are radiation lobes with the same intensity as the main lobe. Element spacing directly affects the radiation pattern, beam steering capability, mutual coupling effects, and the array size.

   Mutual coupling refers to unwanted energy transfer between array elements, which results in input impedance variations, pattern distortion, and reduced efficiency. When $d < \frac{\lambda}{2}$, i.e, close spacing, there is strong mutual coupling; however, when $d > \frac{\lambda}{2}$ (wide spacing), there is reduced coupling, but grating lobes begin to appear. The problem of mutual coupling can be mitigated by using Defected Ground Structures (DGS), decoupling networks, or element isolation techniques.

2.1.6 Practical Considerations

Beyond the theoretical parameters of antenna design, several practical factors influence the system's overall performance and reliability. These include substrate choice, fabrication tolerances, feeding techniques, and the use of Radio Frequency (RF) connectors such as SubMiniature version A (SMA). Attention to these considerations ensures that the designed antenna not only meets simulated specifications but also performs consistently under real-world operating conditions.
The main practical considerations relevant to this work are outlined and discussed below:

1. **Substrate Selection**
   The antenna board's substrate consists of a dielectric material that offers mechanical support for the metallic radiating elements and significantly influences the antenna's electrical performance due to its dielectric constant and loss characteristics. Selecting an appropriate substrate is therefore essential, with key factors including dielectric constant, loss tangent, thermal stability, mechanical strength, and fabrication compatibility.
   A summary of commonly used substrates and their properties is presented in Table 2.2 below.

Table 2.2: Comparison of common antenna substrates at 3.5 GHz

Substrate	ε_r	**Loss Tangent** ($\tan\delta$)	**Gain (dBi)**	**VSWR**	**Return Loss (dB)**	**Price ($/unit)**
FR-4 (Epoxy)	4.4	0.020	5.2	1.90	-12.0	10
Rogers RT/Duroid 5880	2.2	0.0009	7.8	1.15	-22.4	120
Rogers 4003C	3.38	0.0027	7.2	1.20	-21.0	95
Rogers 4350B	3.48	0.0037	7.0	1.22	-20.5	85
Taconic RF-35	3.5	0.0018	7.0	1.25	-20.1	80
Arlon AD350A	3.5	0.0030	6.9	1.28	-19.5	75

   For this project, Rogers 4350B is selected as the most suitable substrate. While Taconic RF-35 offers a slightly lower loss tangent on paper, Rogers 4350B provides superior thermal and electrical stability, ensuring more consistent performance under varying operating conditions. In addition, it is compatible with standard FR-4 fabrication processes, which reduces manufacturing complexity and cost. Considering the balance of dielectric properties, reliability, manufacturability, and price, Rogers 4350B presents the best trade-off for implementing the 4×4 patch antenna array at 3.5 GHz.

2. **SMA Connector Selection**

SubMiniature version A (SMA) connectors are precision RF connectors widely used to interface antennas with measurement equipment or RF front-end circuitry. At high frequencies such as 3.5 GHz, the choice of SMA connector significantly influences signal integrity, insertion loss, and impedance matching. Key factors in selecting an SMA connector include characteristic impedance (typically 50 Ω), voltage standing wave ratio (VSWR), insertion loss, power handling capability, and mechanical robustness.

A summary of commonly used SMA connector variants and their properties is presented in Table 2.3 below.

Table 2.3: Comparison of common SMA connectors at 3.5 GHz

Connector Type	**Impedance** (Ω)	**VSWR** @ 3.5 GHz	**Insertion Loss (dB)**	**Price** ($/unit)
Standard SMA (Brass, Gold)	50	1.15	0.10	5
Precision SMA (Stainless)	50	1.10	0.08	12
RP-SMA (Reverse-Polarity)	50	1.20	0.12	6
SMA Bulkhead (Panel Mount)	50	1.18	0.11	8
SMA Right-Angle (PCB Mount)	50	1.25	0.15	7
Edge-Mounted SMA (PCB Mount)	50	1.22	0.11	7

The gold-plated, edge-mounted SMA connectors are usually employed. Their wide frequency range (3–6 GHz) ensures full compatibility with the 3.5 GHz patch antenna array, while easy matching to the feed line minimizes reflections and maximizes power transfer. Additionally, the connectors' mechanical robustness provides stable and repeatable connections during testing and integration. Considering electrical performance, frequency compatibility, and mechanical reliability, these SMA connectors offer the most suitable solution for the proposed antenna system.

2.1.7 Ansys HFSS

Ansys is short for Analysis Systems. It is a shortened name for both the company and the brand used for its simulation tool. HFSS stands for High Frequency Structure Simulator. It is a software tool developed by Prof. Zoltan Cendes for simulating high-frequency components, including antennas, radio-frequency/microwave components, waveguides, filters, and high-speed interconnects. HFSS has seen significant technological advancements in its software, including solver advances, adaptive meshing, spurious-free vector basis functions, hierarchical and mixed-order basis functions, domain decomposition methods, mesh fusion, and modern solver architecture stability (ANSYS, n.d.). ANSYS was one of the first commercial tools to use the Finite Element Method (FEM) for full-wave electromagnetic problems. This allowed for very accurate modelling of complex geometries. It is

also widely used in 5G research for large Multiple Input Multiple Output (MIMO) antenna arrays, where high efficiency in terms of mutual coupling, beamforming efficiency, and radiation patterns stability is required (Balanis et al. 2007). Many IEEE papers on antenna design and fabrication use HFSS because of its reliability (Wong 2016).

ANSYS has some core simulation guidelines. It has accurate material modelling, allowing one to define the material type based on reliable datasets. These manufacturer-provided values are crucial for simulation. ANSYS also sets appropriate boundary conditions, such as using Perfect Electric Conductor (PEC) for metallic surfaces, radiation boundaries for open-space antenna simulation, and symmetrical planes where necessary to reduce the simulation time (ANSYS, n.d.).

2.1.8 Available Resources

- Simulation Software (ANSYS HFSS)
  Simulation software is used to reduce development and implementation time and avoid material wastage due to design errors. It improves productivity and provides high-accuracy, complete measurements of antenna characteristics. ANSYS HFSS is used in this project because of its availability, reliability, and its ability to perform 3D electromagnetic simulations and provide detailed visualisation.

- Substrate (Rogers 4350B)
  It has low dielectric strength ($\varepsilon_r = 3.48$), return loss (-20.5dB), and extremely low loss tangent ($\tan\delta = 0.0037$). These properties minimize signal loss and result in a good radiation pattern.

- Defective Ground Structures (DGS)
  It is used to improve impedance matching, enhance bandwidth, simplify design, and reduce size.

2.1.9 Review of Related Works

The swift rollout of 5G networks has accelerated investigations into advanced antennas for sub-6 GHz bands (3.3–7.1 GHz). This section offers an overview of key research and advancements in the design of patch antenna arrays for sub-6 GHz and mmWave 5G applications. The aim is to highlight current trends and methodologies, and to identify areas requiring further investigation.

Padire et al. (2025) carried out the design of a 4×4 microstrip patch antenna (MPA) for 5G mmWave applications, based on the premise that the mmWave spectrum offers increased bandwidth due to its high frequency range, thereby enabling high data rates, low latency, and ultra-high capacity. They emphasized the benefits of MPAs, such as their small size, adaptability to various surfaces, simplicity in manufacturing, and compatibility with integrated circuit technologies. According to the authors, MPAs have seen widespread industrial and commercial applications over the past decade, prompting numerous research efforts to enhance their performance.

The novelty of their research lies in the optimization of key antenna parameters—gain, directivity, bandwidth, and efficiency—for a 4×4 MPA specifically tailored for mmWave applications. The authors chose the mmWave frequency band, specifically the 24-40 GHz range, to meet the increasing need for faster data speeds, wider bandwidth, and enhanced network capacity, as mmWave spectrum presents a potential solution to these issues. However, they recognized the fundamental drawbacks of mmWave frequencies, including significant path loss and restricted penetration, which require sophisticated antenna designs to surmount these challenges.

The antenna was designed and simulated using CST Microwave Studio, yielding the following performance metrics: gain = 9.54 dB, $S_{11} = -26.71$ dB, directivity = $10.13dB$, bandwidth = $2.52GHz$, Voltage Standing Wave Ratio (VSWR) = 1.23, and efficiency = 86.82%. These results demonstrate a balanced performance across critical antenna characteristics.

A thorough analysis of Defective Ground Structure (DGS) as a valuable method for improving the functionality of microwave and antenna systems was provided by Khandelwal et al. (2017) in 2017. To enhance mutual coupling, gain, and bandwidth, DGS involves etching compact defects into the ground plane. The study highlighted DGS's smaller size, simpler design, and simpler parameter extraction compared to Photonic Band Gap (PBG) and Electromagnetic BandGap (EBG) structures. The usefulness of DGS in reducing surface waves and enhancing radiation properties was demonstrated by its use in filters, amplifiers, waveguides, and antennas.

To improve gain, bandwidth, and efficiency, Nadar et al. (2023) proposed an E-shaped Microstrip Patch Antenna Array (MSPAA) using the RT/Duroid 5880 substrate. The study examined 2×2 and 3×3 MSPAAs with different patch sizes and substrate thick-

nesses, and simulation and hardware results demonstrated that the proposed arrays outperformed previous designs, achieving low sidelobes, high gain (up to 8.9 dBi), and effective beam steering across 3.8–4.2 GHz. CST and MATLAB tools were utilized for design and analysis.

An overview of microstrip patch antennas, including their design, structure, and radiation principles, was presented at (Mehta 2015). The antenna features a ground plane on one side of a PCB and a metallic patch on the opposite side. This encompasses an examination of different feeding tgechniques, such as coaxial, strip line, aperture, and proximity coupling. The report emphasizes the antenna's widespread use in commercial, industrial, and military settings.

(E. A.-A. Fubara et al. 2023) used the Advanced Design System (ADS) with the Method of Moments (MoM) and FEM to present a numerical study of microstrip patch antennas. FEM assessed the behavior of high-frequency electromagnetic waves, while MoM used integral formulations to solve Maxwell's equations. To regulate impedance bandwidth and facilitate dual-band operation at 2.4 and 5.8 GHz, the study focused on reactive loading. To measure reflection reduction, a perturbed E-patch design was suggested, and the Driving Point Impedance Function (DPF) was examined. The outcomes demonstrated enhanced RF output in both frequency ranges and superior antenna performance.

The effect of various feeding strategies on the functionality of microstrip patch antennas used for wireless communication was investigated by Thakur et al. (2018) in 2025. Coaxial probe feed, quarter-wavelength transformer feed, and microstrip inset feed are among the feeding techniques examined. Key metrics for antenna performance, including radiation efficiency, gain, directivity, and return loss, were evaluated and compared among the different methods. The coaxial probe feed demonstrated the best directivity at 5.43 dBi and a gain of 5.33 dB, as indicated by the study. These findings show that antenna properties are strongly influenced by the choice of feeding technique, making coaxial probe feeding a desirable alternative for effective, high-performance antenna design.

An E-patch microstrip antenna was numerically analyzed by Rashid et al. (2019) utilizing the Advanced Design System (ADS) with the Method of Moments (MoM) and Finite Element Method (FEM). While FEM examined the behavior of high-frequency electromagnetic waves, MoM solved Maxwell's equations by transforming them into integral form. To increase impedance bandwidth and facilitate dual-band operation at 2.4 GHz and 5.8 GHz, the study focused on reactive loading. The Driving Point Impedance Function (DPF) was investigated to reduce reflections, and a perturbed patch design was employed to increase speed and range. The results demonstrated improved RF performance and efficient dual-frequency response.

Using ANSYS HFSS, A. Kumar et al. (2017) investigated different feeding techniques

for microstrip patch antennas functioning at 2.4 GHz. The primary emphasis of the research was on how inset, transmission-line, coaxial, and aperture-coupled feeds affected the performance of the antenna. A patch antenna featuring both an inset feed and a coaxial feed was developed and simulated to evaluate return loss and gain. The inset feed achieved a return loss of –23.01 dB and a gain of 7.67 dB, while the coaxial feed resulted in a return loss of –19.6 dB and a gain of 7.69 dB. The findings of the study indicated that microstrip patch antennas are highly suitable for RF and microwave communication systems, owing to their compact design and advantageous radiation characteristics, even when bandwidth is limited.

Microstrip patch antennas (MPAs), which have been in widespread usage for the past thirty years because of their low profile, ease of manufacture, and planar construction, were examined by M. U. Khan et al. (2015) for their evolution and miniaturization. The size of traditional MPAs is usually half a wavelength, although contemporary wireless requirements have necessitated smaller designs. The study explored various strategies for reducing size, including altering material distribution, reshaping, shortening, folding, creating slots and defects in the ground plane, and applying metamaterials. The benefits and drawbacks of each method were evaluated concerning their impact on key antenna performance metrics such as efficiency, bandwidth, and gain.

A thorough review of microstrip patch antennas was given by R. Singh et al. (2011), who emphasized their benefits over traditional antennas. This encompasses aspects such as ease of manufacturing, affordability, a slim profile, lightweight construction, and compact dimensions. The research highlighted the significance of dual and circular polarizations, operation at dual frequencies, frequency flexibility, broad bandwidth, different feeding methods, and the capability for beam scanning. The strengths and weaknesses of microstrip antennas in comparison to traditional microwave antennas were analyzed, along with various types of microstrip antennas, feeding techniques, and their applications.

Barnardo (2024) conducted electromagnetic modeling research on microstrip patch antennas (MPAs) intended for 5G applications. The study assessed scattering and impedance matrices based on feeding-point modifications and examined two popular feeding techniques: a coaxial probe and a transmission line. The effects of relative permittivity, patch length, width, and substrate height on antenna performance were evaluated using a thorough parametric analysis. The findings indicated that while variations in height and length also altered resonance without significantly altering radiation patterns, changes in permittivity also shifted resonance frequencies and decreased gain. Modifications to the patch width enhanced impedance matching with negligible radiation impact.

A thorough analysis of current developments in antenna-array design for 5G communication systems was provided by Ahmed et al. (2024). To meet the needs for faster

data rates, reduced latency, and improved spectrum utilization, the research pointed out the increasing necessity for advanced antenna technologies. It explored the benefits and drawbacks of various array designs, such as phased arrays, MIMO systems, and beamforming techniques. It was also investigated how to improve antenna performance by combining cutting-edge materials and new technology. Size, cost, and power efficiency were emphasized as important design factors, offering insights for optimizing antenna arrays in next-generation wireless networks.

Saeed et al. (2024) identified five essential techniques necessary to achieve reliable and high-capacity communication, with beamforming being a critical component. In their study, the authors provided a comprehensive review and analysis of microstrip patch antenna (MPA) array beamforming techniques tailored for 5G communication systems. They examined various beamforming strategies—namely, analog, hybrid, and digital—highlighting their respective advantages, limitations, and suitability for 5G applications. Furthermore, the study reviewed several types of couplers used in antenna feeding networks, including hybrid couplers, Wilkinson power dividers, branch-line couplers, and Butler matrices, all of which play significant roles in optimizing antenna performance in 5G systems.

Gemeda et al. (2021) developed and assessed the performance of a 28 GHz microstrip patch antenna (MPA) designed for 5G communication systems. The antenna was fabricated using an FR-4 substrate with a thickness of $0.244mm$, a dielectric constant (ε_r) of 4.4, and a loss tangent of 0.0025. Simulations were carried out using CST Microwave Studio. An inset feed technique was utilized, and impedance matching was accomplished with a quarter-wavelength transformer. MPAs were chosen for this design due to their cost-effectiveness, lightweight construction, compact size, and low-profile design in comparison to larger antenna types. The simulated results demonstrated a gain of $7.587dBi$, a directivity of $7.509dBi$, a radiation efficiency of 98.214%, and a bandwidth of $1.046GHz$, indicating optimal performance for the target frequency band.

R. Tiwari et al. (2020) analyzed the configuration and functionality of various microstrip patch antenna arrays, concentrating on essential performance indicators such as return loss, voltage standing wave ratio (VSWR), bandwidth, resonant frequency, and gain. The authors state that a return loss lower than $-10dB$ signifies effective impedance matching and efficient radiation, while an ideal VSWR around 1.2 suggests minimal reflection and effective power transfer. The evaluations and simulations were performed using CST Microwave Studio, enabling a comprehensive analysis of antenna characteristics across various design configurations.

P. Gupta et al. (2022) created a linear microstrip patch antenna (MPA) array with a configuration of 1×4, featuring a slotted circular patch specifically for 5G communication purposes. This antenna was designed to function at a central frequency of $28GHz$ and utilized the TM_{11} mode as its primary resonant mode. To achieve excitation, a microstrip

line feeding method was employed. The design incorporated a Rogers RT/Duroid 5880 substrate, chosen for its low dielectric constant ($\varepsilon_r = 2.2$) and low dielectric losses, with a thickness of $0.254mm$. The performance assessment was carried out using a vector network analyzer (VNA) in an anechoic environment. Simulations were conducted in CST Microwave Studio, and the findings exhibited a return loss of $16dB$ and an impedance bandwidth of around 10% within the millimeter-wave frequency range (24.6-27.24 GHz), validating the antenna's applicability for 5G technologies.

Shamim et al. (2021) introduced a design for a 37 GHz millimeter-wave square-slotted microstrip patch antenna (MPA) aimed at 5G mobile applications. The authors highlighted the critical role of millimeter-wave wireless technology in contemporary society for its capability to facilitate rapid and secure data transmission. The antenna's design featured an H-shaped slot and an inverted T-slot, strategically placed above the radiating patch to improve bandwidth and impedance matching. Rogers RT5880 was chosen as the dielectric substrate due to its low dielectric constant ($\varepsilon_r = 2.2$) and a very low loss tangent of 0.0009, which both support minimal loss operation at high frequencies. The simulation conducted with CST Microwave Studio yielded positive results, including a return loss of -43.05dB, a gain of 8.18dB, and an impedance bandwidth of 16.22% centered around a resonant frequency of 37 GHz, showcasing the antenna's suitability for high-frequency 5G communication.

Irfansyah et al. (2021) highlighted the advantages of microstrip patch antennas (MPAs) for contemporary communication systems due to their compact dimensions, lightweight design, and straightforward integration. Their study involved the design of a 1×2 rectangular patch MPA array intended to function at a frequency of 3.5 GHz, which is important for sub-6 GHz 5G applications. Each patch was sized at 19mm $\times$ 26.5mm and made of copper as the conducting material. The antenna employed an FR-4 substrate with a relative permittivity of 4.3. An inset feeding approach was used to effectively supply power to the radiating elements. After optimization, the antenna achieved a return loss of $-12.54, \text{dB}$ over the frequency range of 3.47 GHz to 3.53 GHz, resulting in a bandwidth of 66.5 MHz, a VSWR of 1.6, and a gain of 5.5dB. These findings support the antenna's potential for incorporation into mid-band 5G communication systems.

Didi et al. (2022) introduced a design for a rectangular microstrip patch antenna (MPA) that incorporates a rectangular slot, specifically optimized for operation at 28 GHz in fifth-generation (5G) wireless applications. The antenna feeding was implemented using the microstrip line method, with the slot added to improve the overall performance of the antenna by enhancing impedance matching and bandwidth. For the dielectric substrate, Rogers RT5880 was selected because of its beneficial electrical characteristics, which include a low relative permittivity ($\varepsilon_r = 2.2$), a loss tangent of 0.0009, and a substrate height of $h = 0.5, \text{mm}$. The dimensions of the antenna were $4.2, \text{mm} \times 3.3, \text{mm} \times 0.5, \text{mm}$. To verify the design, simulations were conducted using Ansys HFSS and CST

Microwave Studio. The simulation results indicated a resonant frequency of 27.97 GHz, a reflection coefficient (S_{11}) of -20.95, dB, a bandwidth of 1.06 GHz, a gain of 7.5, dB, a radiated power of 29.9 dBm, and an efficiency of 99.83%, thereby affirming the antenna's excellent performance for 5G millimeter-wave applications.

Smartphone-oriented antenna arrays leverage compact geometries for seamless integration. A. Gupta et al. (2023) developed a 4×4 MIMO array using parasitic strips and a Defected Ground Structure (DGS) to achieve over 18 dB port isolation and 71% radiation efficiency at 3.5 GHz, making it ideal for smartphone bezels. Sharma et al. (2024) cataloged advancements in multiband operation techniques, emphasizing trade-offs between bandwidth (greater than 1.5 GHz), gain (4–8 dBi), and the physical constraints of modern handsets. Further miniaturization was demonstrated by T. Chen et al. (2024), using a rectangular patch with multiple slits and slots that resonated at 3.45, 5.2, and 5.9 GHz, with a 160 MHz bandwidth at the lower band, enabling multi-protocol support in compact devices.

In IoT applications, wideband antennas prioritize spectrum agility and gain stability. Ibrahim et al. (2024) designed an ultra-wideband elliptical resonator antenna covering 2.37–8 GHz (108.58% fractional bandwidth) using circular slot loading, achieving a peak gain of 7.91 dBi. Similarly, Kumar Dash et al. (2022) delivered an 863 MHz bandwidth (4.921–5.784 GHz), 6.21 dBi gain, and –8 dB back-lobe suppression—crucial in cluttered RF environments.

High-gain antenna arrays address 5G infrastructure needs. Martínez et al. (2024) engineered a 4×4 patch rectenna array that merges communication and energy harvesting at 3.5 GHz, producing 20.5 dBi gain and 4.2 V DC output. Though outside the sub-6 GHz range, S. Rahman et al. (2020) developed a Ku/K-band 2×2 array using U-slot patches to attain 7.15 dBi at 12 GHz and 8.2 dBi at 18 GHz, demonstrating the scalability of array techniques.

Bandwidth expansion is a central goal of many single-element designs. F. Khan et al. (2020) used an air-gap layered E-shaped patch to achieve 700 MHz bandwidth (3.3–4.0 GHz) while maintaining 7.1 dBi gain. Zhao et al. (2023a) introduced a theta-shaped slotted patch combined with DGS, resulting in 400 MHz bandwidth (3.3–3.7 GHz) and a front-to-back ratio exceeding 15 dB.

Emerging designs aim to future-proof antennas for the upcoming 5G bands. Tan et al. (2023) developed a parasitic-element-loaded patch covering both sub-6 GHz (3.5 GHz) and sub-7 GHz (6.5 GHz), delivering gains of 5.25 dBi and 6.85 dBi, respectively. This anticipates the expansion of 5G-Advanced and 6G spectrum.

For high-gain millimeter-wave antenna arrays operating at 60 GHz, A. Farahbakhsh et al. (2017) introduced a wideband design of power dividers, T-junctions, and transitions using Groove-Gap Waveguide (GGW) technology. The GGW method eliminates electrical contact between metal layers, reducing fabrication complexity and cost. Two

GGW-to-rectangular waveguide transitions were created, and the designed components accomplished a wide bandwidth with low power and phase imbalance. Testing and prototyping of a 64-way power divider with 256 radiating slots revealed good agreement with simulations. The outcomes showed sidelobe levels that matched simulations, over 32.5 dBi gain, and over 80% radiation efficiency spanning 57–67 GHz.

In order to improve antenna gain, Sahana (2024) developed and examined an inset-fed planar rectangular microstrip patch antenna array that incorporates a corporate-feed network. The array consists of 16 elements connected through quarter-wave transformers and T-junction power dividers, operating at a frequency of 2.4 GHz on an FR-4 substrate ($\varepsilon_r = 4.4$, loss tangent = 0.002). The utilization of multiple radiating patches enhanced the gain, directivity, and bandwidth. The proposed array demonstrated its suitability for wireless communication applications, achieving a gain of 9.284 dB, a directivity of 16.2 dBi, and a bandwidth of 0.361 GHz.

Ghimire et al. (2021) used a unique feed system based on binary T-junction splitters, frequency-independent phase shifters, and T-branches to propose a compact, wideband, high-gain six-slot Vivaldi antenna array. To preserve beam symmetry and produce highly directional patterns, the system uses three Vivaldi antennas on each arm, with the right arm being coupled via a phase shifter. Radiation performance and return loss were enhanced by optimized feeds and slots. With a front-to-back ratio of 23.23 dB and a realized gain of 14.12 dBi, the array is appropriate for position detection, sensing, and Ultra Wide Band (UWB). With produced findings that closely match predictions, its excellent directivity over the UWB band facilitates applications like ground penetration radar and through-wall microwave imaging.

A microstrip-fed patch antenna with T-slot and Pi-slot configurations, featuring a flawed ground structure, was presented by (Jabeen et al. 2023). The T-slot ground plane improved the radiation performance, gain, and bandwidth on an RT/Duroid 5880 substrate ($\varepsilon_r = 2.2$, thickness = 1.6 mm). To achieve ultra-wideband functionality from 7.15 to 10.925 GHz with an impedance bandwidth of 3.775 GHz (S11 = -10 dB), enhancements were made to a standard Pi-slotted patch antenna that operates at 9.74 GHz with a 19.7 dB return loss. The proposed design attained a peak gain of 6.99 dBi at 8.95 GHz, and the calculations were consistent with experimental results. Potential applications include radar, satellite communication, weather monitoring, and vehicle speed detection.

To overcome issues related to efficiency and bandwidth caused by surface wave effects in microstrip antennas, Venkatachalam et al. (2019) introduced a miniaturized planar antenna designed for UWB applications. The design employs multiple slots and a Defected Ground Structure (DGS) to minimize the effects of the ground plane. This compact antenna, which integrates the ground and radiator on a PCB, measures $17 \times 22 \times 1.588$ mm. By using an asymmetric strip and etched slots, the operational bandwidth was expanded to 2.9–11.4 GHz (with a 10 dB return loss) and demonstrated an average radiation

efficiency of 88.5%. The antenna is suitable for wideband applications since it produces an omnidirectional radiation pattern, has a gain of 2 dB, and maintains a VSWR between 1 and 2.

Employing a defective ground structure and slots within the patch, Mabaso et al. (2019) developed a microstrip antenna with triple-band functionality. Optimization and simulations were carried out in CST Microwave Studio before the antenna was prototyped for validation. The measured outcomes closely align with calculations at 1.2 GHz, 2.45 GHz, and 5.6372 GHz, where the design operates effectively. The performance analysis included various aspects such as reflection coefficient, gain, directivity, and radiation patterns in both E- and H-planes. The antenna's triple-band capabilities were verified by its maximum gain of 6.307 dB and directivity of 7.279 dBi. Applications including Wide Local Area Networks (WLANs), Industrial, Scientific, and Medical (ISM) bands, security systems, and wireless video transmission can all benefit from the suggested design.

A compact Ku-band microstrip patch antenna (MSPA) measuring 40 × 48 × 1.59 mm for satellite applications was introduced by Davuluri et al. (2021). It is powered through a 50 Ω coaxial probe. Constructed on an FR4 substrate, this antenna employs a defective ground structure (DGS) along with etched slots on the radiating component to achieve a broad operational bandwidth of 3.03 GHz (12.8–15.8 GHz). The simple circular patch enabled dual-frequency operation, further enhanced by incorporating both a square ring slot and a circular ring slot. Its unique performance in the Ku-band and compact size make it suitable for satellite as well as UWB wireless applications. Additionally, it exhibited a $VSWR < 2$ and an average gain of 3.6 dB.

Using the finite element method, Kaur et al. (2017) showcased an optimal design for a multiband slotted microstrip patch antenna aimed at wireless applications. To enhance gain, circular and rectangular slots were etched into the patch, leading to improved performance with every design iteration. The final design achieved gains of 1.07 dB, 2.53 dB, 5.94 dB, 6.2 dB, and 9.3 dB at frequencies of 2.81, 5.81, 7.81, 8.00, and 8.72 GHz, respectively, resonating at five distinct frequencies ranging from 2 to 9 GHz. For each resonance, the return loss was under -10 dB. The results showed strong consistency when validated experimentally with a VNA and simulated using HFSS V13. Applications including Worldwide Interoperability for Microwave Access (WiMAX), LTE, GSM, Code Division Multiple Access (CDMA), Bluetooth, WLANs, and femtocell systems can use the antenna.

For the 28 GHz band, Gaid et al. (2024) created a straightforward, low-profile rectangular microstrip patch antenna. Performance was increased by applying an inset feed for better impedance matching and adding a rectangular slit on the patch edge to reduce size, starting with a traditional rectangular patch. The antenna's compact dimensions were 8 × 8.489 × 0.508 mm^3 ($\approx 0.75\lambda \times 0.79\lambda \times 0.05\lambda$), and it was constructed on a Rogers RT/Duroid-5880 substrate (εr = 2.2, thickness = 0.508 mm, loss tangent = 0.0009). The

findings revealed an impedance bandwidth of 1.43 GHz (27.28–28.71 GHz), a maximum S11 of –45 dB, a radiation gain of 8 dBi, and an efficiency of roughly 99%. The antenna's suitability for millimeter-wave applications was confirmed by the high agreement between simulations conducted in HFSS and validated in CST.

In the context of 5G mobile communication, Khattak et al. (2019) proposed a dual-band circular microstrip patch antenna that features an elliptical slot. With bandwidths of 1.3 GHz and 1 GHz, the antenna resonates at 28 GHz and 45 GHz, with efficiencies of 85.6% and 95.3% at those frequencies, respectively. It offers a return loss of -40 dB and gain of 7.6 dB at 28 GHz and a return loss of -14 dB and gain of 7.21 dB at 45 GHz on a small Rogers RT5880 substrate ($6 \times 6 \times 0.578mm^3$, $\varepsilon_r = 2.2$, $tan\delta = 0.0013$). To achieve greater gain requirements, an array arrangement was used, resonating at 28, 34, and 45 GHz with a radiation efficiency of 98.75% and a maximum gain of 13.5 dB.

To get around the constrained bandwidth of conventional microstrip antennas, Pan et al. (2024) suggested a broadband patch antenna with a Y-shaped microstrip feeder. With slots added and dimensions adjusted for impedance matching, the design uses a strip-slot hybrid structure on a square patch. The antenna, when simulated in HFSS, maintained radiation properties comparable to traditional slot antennas while achieving a relative bandwidth of 22% (4.48–5.60 GHz) with a reflection coefficient below –10 dB. The maximum gain observed was 10.72 dB, illustrating the efficiency of the Y-shaped feed in enhancing bandwidth without decreasing radiation performance.

In the context of 5G connectivity, Kishore et al. (2022) introduced a microstrip line-fed patch antenna functioning at 30 GHz. Designed for the FR-2 band (28–33 GHz), this antenna was fabricated using a Rogers RT5880 substrate and optimized for reflection coefficient and gain. A C-slot with a dimension of 0.4 mm was integrated to boost directivity through a dipole effect, while a quarter-wave feed cut was employed for better impedance matching. The design achieved a gain of 8.45 dB, a reflection coefficient of -8 dB, a VSWR of 2.3, a bandwidth of 3.5 GHz, and a directivity of 5°. Its compact dimensions and dependable performance make it ideal for various applications in the 5G mobile, automotive, medical, and Internet of Things sectors within the mmWave range.

For L-band applications, O. Singh et al. (2025) developed an O-shaped slot microstrip patch antenna (MPA) that uses an Artificial Neural Network (ANN) to predict antenna bandwidth. Six patch dimensions were used to train a Feedforward Back Propagation Network (FFBP-ANN) with Levenberg–Marquardt training, and the output was fractional bandwidth. With an average error of 1.308%, the ANN demonstrated the ability to make accurate predictions. With an S11 of –26.44 dB at 1.68 GHz, the antenna, mounted on a 70 x 50 mm^2 ground plane, achieved a wideband fractional bandwidth of 35.89% (660 MHz) covering 1.51–2.17 GHz. The correctness and strong performance of the suggested ANN-aided antenna design were confirmed by the close match between the measured and simulated results.

To address the limitations of traditional microstrip patch antennas — restricted bandwidth and low gain — V. P. Patil (2024) introduced a circular patch design featuring an air substrate and asymmetrical U-shaped slots. The optimized design includes two U-slots that are strategically placed to achieve dual bandwidths of 0.8 GHz (4.6–5.4 GHz) and 0.3 GHz (3.1–3.4 GHz). Simulation outcomes reveal peak gains of 8.87 dBi at 3.6 GHz, 9.15 dBi at 5.2 GHz, and 6.8 dBi at 5.8 GHz, exceeding the performance of earlier U-slot circular patch designs. With its improved bandwidth, gain, and reliability, the antenna is ideally suited for modern high-speed wireless communication systems like Wi-Fi and 5G.

The design of a symmetrical T-junction power divider tailored for 2.45 GHz applications was described by A. Tiwari et al. (2024). To ensure equitable power distribution and improved wideband performance, the proposed structure employs a quarter-wave transformer, a stepped-impedance transformer, and mitered corners. Low reflection and superior transmission properties are achieved through thorough optimization of these components. The divider's effectiveness was validated through simulations in CST Microwave Studio, which showed a very low VSWR of 1.006. The findings demonstrate the T-junction power divider's ability to split power steadily and effectively, making it a good fit for incorporation into contemporary wireless communication systems that require reliable signal distribution.

A W-band T-junction power divider with a rectangular microcoaxial structure was presented by Huang et al. (2021). This 3D transmission line is appropriate for RF device applications due to its large bandwidth, low loss, and good integration. To show the design approach's scalability, a two-way power divider was initially created and subsequently expanded to a four-way configuration. A back-to-back configuration of two identical two-way dividers was constructed and measured to verify functionality. A W-band insertion loss of 0.11–1.18 dB was observed, which closely matched simulations and validated the divider's effectiveness and suitability for high-frequency applications.

A small Wilkinson Power Divider (WPD) with integrated bandpass characteristics and ultra-wideband harmonic reduction was proposed by Wang et al. (2017). To achieve three transmission zeros for wideband suppression, the design integrates a frequency-selective coupling structure into a traditional quarter-wavelength transmission line. Furthermore, both output ports have short-ended meander-line stubs connected, which provide DC blocking and an additional transmission zero in the passband. The WPD successfully suppresses DC, $3f_0$, $5f_0$, and $7f_0$ harmonics while achieving a –20 dB bandwidth of 1.74-3.71 GHz. With a small footprint of 14.65×19.64 mm^2 ($0.19\lambda g \times 0.25\lambda g$), the design is adequate and appropriate for contemporary radio frequency systems.

To increase bandwidth in a single-stage setup, Zhou (2023) proposed a miniature broadband Wilkinson power divider that uses microstrip branch lines in place of the many resistors used in multi-stage systems. Four microstrip branches in an upgraded

single-stage divider were created and assessed. The simulation results showed strong performance, with isolation above 15 dB, input and output return losses over 15 dB, and insertion loss better than 3.2 dB over a broad 76% bandwidth from 18 to 40 GHz. The design demonstrates a small and effective method for high-frequency broadband applications.

To improve the design of Wilkinson power dividers (WPDs), Jamshidi et al. (2021) presents a hybrid approach that focuses on performance enhancement, size reduction, and harmonic suppression. The technique substitutes two LC branches—each consisting of a series LC circuit, a miniaturizing inductor, and two transmission lines—for the traditional quarter-wavelength branches. Theoretically, this adjustment provides limitless harmonic suppression, high-frequency selectivity, and 100% downsizing. Compared to conventional designs, the proposed Filtering Power Divider (FPD) performs better in practice. Through LC circuit tuning, designers can modify the operating frequency, stopband bandwidth, and operating bandwidth while blocking arbitrary harmonics. The method's efficiency and potential to improve other microstrip components are confirmed by experimental results that corroborate the theoretical analysis and simulations.

The microstrip Wilkinson power divider (WPD) described by (Jamshidi et al. 2021) is intended to address the drawbacks of traditional WPDs, such as their size and subpar out-of-band performance. A lowpass filter is integrated into both branches of the proposed design to enhance isolation and suppress harmonics. The simulation and measurement results demonstrate excellent performance, featuring an input return loss ($|S_{11}|$) of under 34.2 dB, an output return loss ($|S_{22}|$) of less than 26.2 dB, an insertion loss ($|S_{21}|$) of 3.52 dB, and an isolation ($|S_{32}|$) exceeding 31.2 dB. From 2.54 GHz to 13.48 GHz, the WPD exhibits a broad 20 dB stopband, attenuating the second to seventh harmonics by more than 20 dB. Additionally, it is suitable for space-efficient designs due to its small footprint of 33.8 mm × 27 mm (0.42 λg × 0.33 λg at 1.8 GHz).

(Liu et al. 2025) presents a straightforward hybrid electric and magnetic coupling decoupling technique for planar square patch antenna arrays. The 2D coupling problem is simplified to 1D by utilizing the orthogonal TM_{10} and TM_{01} modes of a square patch to create a superposed mode with uniform field distribution by feed modification. In order to reduce mutual coupling and balance coupling strengths, metallic pins and connecting strips are introduced. Across the passband, isolation is improved from 4 dB to 17 dB using a 1×2 array spaced 1 mm apart ($\approx 0.0117\lambda_o$). The efficacy of the technique for small linear and planar antenna arrays is confirmed by validating its scalability using 1×3, 2×2, and 4×4 arrays.

A θ-shaped slotted patch antenna with a special defected ground structure (DGS) for sub-6 GHz 5G communication is presented by (Nafi et al. 2024). With a return loss of up to -30 dB, the antenna, which is mounted on a FR-4 substrate, operates in two bands at 4.19 GHz and 4.91 GHz with bandwidths of roughly 130 MHz and 890 MHz. The single-

band design is changed into a dual-band structure with better bandwidth and impedance matching by the modified DGS. Although efficiency and radiation pattern performance need more research, this small configuration shows promise for sub-6 GHz 5G systems.

A slotted patch antenna featuring parasitic strips is proposed by (Noor et al. 2023) for use in 5G applications at frequencies under 6 GHz and 7 GHz. The antenna operates in two frequency bands, approximately at 3.45 GHz and 5.9 GHz, utilizing an FR-4 substrate. It has bandwidths of 160 MHz and 220 MHz, along with gain values of 3.83 dBi and 0.58 dBi, correspondingly. Compared to a conventional patch antenna, the parasitic elements enhance both bandwidth and gain, offering a compact and cost-effective solution for 5G devices.

The design challenges faced by Multiple-Input Multiple-Output (MIMO) antennas for mobile phones in the context of 5G and future developments were explored by (Gao 2019). The author pointed out that a significant issue in compact MIMO configurations is maintaining high isolation between antenna elements that are closely arranged. The study examined several techniques for enhancing isolation that have emerged in recent years, such as the integration of parasitic elements, neutral lines, metamaterials, and electromagnetic band gap (EBG) structures. It was noted that while these methods can achieve isolation levels of up to 20 dB when antenna elements are spaced about half a wavelength apart, their effectiveness notably declines as the spacing between elements decreases. To overcome this constraint, Zhang proposed the Common-Mode/Differential-Mode (CM/DM) antenna design technique, which showed isolation levels surpassing 20 dB even when the antenna elements are in direct contact (zero spacing). The author concluded that the CM/DM approach holds great promise for developing compact, highly integrated MIMO antenna systems that are suitable for 5G and upcoming wireless technologies.

- **Isolation Techniques:** DGS and parasitic elements remain pivotal for MIMO systems, achieving over 15 dB isolation(A. Gupta et al. 2023; P. Kumar et al. 2024; Zhao et al. 2023a).
- **Bandwidth-Gain Tradeoffs :** Air gaps and slots effectively increase bandwidth, though often limiting peak gain to below 8 dBi(F. Khan et al. 2020; T. Chen et al. 2024).
- **Multi-Functionality:** Rectenna arrays represent a convergence of energy harvesting and wireless communication (Martínez et al. 2024).

2.1.10 Research Gap

In recent years, extensive research has been conducted on microstrip patch antennas and array configurations for 5G applications, particularly within the sub-6 GHz frequency

range. Although several designs have achieved notable improvements in parameters such as gain, bandwidth, and radiation efficiency, certain limitations persist in existing works. Most conventional 4×4 microstrip patch antenna arrays designed for the 3.5 GHz ($n78$) band tend to suffer from narrow impedance bandwidths, poor mutual coupling suppression, and increased surface wave propagation, all of which degrade radiation performance and reduce the array's suitability for broadband 5G communication systems. Furthermore, while high-frequency laminates such as Rogers RO4003C or FR-4 are commonly used, their performance either comes at high cost or results in undesirable dielectric losses at higher frequencies, making them less ideal for cost-effective and energy-efficient implementations.

Several previous studies have explored techniques such as slot loading and defected ground structures (DGS) to enhance antenna performance; however, most have focused on single-element configurations or small arrays (e.g., 1×2 or 2×2), which do not adequately address the challenges associated with large-scale array integration. In addition, few researchers have examined the **combined use of U-slots and DGS** in a 4×4 **array** configuration operating within the **sub-6 GHz 5G** $n78$ **band**, where achieving a balanced trade-off between bandwidth, gain, compactness, and mutual coupling remains a challenge. While some designs achieve high gain, they often do so at the expense of bandwidth or increased fabrication complexity, indicating a need for more efficient design strategies that improve impedance matching and radiation characteristics without excessive design overhead.

Moreover, many existing works rely solely on high-end materials or complex feeding networks, which increase cost and design difficulty. There is therefore a need to demonstrate that **affordable substrates such as Rogers RO4350B** can still achieve competitive performance when combined with effective structural modifications such as U-slots and DGS. In addition, a lack of comparative analysis between conventional arrays and modified structures (U-slot and DGS integrated) limits the understanding of how these modifications influence bandwidth enhancement and coupling reduction in array environments.

A persistent challenge in antenna design for 5G and Internet of Things (IoT) devices is achieving compact, miniaturized configurations without significantly compromising key performance metrics such as bandwidth, gain, and radiation efficiency. As modern wireless systems demand integration into increasingly smaller platforms—such as smartphones, wearables, and compact IoT nodes—traditional antenna designs often face trade-offs between physical size and electromagnetic performance. These limitations are especially pronounced in sub-6 GHz microstrip patch antennas (MPAs), which typically exhibit narrow bandwidths (< 500 MHz) and poor isolation when scaled down. While techniques such as multilayer stacking and electromagnetic bandgap (EBG) structures have been proposed to mitigate these effects, they introduce additional complexity and

fabrication cost. Therefore, a critical gap remains in developing antenna architectures that balance miniaturization with performance enhancement. This study addresses this gap by incorporating **Defected Ground Structures (DGS)** into a 4×4 MPA array to improve bandwidth and mutual coupling performance while maintaining a compact, fabrication-friendly design suitable for 5G sub-6 GHz applications.

While substantial research has focused on antenna array designs targeting millimeter-wave (mmWave) bands for 5G applications, there remains a relative scarcity of low-loss, wideband solutions in the sub-6 GHz spectrum that leverage premium yet cost-effective substrates such as Rogers RO4350B. Furthermore, the integration of compact DGS within multi-element arrays—such as 4×4 configurations optimized for the critical 3.5 GHz band—has not been extensively investigated. This gap is significant because sub-6 GHz frequencies offer superior coverage and penetration compared to mmWave frequencies, making them indispensable for real-world 5G deployments. The present project therefore focuses on addressing this gap by developing and simulating a 4×4 microstrip patch antenna array that utilizes advanced feeding techniques, U-slots, and ground-plane modifications to achieve enhanced bandwidth, gain, and reduced mutual coupling, explicitly tailored for sub-6 GHz 5G small-cell applications.

This research tackles the identified issues by designing and simulating a 4×4 microstrip patch antenna array utilizing a **RO4350B** substrate, featuring **U-slots** in the radiating elements and incorporating a **Defected Ground Structure (DGS)** beneath the feeding network. This setup is intended to boost bandwidth, minimize mutual coupling, and enhance overall gain performance within the **3.5 GHz** $n78$ **sub-6 GHz band**. The resulting **bandwidth of 180 MHz** and a **peak gain of 10.64 dB** highlight a notable advancement over traditional arrays, validating that the combination of U-slot and DGS offers an efficient, cost-effective, and performance-oriented solution for upcoming 5G antenna systems.

Chapter THREE

METHODOLOGY

3.1 Introduction to Methodology

The chapter details the methodology used for optimizing, simulating, and designing a 4x4 microstripline-patched antenna array. This array features a defective ground structure (DGS) and a U-slot on each patch. The main objective of this methodology is to develop an antenna functioning effectively in the frequency range of 3.3 to 3.8 GHz, essential for 5G applications, particularly at the mid-range frequency of 3.5 GHz. We used a simulation-based approach that simplified the analysis and optimization of the antenna before fabrication. Our methodology relies heavily on computer-aided design, particularly using ANSYS HFSS for electromagnetic simulation, parametric optimization, and fine-tuning of the array.

The sections below offer a detailed description of the research design, which includes the theoretical design process, substrate selection, array arrangements, integration of slots and DGS, simulation setup, optimization process, and performance evaluation.

3.2 Research Design

3.2.1 Overview

This research employs a quantitative, experimental research design to investigate the performance of a patch antenna array. The study will follow a systematic process involving theoretical calculations, computer-aided design (CAD), electromagnetic (EM) simulation, and physical prototyping to validate the results. The core objective is to iteratively optimize the antenna specifications to meet the target performance criteria, including gain, bandwidth, and return loss, for 5G wireless communication.

3.2.2 Design and Analysis Methods

The Methodology is a step-by-step technical process that combines design, analysis, and optimization. It begins with a single radiating element and progressively builds up to the entire array.

1. **Single Patch Element Design**
   The core radiating component utilized in this design is a **rectangular microstrip patch antenna**. This selection is motivated by its slim profile, ease of integration, and economical fabrication. The initial dimensions (length and width) were determined using established equations from the **transmission-line model**, targeting a

resonant frequency of **3.5 GHz**. The chosen substrate material is **Rogers 4350B**, which possesses a relative permittivity (ϵ_r) of **3.48** and a thickness (h) of **1.6 mm**. The dimension calculations for the patch were performed as follows:

(a) **Width (W) Calculation**
The patch width is computed to control the resonant frequency.

$$W = \frac{c}{2f_r}\sqrt{\frac{2}{\varepsilon_r + 1}} \tag{3.1}$$

$$W = \frac{3 \times 10^8 \text{ m/s}}{2 \times (3.5 \times 10^9 \text{ Hz})}\sqrt{\frac{2}{3.48 + 1}}$$

$$W = (0.04286 \text{ m})\sqrt{0.4464}$$

$$W = (0.04286 \text{ m})(0.6681)$$

$$W \approx 0.0286 \text{ m} \approx 28.6 \text{ mm}$$

(b) **Effective Dielectric Constant (ε_{re}) Calculation**
It takes into consideration the fringing fields present at the borders of the patch.

$$\varepsilon_{re} = \frac{\varepsilon_r - 1}{2} \times \left[1 + 12\frac{h}{W}\right]^{-0.5} + \frac{\varepsilon_r + 1}{2} \tag{3.2}$$

$$\varepsilon_{re} = \frac{3.48 + 1}{2} + \frac{3.48 - 1}{2}\left[1 + 12\frac{1.6 \text{ mm}}{28.6 \text{ mm}}\right]^{-0.5}$$

$$\varepsilon_{re} = 2.24 + 1.24\left[1 + 12(0.0559)\right]^{-0.5}$$

$$\varepsilon_{re} = 2.24 + 1.24\left[1.6708\right]^{-0.5}$$

$$\varepsilon_{re} = 2.24 + 1.24 \times 0.7735$$

$$\varepsilon_{re} \approx 3.208$$

(c) **Length Extension (ΔL) Calculation**
It accounts for the increase in electrical length due to fringing.

$$\Delta L = \frac{(\varepsilon_{re} + 0.3)(\frac{W}{h} + 0.264)}{(\frac{W}{h} + 0.8)(\varepsilon_{re} - 0.258)} \times 0.412h \tag{3.3}$$

$$\Delta L = 0.412(1.6 \text{ mm})\frac{(3.208 + 0.3)(\frac{28.6}{1.6} + 0.264)}{(3.208 - 0.258)(\frac{28.6}{1.6} + 0.8)}$$

$$\Delta L = 0.6592 \text{ mm}\frac{(3.508)(18.139)}{(2.95)(18.675)}$$

$$\Delta L = 0.6592 \text{ mm} \frac{63.635}{55.08}$$

$$\Delta L = 0.6592 \text{ mm} \times 1.155$$

$$\Delta L \approx 0.7617\text{mm}$$

(d) **Length (L) Calculation**

The true length of the patch is calculated by taking the effective length and subtracting the length extension from it.

$$L = \frac{c}{2f_r\sqrt{\varepsilon_{re}}} - 2\Delta L \tag{3.4}$$

$$L = \frac{3 \times 10^8 \text{ m/s}}{2 \times (3.5 \times 10^9 \text{ Hz})\sqrt{3.208}} - 2(0.7617 \text{ mm})$$

$$L = \frac{0.04286 \text{ m}}{1.791} - 1.5234 \text{ mm}$$

$$L = 0.02393 \text{ m} - 1.5234 \text{ mm}$$

$$L \approx 23.93 \text{ mm} - 1.5234 \text{ mm}$$

$$L \approx 22.4 \text{ mm}$$

(e) **Single Patch Dimensions and Layout**

The dimensions of the single patch antenna have been calculated and are summarized in Table 3.1, as visually depicted below. The antenna features a width of **28.6 mm** and a length of **22.4 mm**, and is constructed on a **Rogers 4350B** substrate with a thickness of **1.6 mm**. The feed line is centrally located and optimized for a 50Ω impedance to facilitate efficient power transfer.

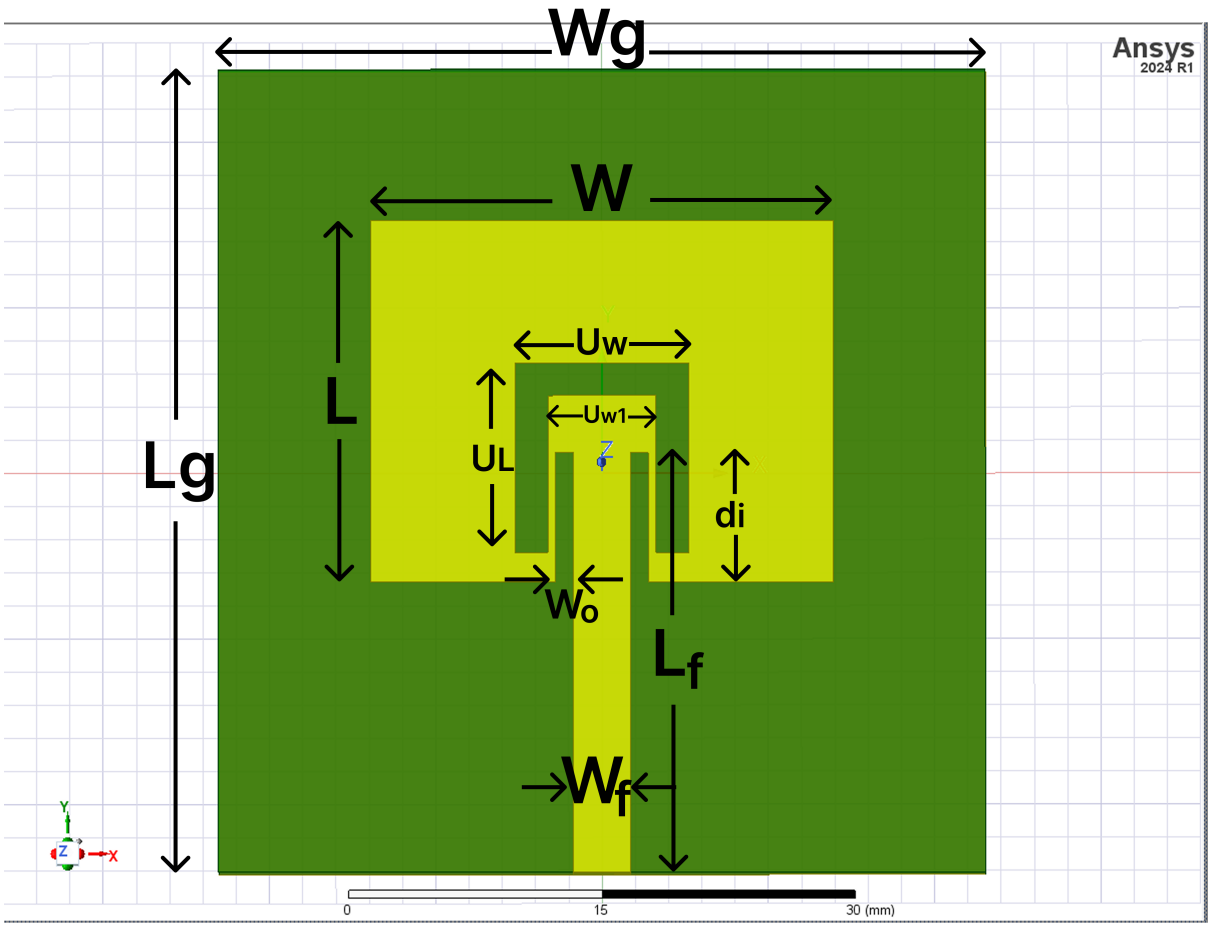

Figure 3.1: Single Patch Layout

Table 3.1: Overview of the performance metrics for the simulated antenna.

Parameter	Simulated Value
W_g	47.335 mm
L_g	41.32 mm
W	27.82 mm
L	21.81 mm
U_W	6.5 mm
U_L	9.48 mm
U_{w1}	41.32 mm
d_i	6.72 mm
W_o	1.05 mm
W_f	3.46 mm
L_f	14.23 mm

(f)

2. **Optimization and Enhancement of Performance**
   In order to enhance the performance of the single patch antenna beyond its inherent properties, two strategic alterations were introduced: a **U-slot on the radiating patch** and a **Defected Ground Structure (DGS)**. These features are not merely additions; they are meticulously designed to manipulate the antenna's current distribution and electromagnetic fields, thereby creating new resonant modes that operate in conjunction with the fundamental mode. This multi-resonance phenomenon is crucial for achieving a wider operational bandwidth.

   (a) **U-Slot Design and Analysis**
   The U-shaped groove, engraved on the surface of the rectangular patch, serves as a parasitic component.The antenna's input impedance and resonant frequency are directly affected by its dimensions, particularly its length, width, and placement. By introducing the U-slot, an additional resonant path is created, which can be tuned to a frequency slightly offset from the main patch resonance. The goal is for these two resonant frequencies to merge into a single, broader-band response.Enhancing the U-slot is an essential process that entails adjusting its physical characteristics—such as the length, width, and its placement in relation to the feed point—to attain maximize impedance matching and frequency range.

   (b) **Design and Analysis of Defected Ground Structure (DGS)**
   A Defected Ground Structure (DGS) is characterized by a pattern that is either periodically or non-periodically etched into the ground plane of a microstrip antenna. Unlike modifications to the radiating element, such as the U-slot, the DGS alters the flow of charges within the substrate.This modification enhances the effective transmission line length, aids in minimizing surface interference, and reduces coupling effects among array elements. Additionally, the DGS creates a stopband that filters out unwanted frequencies and enhances the antenna's gain within the specified frequency range.
   The geometry of the DGS, including its shape, size, and spacing, must be optimized to achieve the intended effects on antenna performance. The final DGS design is developed through several simulation iterations to strike a balance between improved performance and added complexity.

   (c) **Simulation-Based Optimization**
   Optimization of both the U-slot and the DGS is performed iteratively using Ansys HFSS. The process begins with calculating the initial dimensions for both features, followed by a parametric analysis in which their dimensions are varied within a defined range. The assessment of each iteration's effectiveness relies on important metrics, which consist of:

- **Return Loss (S_{11}):** The aim is to achieve a return loss below **-10 dB** across the target bandwidth, indicating that less than 10% of the incident power is reflected.
- **Voltage Standing Wave Ratio (VSWR):** An optimal VSWR close to 1:1, or typically below 2:1, is targeted within the operational band.
- **Antenna Gain and Radiation Characteristics:** The effects on gain and the radiation characteristics are regularly assessed to make certain that the changes do not negatively impact the antenna's directivity.

The optimization process concludes when the design achieves the maximum possible bandwidth while maintaining optimal return loss and gain. The final optimized single patch, featuring both a U-slot and a DGS, acts as the essential foundational component for the antenna array.

3. **Array Configuration and Feed Network**
After the single patch element was fully optimized, the design process transitioned to systematically and progressively building the complete antenna array. This approach involved an iterative design process, starting with scaling the design to a **2x2 array** before advancing to the final **4x4 configuration**.

   (a) **Element Spacing and Array Layout**
   The construction began with a **2x2 planar antenna array**, where the optimized single-patch elements were arranged in a grid. This intermediate step allowed for the characterization of fundamental array properties, such as **mutual coupling** between adjacent elements, prior to the full-scale assembly. A key design parameter, the inter-element spacing, denoted as dx and dy for the x and y directions, was carefully optimized to be slightly less than a half-wavelength ($\lambda/2$). This spacing is essential for controlling the array's radiation pattern and for suppressing unwanted **grating lobes**, which can occur when the element spacing is too large. Additionally, the spacing was optimized to minimize mutual coupling, the electromagnetic interaction between adjacent elements that can degrade the array's performance. Following the successful validation of the 2x2 array, a **4x4 planar antenna array** was constructed by arranging four of the previously optimized 2x2 array modules into a larger grid.

   (b) **Corporate Feed Network Design**
   A **corporate feed network** was implemented to distribute RF power from a single input port to all individual antenna elements. This network type was chosen for its capability to provide a consistent and equal amplitude and phase distribution across each element, which is vital for achieving a well-

defined main beam. The network comprises a series of power splitters (such as T-junctions or Wilkinson dividers) and microstrip transmission lines. Each section of the transmission line and each power splitter was meticulously designed and matched to the appropriate impedance to reduce reflections and power losses. Additionally, the lengths of the transmission lines were optimized to ensure that the signal reached each patch element with the correct phase, a requirement for a high-performance array.

(c) **Final Simulation and Analysis**
Once the complete **4x4 array**, incorporating both the optimized elements and the corporate feed network, was designed, it underwent a final round of **full-wave electromagnetic simulations** using Ansys HFSS. This crucial step allowed for a comprehensive analysis of the array's performance. Key metrics evaluated included the overall **return loss (S_{11})** of the array, the **radiation pattern**, the **directivity**, and the overall **gain**. The simulation also confirmed that the inter-element spacing was optimal for minimizing mutual coupling and that the feed network was properly matched and balanced.

(d) **Simulation Tools and Environment**
All design, analysis, and optimization procedures were performed using **Ansys HFSS**. This software was selected for its powerful **3D full-wave electromagnetic (EM) solver**, essential for accurately modeling the complex geometries of the patch antenna and its modifications (U-slot and DGS), as well as for simulating intricate interactions within the array, such as **mutual coupling**. The solver's capability to handle high-frequency behavior ensures accurate forecasts regarding the antenna's performance.

Essential Performance Indicators
During the modeling phase, the antenna's efficacy was evaluated using various crucial indicators to verify that the design aligned with the project's goals. These indicators were examined at each design phase, from the individual element to the complete array, and include:

- **Return Loss (S_{11}):** This metric quantifies the energy reflected from the antenna's input terminal. A slight return loss (generally less than -10 dB) indicates effective energy transmission from the source to the antenna, helping reduce signal reflections.
- **Voltage Standing Wave Ratio (VSWR):** VSWR assesses the resistance difference pertaining to the antenna and the transmission line. An optimal VSWR ratio is around 1:1, signifying a flawless match, while a ratio of 2:1 or less is typically considered satisfactory for most applications.
- **Radiation Pattern:** This visual depiction of the antenna's emission

traits illustrates how energy is spread throughout space, highlighting the main beam, side lobes, and rear lobes. Grasping this configuration is vital for evaluating the antenna's directionality and its capability to concentrate energy in a particular direction.

- **Gain:** Gain evaluates the antenna's capacity to focus or direct energy towards a particular direction in relation to an isotropic source. It is directly connected to the radiation pattern and acts as a crucial measure of the antenna's effectiveness and performance.
- **Axial Ratio:** For circularly polarized antennas, the Axial Ratio represents the proportion of the major axis to the minor axis of the polarization ellipse. An axial ratio close to 1 dB (or 0 dB) denotes ideal circular polarization, which is essential for uses like satellite communications.

The consistent use of Ansys HFSS and the rigorous analysis of these metrics ensured that the design was systematically optimized and validated before proceeding to physical prototyping.

(e) **Ethical Considerations and Limitations**

This research is fundamentally technical, concentrating on the design and efficiency of an antenna array without involving human subjects, animal testing, or the collection of sensitive data. Therefore, the ethical considerations are limited to ensuring academic integrity and proper citation of all referenced works. The primary limitations of this study arise from the practical constraints of the design and fabrication process.

- **Simulation Model Inaccuracies:** Although the Ansys HFSS simulator provides a powerful and highly accurate tool for predicting antenna performance, its results are based on a perfect model, which may not always reflect real-world conditions.

These limitations highlight the difference between a theoretical, idealized model and a tangible, real-world prototype. Despite these constraints, the systematic Methodology employed ensures that the results provide a strong and reliable foundation for the conclusions drawn.

3.3 Design Methodology

3.3.1 Flowchart of Methodology

The overall design and simulation procedure adopted in this work is illustrated in the flowchart shown in figure 3.2.

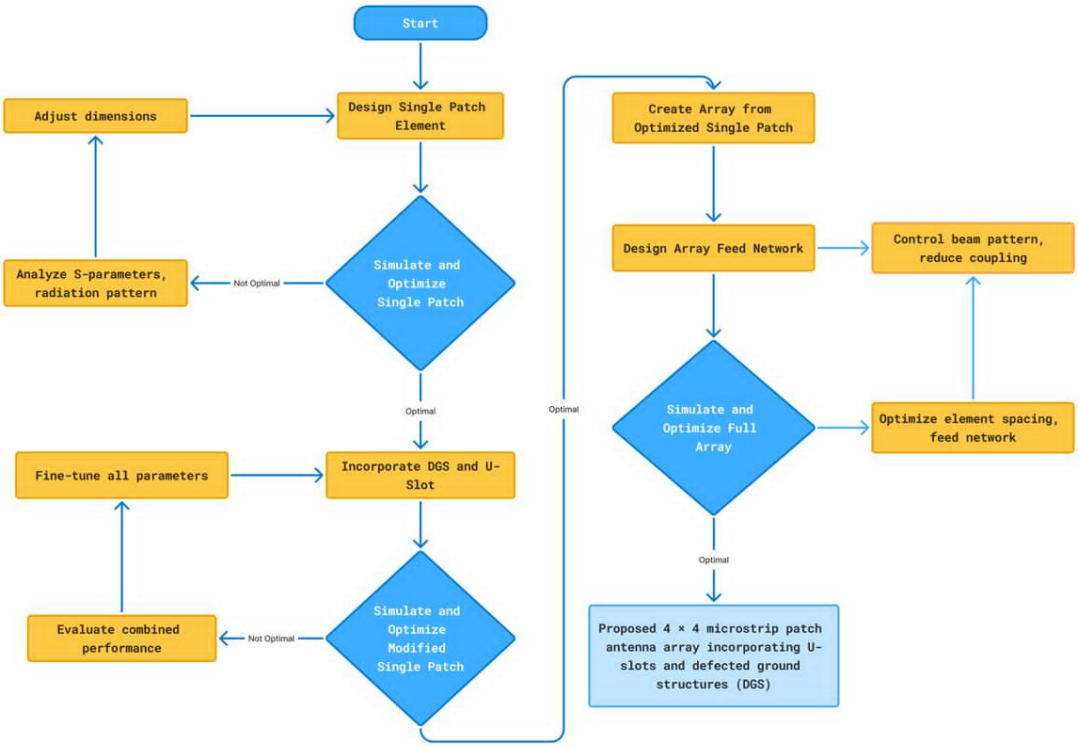

Figure 3.2: Flow Chart of Methodology

3.3.2 Single Patch Antenna Design and Optimization

This phase details the initial setup and construction of the single radiating element in Ansys HFSS.

1. **Project Setup and Parameter Definition**

   (a) Open Ansys Electronics and select the HFSS module as shown in figures 3.3 and 3.4 respectively.

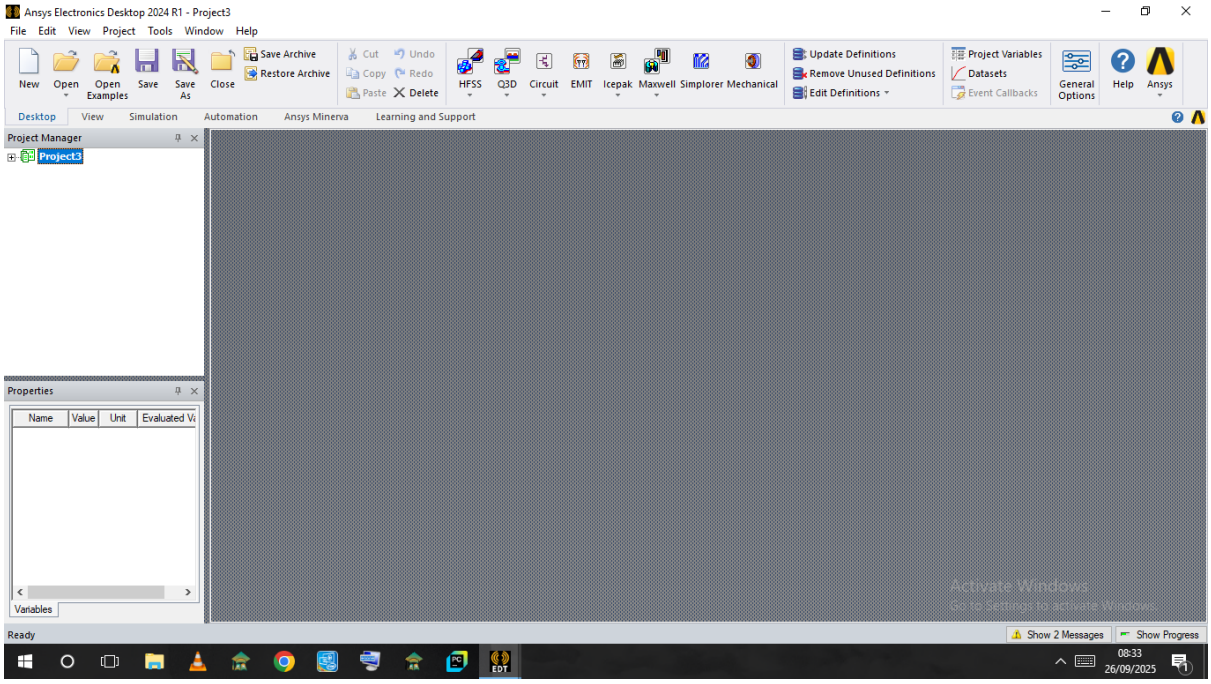

Figure 3.3: Open Ansys

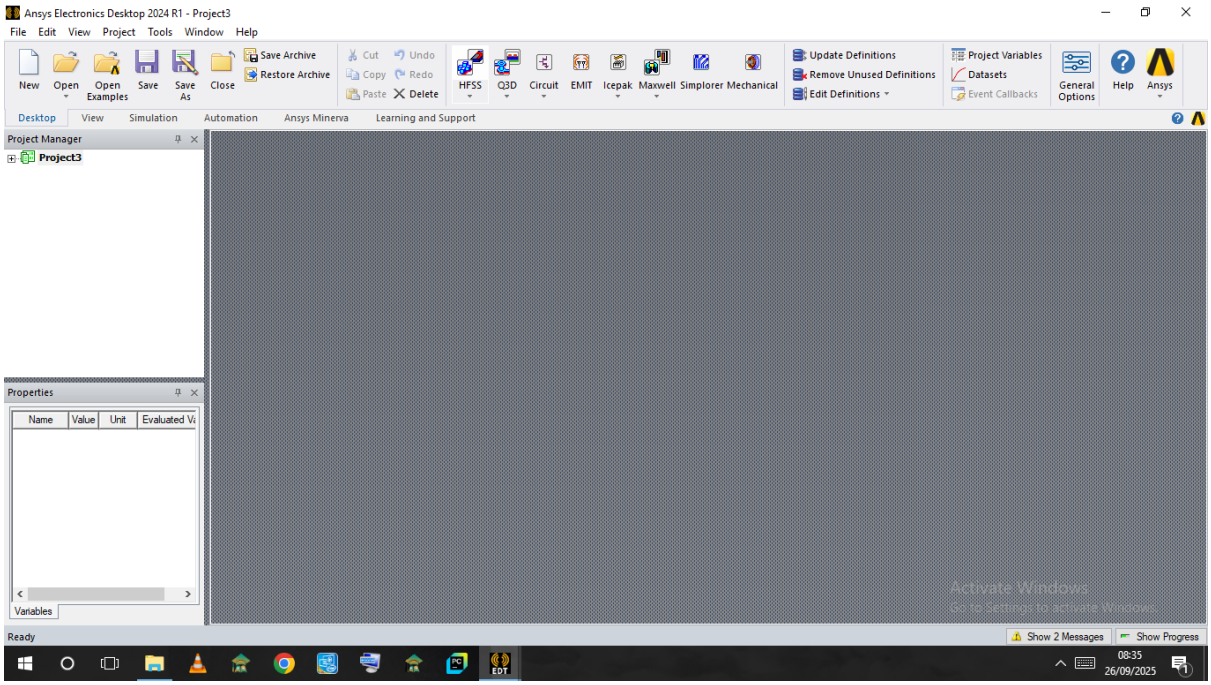

Figure 3.4: Select the HFSS module

(b) In the menu bar, navigate to **HFSS** → **Design Properties** → **Add** to define design variables as shown in figure 3.5.

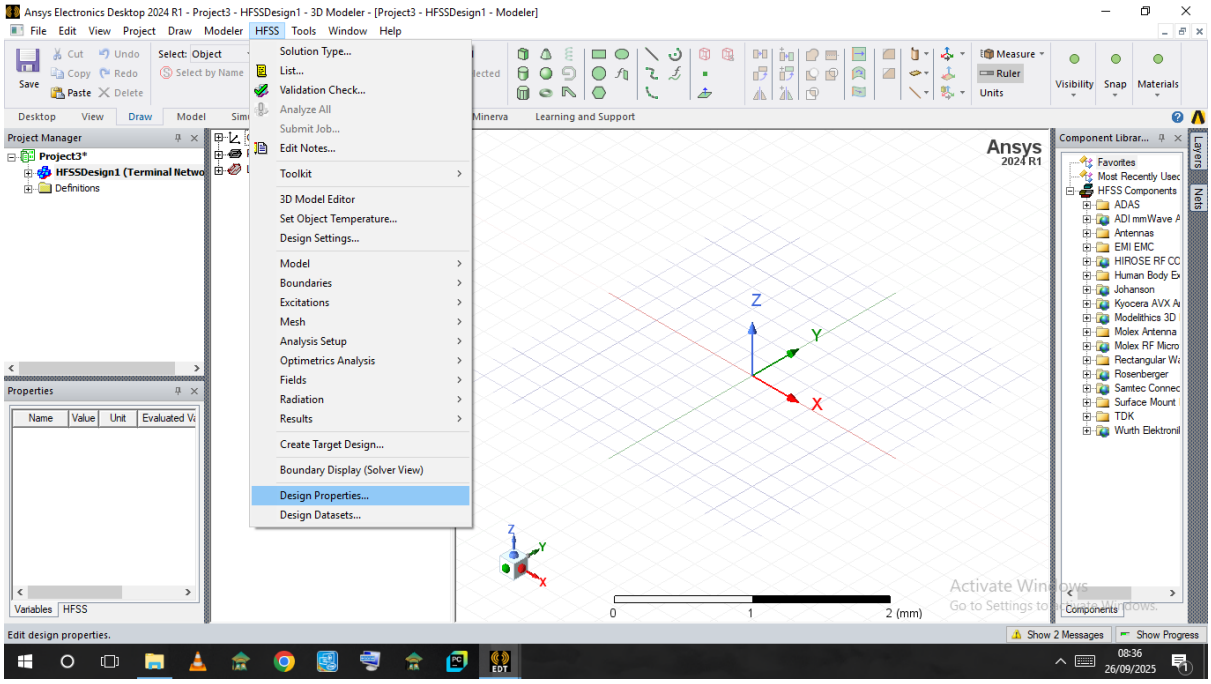

Figure 3.5: Navigate to Design Properties

(c) Add all necessary parameters: *L, Lf, Lg, slit 4Y, substrate_height, e.t.c.* as shown in figure 3.6 to 3.8.

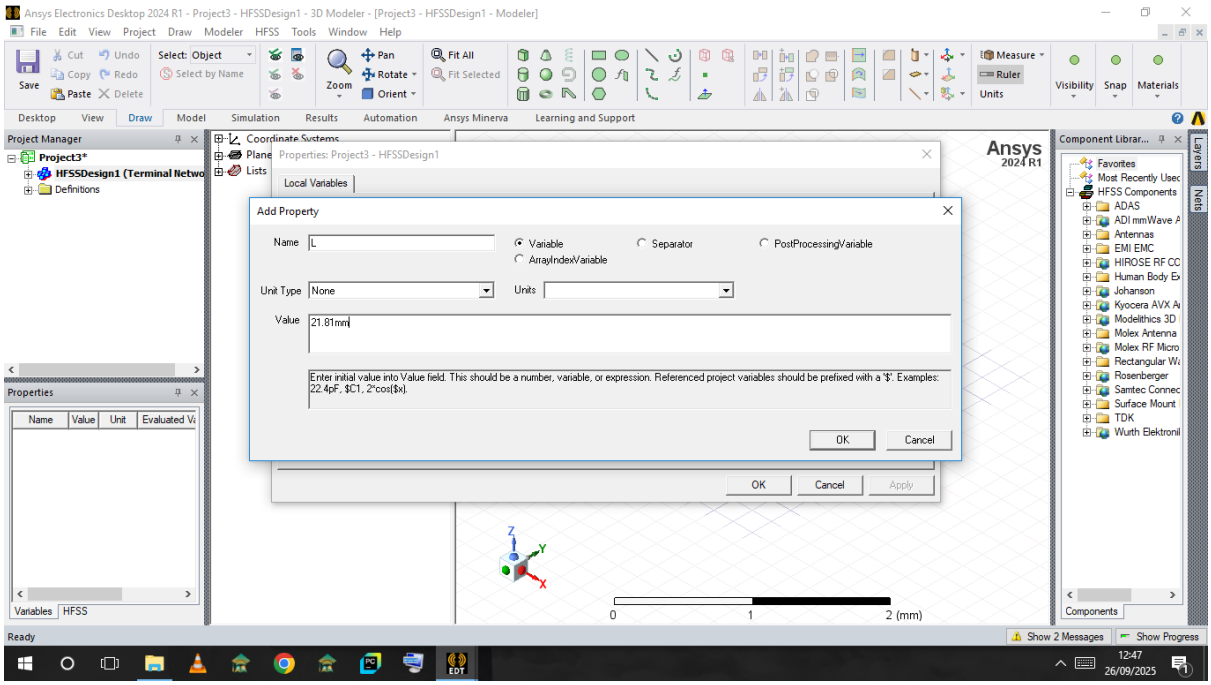

Figure 3.6: Add Variables

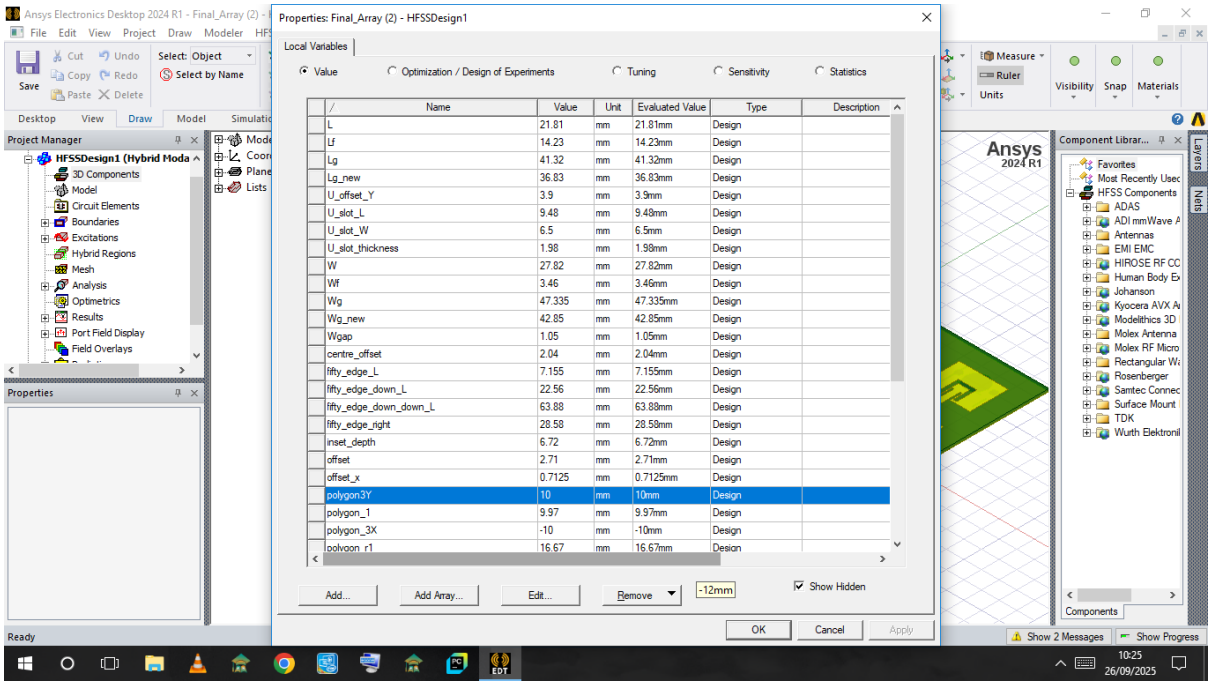

Figure 3.7: A list of all necessary parameters

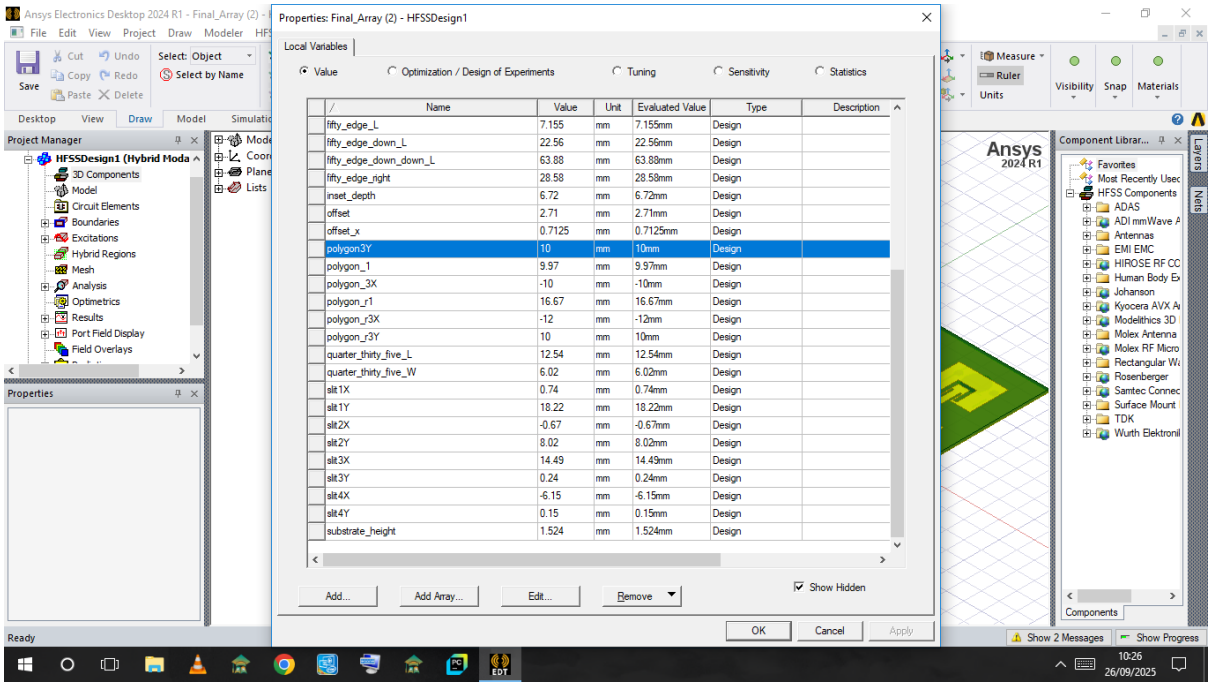

Figure 3.8: A list of all necessary parameters

(d) Click **OK**.

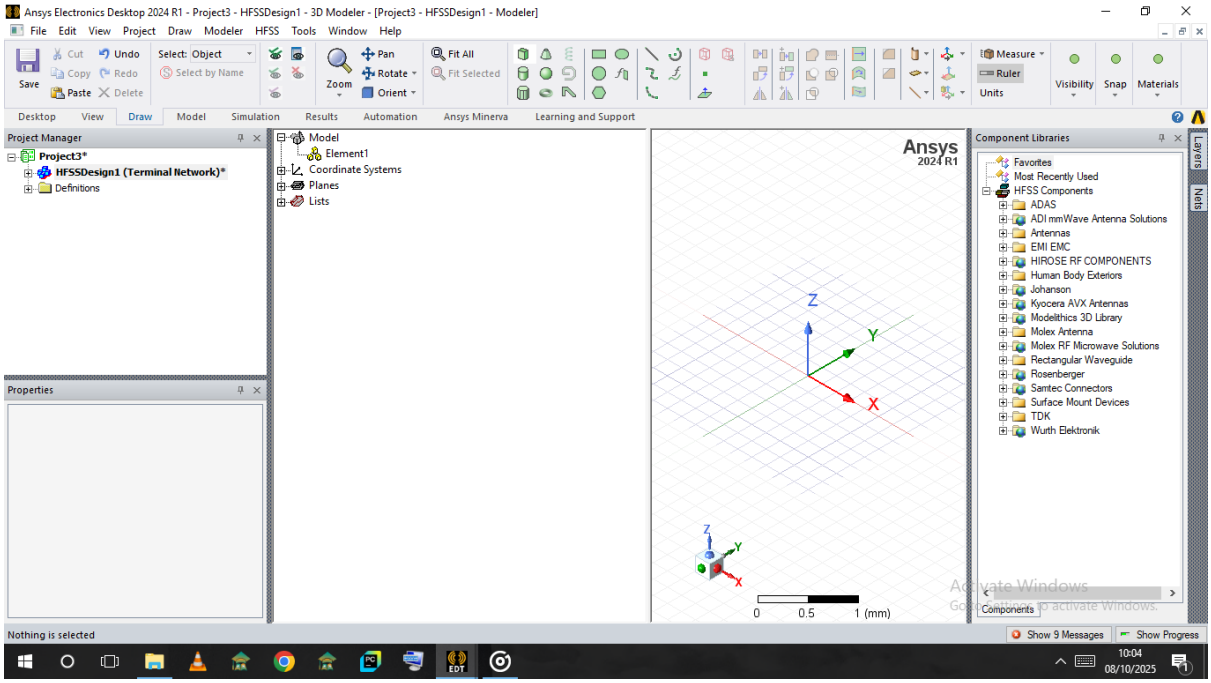

Figure 3.9: Parameters have been added successfully

2. Substrate and Ground Plane Creation

(a) Click the **Draw Box** icon (cube) on the Draw menu and create a cuboid in the modeler space as shown in figure 3.10 and 3.11.

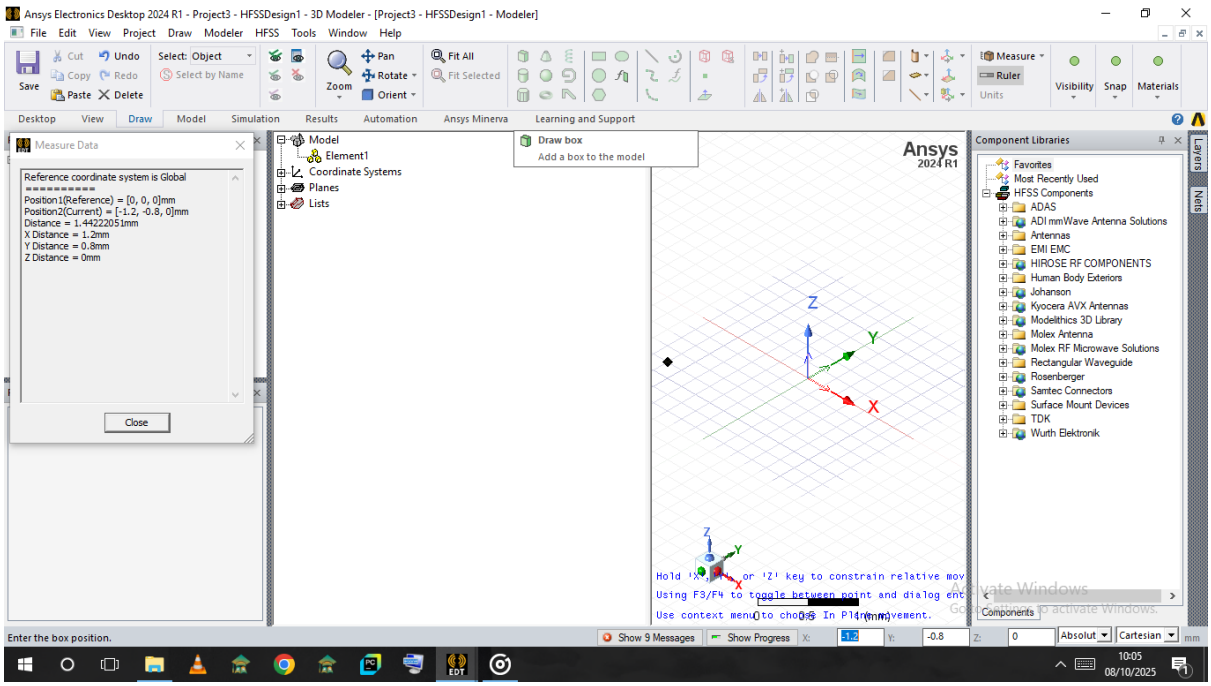

Figure 3.10: Click on the Draw box icon

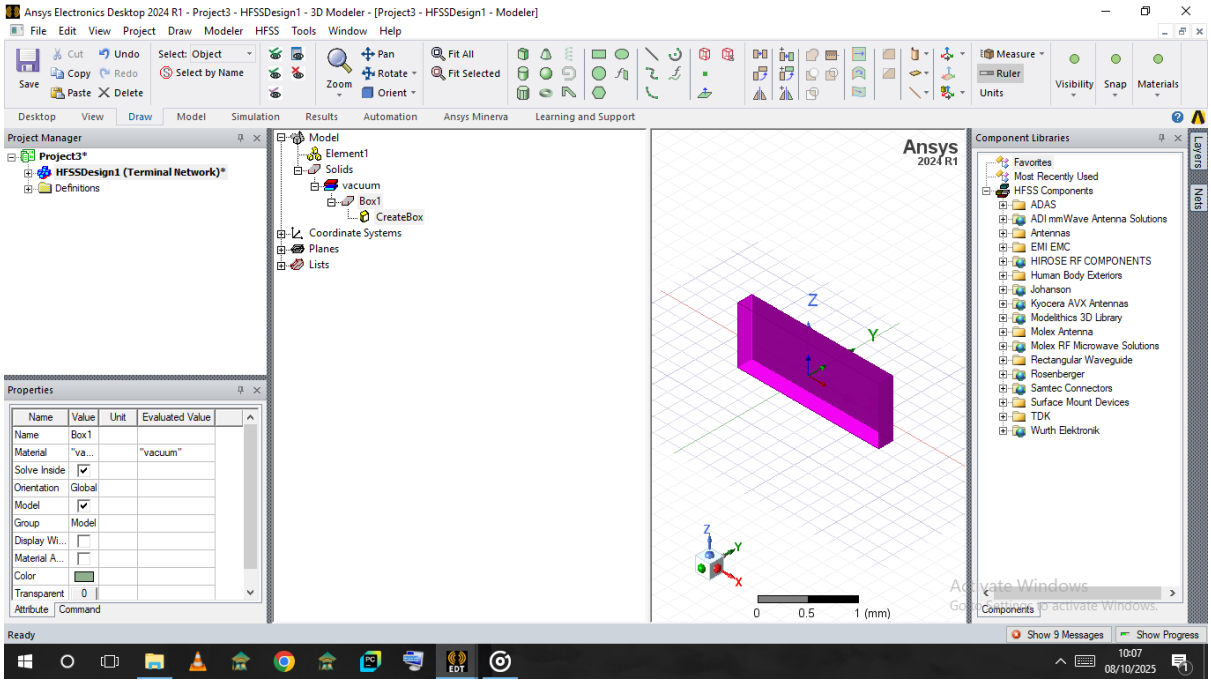

Figure 3.11: Create a cuboid in the modeler space

(b) In the Modeler Tree, select `createBox` and set the dimensions according to your defined parameters as shown in figure 3.12 and 3.13.

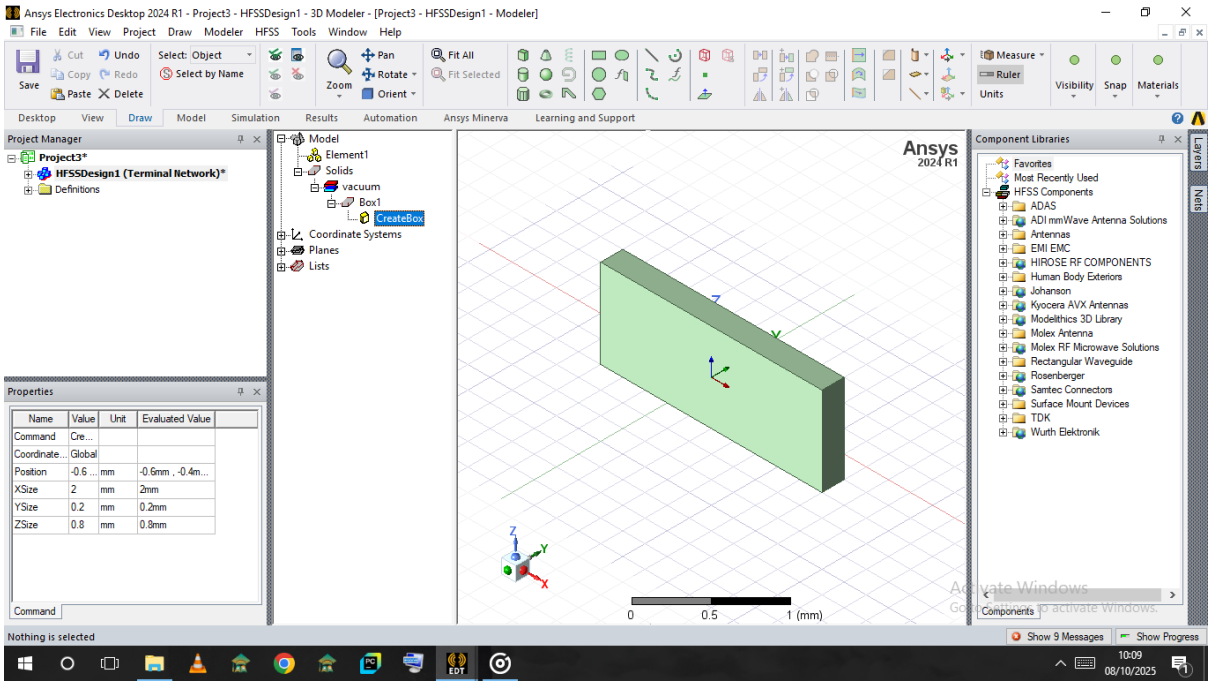

Figure 3.12: Select CreateBox

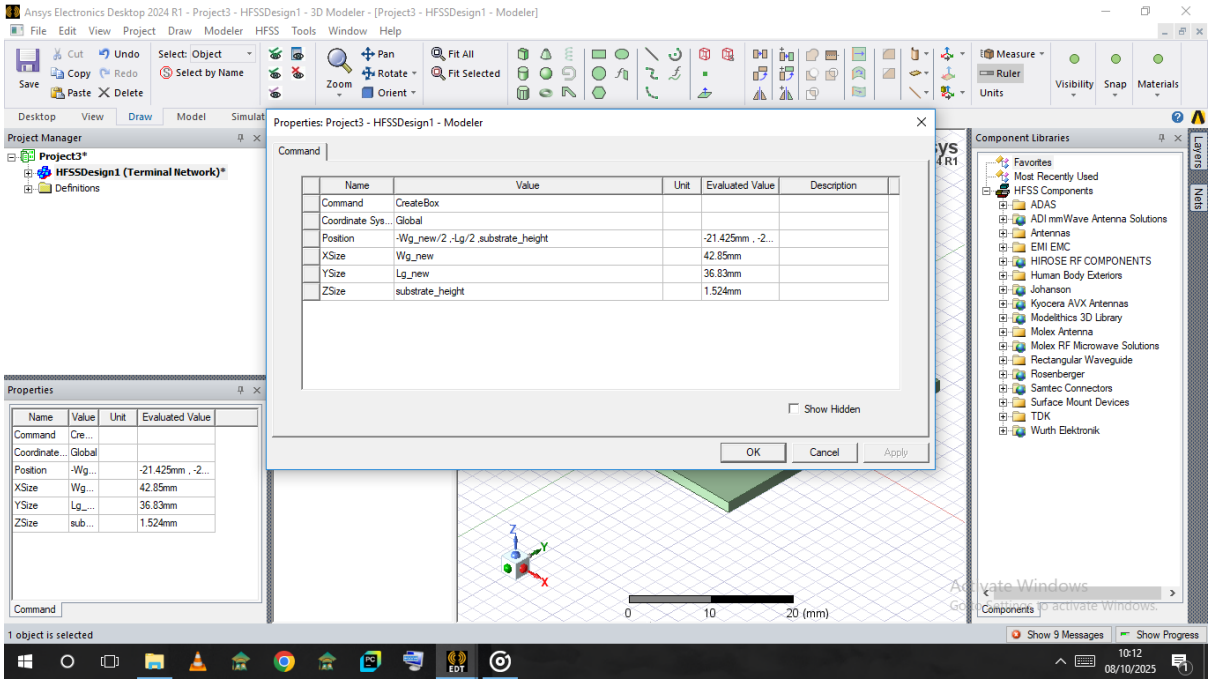

Figure 3.13: Set the dimensions according to your defined parameters

(c) Rename the object to **substrate**. In the Properties window, assign the material to **RO4350B** and set transparency and color as shown in figure 3.14 and 3.15 respectively.

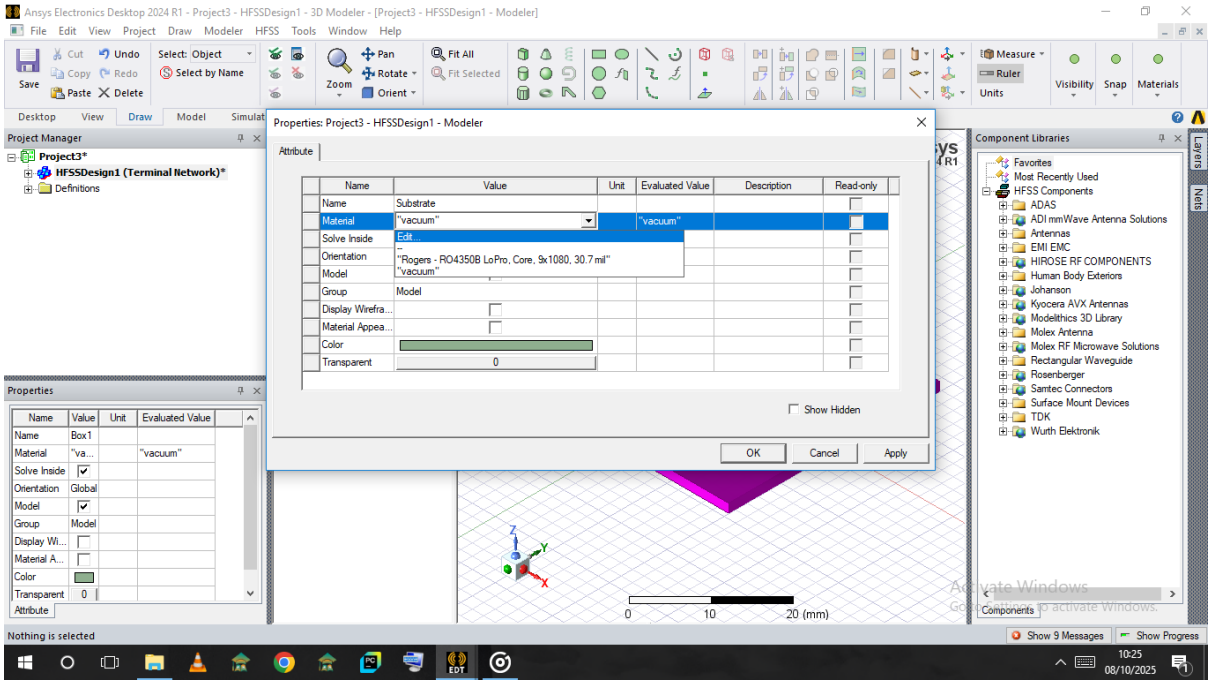

Figure 3.14: Rename the object to substrate

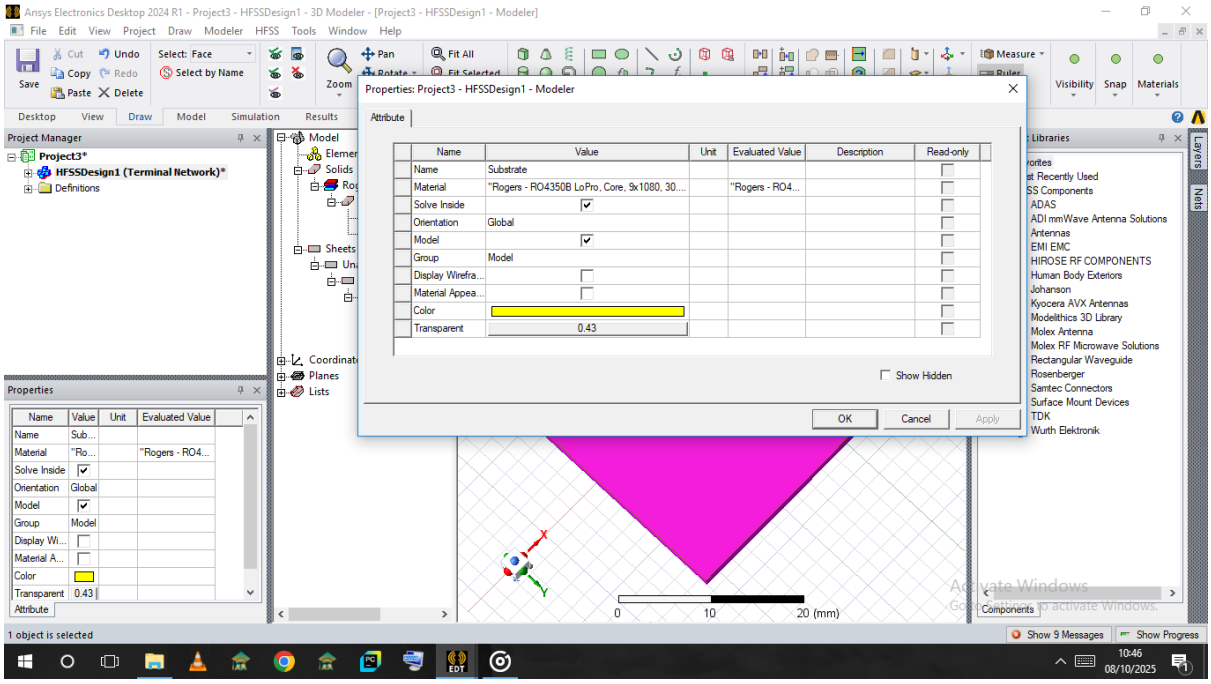

Figure 3.15: Assign the material to **RO4350B** and choose a desired transparency and color

(d) Create a ground plane by drawing a rectangle with the same width and length as the substrate's Surface. Rename it **GND**.

(e) Right-click on the selected face and go to **Edit** → **Surface** → **Create Object from Face**.

(f) Rename the new object to **GND** as shown in figure 3.16.

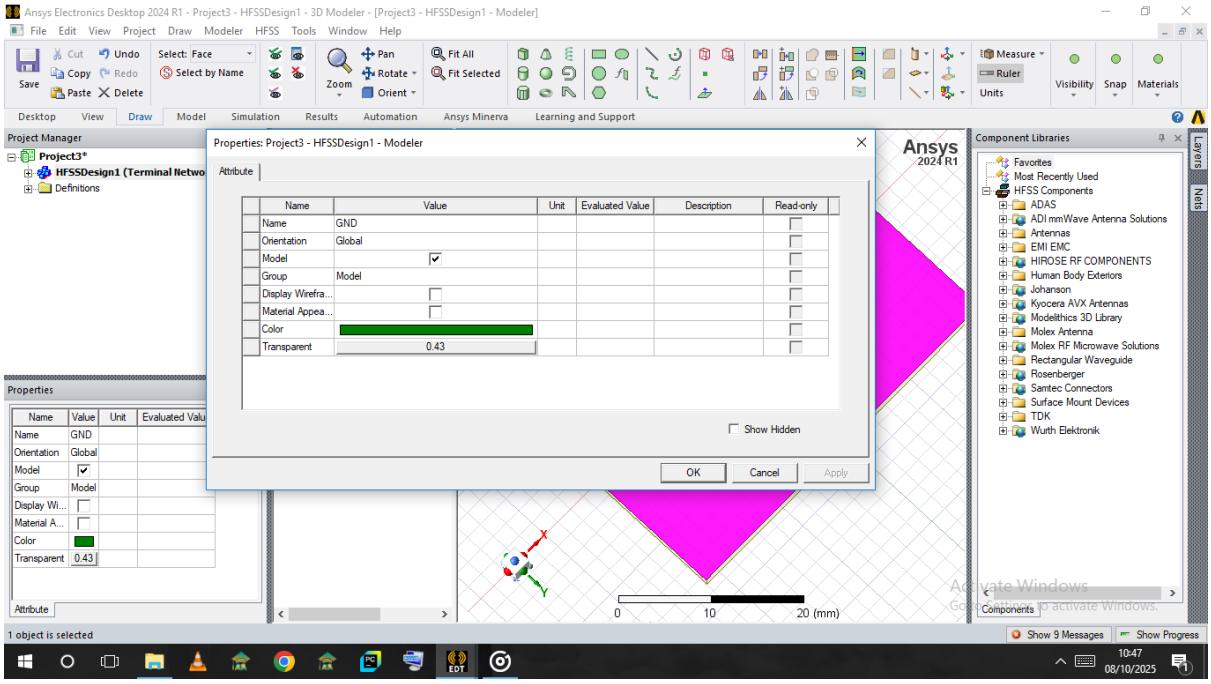

Figure 3.16: Create a ground plane and rename it GND

3. Patch, Feedline, and Port Creation

(a) Draw a rectangle on top of the substrate to create the patch. Set the dimensions in the `createRectangle` properties as shown in figure 3.17.

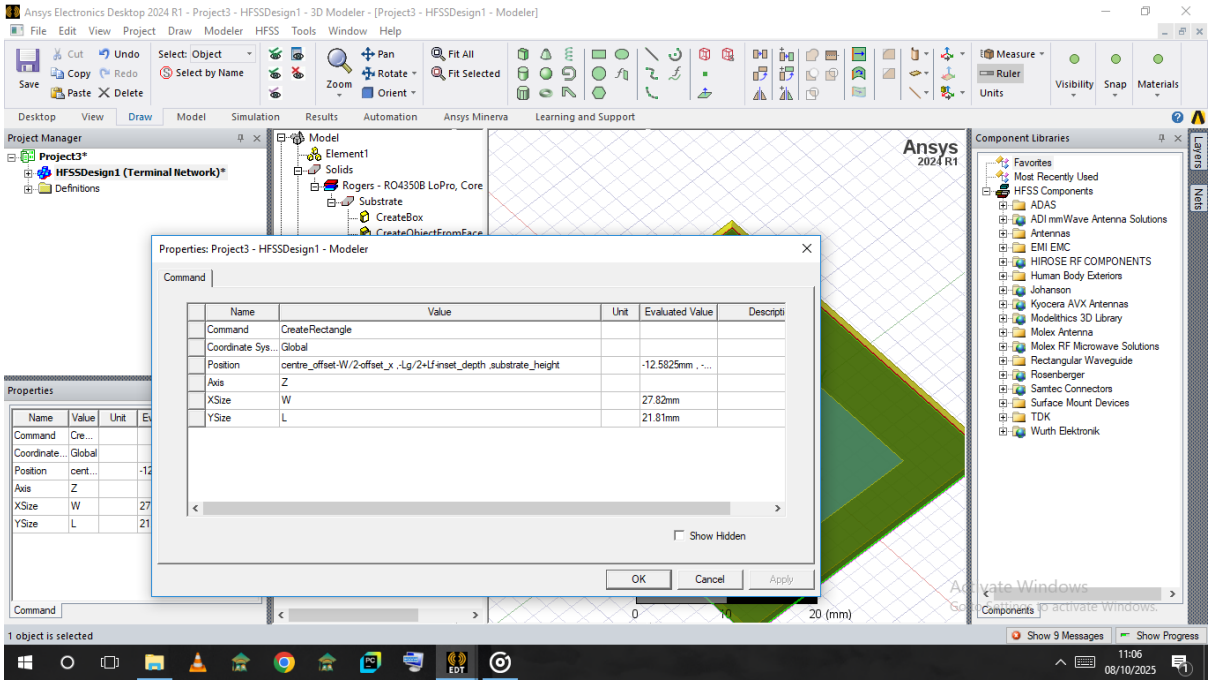

Figure 3.17: Create the patch and set its dimensions

(b) Rename the rectangle to **patch**.

(c) Draw another rectangle for the feed line, set its parameters, and name it **feed** as shown in figure 3.18 to 3.20.

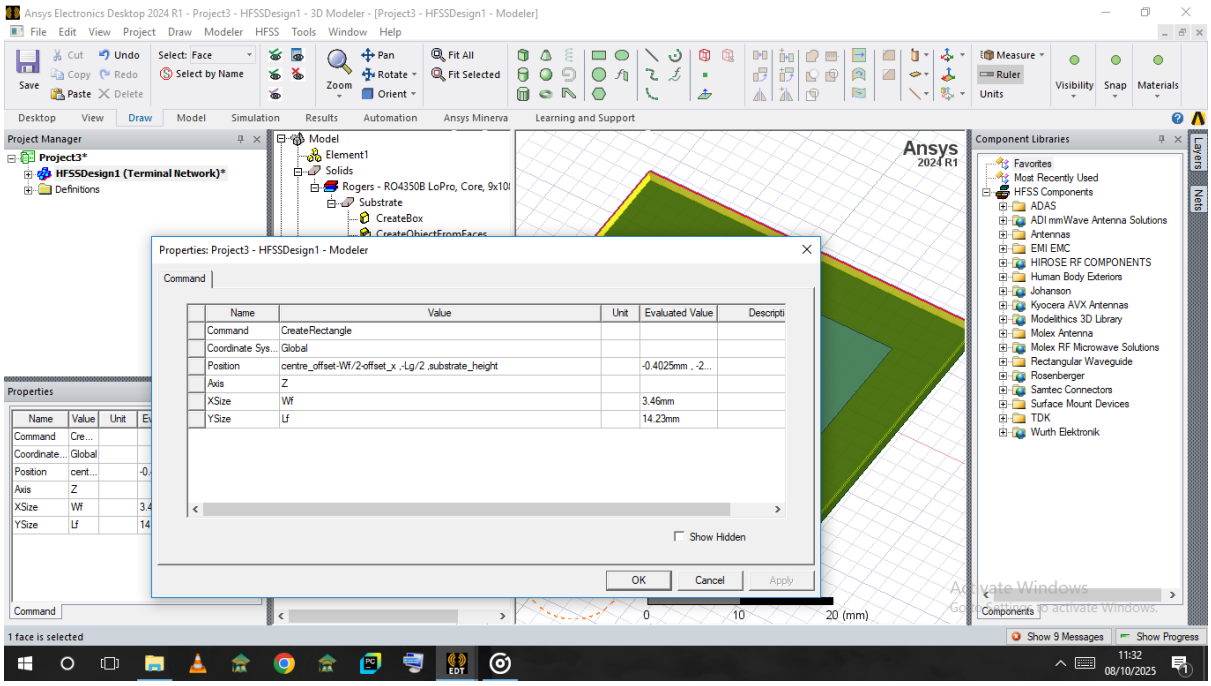

Figure 3.18: Create the feedline and set its parameters

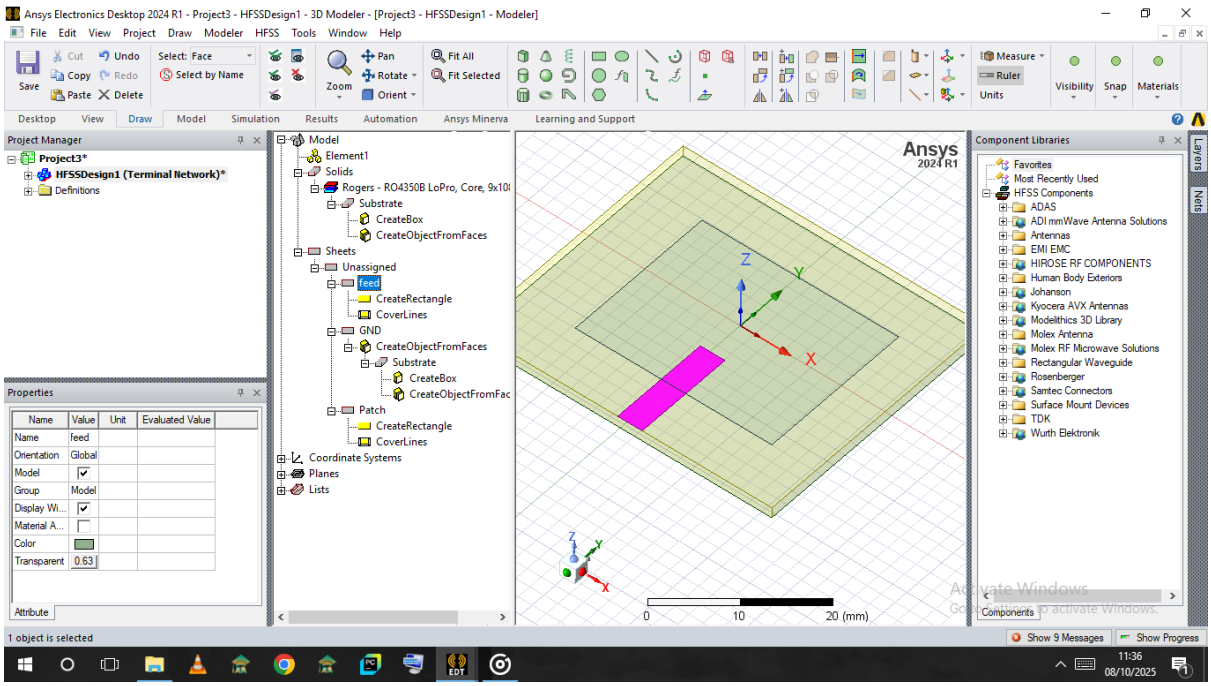

Figure 3.19: Created feedline

(d) To create a gap, draw a small rectangle on the feed line. Set its dimensions and name it **Gap** as shown in figure 3.21 and 3.22.

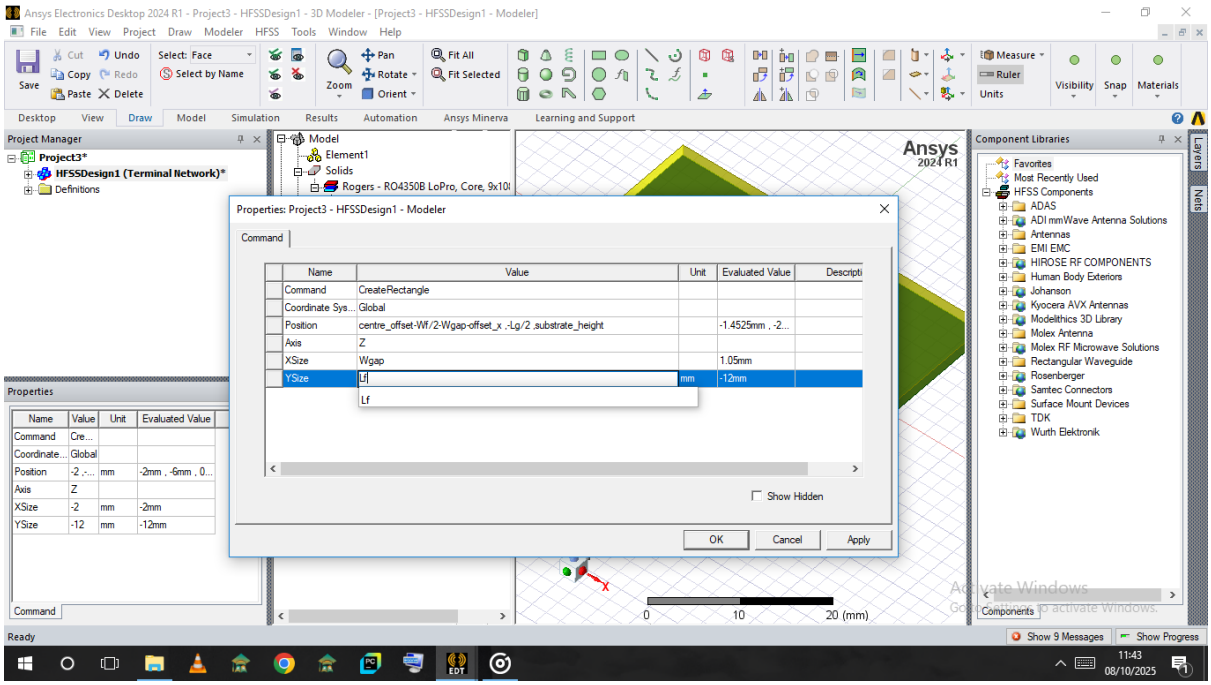

Figure 3.20: Feedline Dimensions

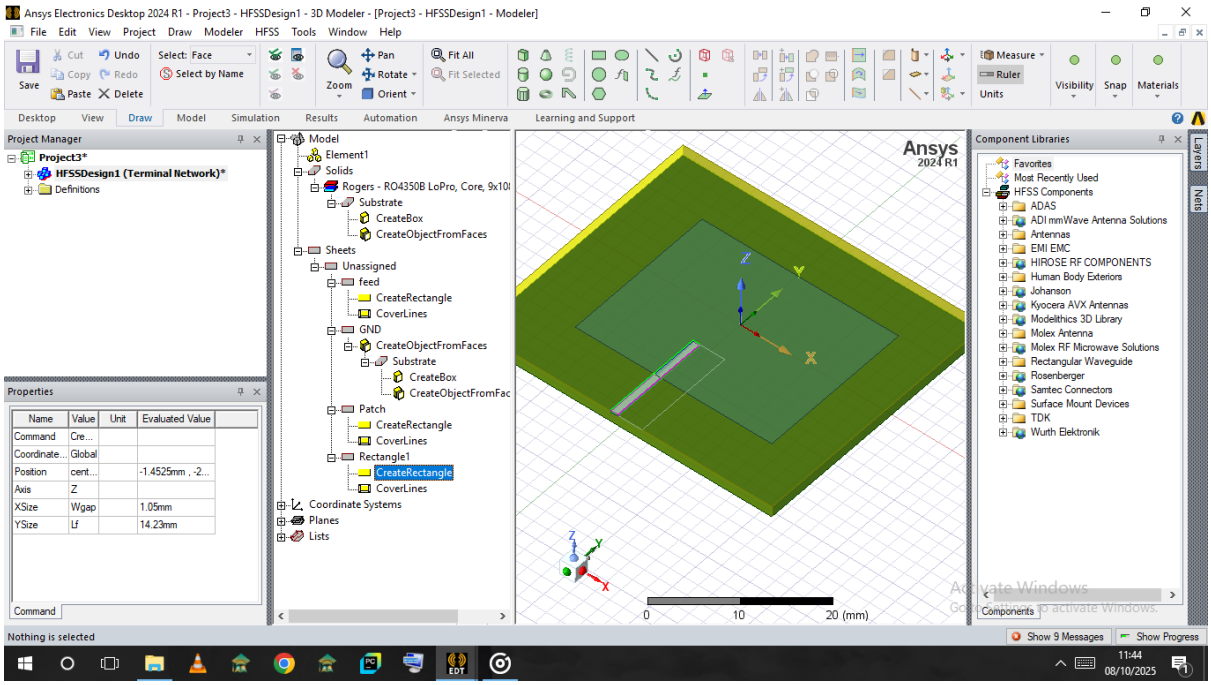

Figure 3.21: Draw a thin rectangle on the feedline

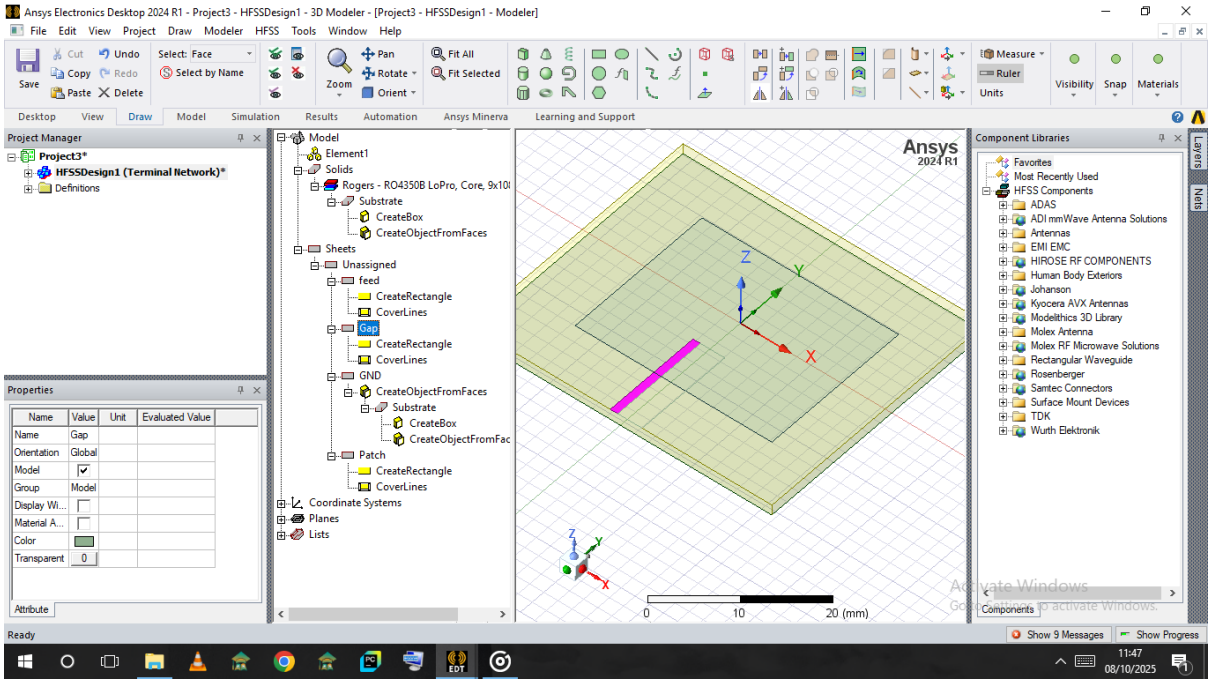

Figure 3.22: Select the newly created rectangle

(e) Use the **Duplicate Mirror** icon to mirror the gap to the opposite side of the feed line as shown in figure 3.23.

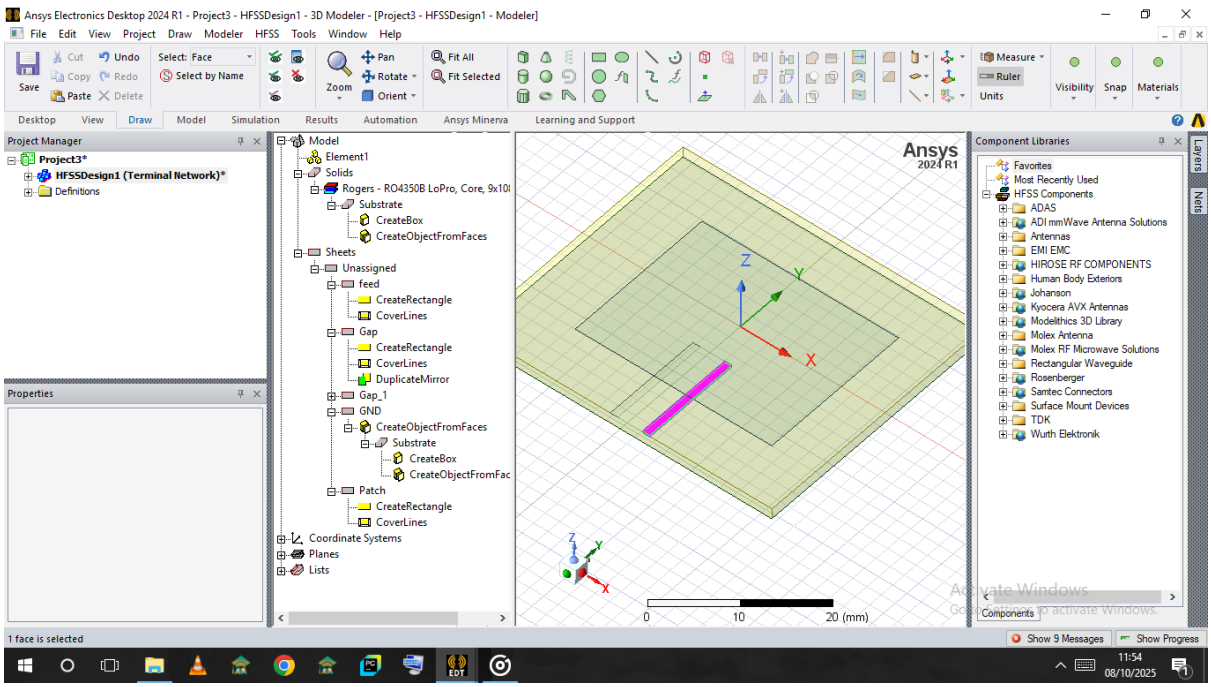

Figure 3.23: Duplicate the gap

(f) Select the `feed` and `patch` elements and click the **Unite** icon to combine them

as shown in figure 3.24 and 3.25.

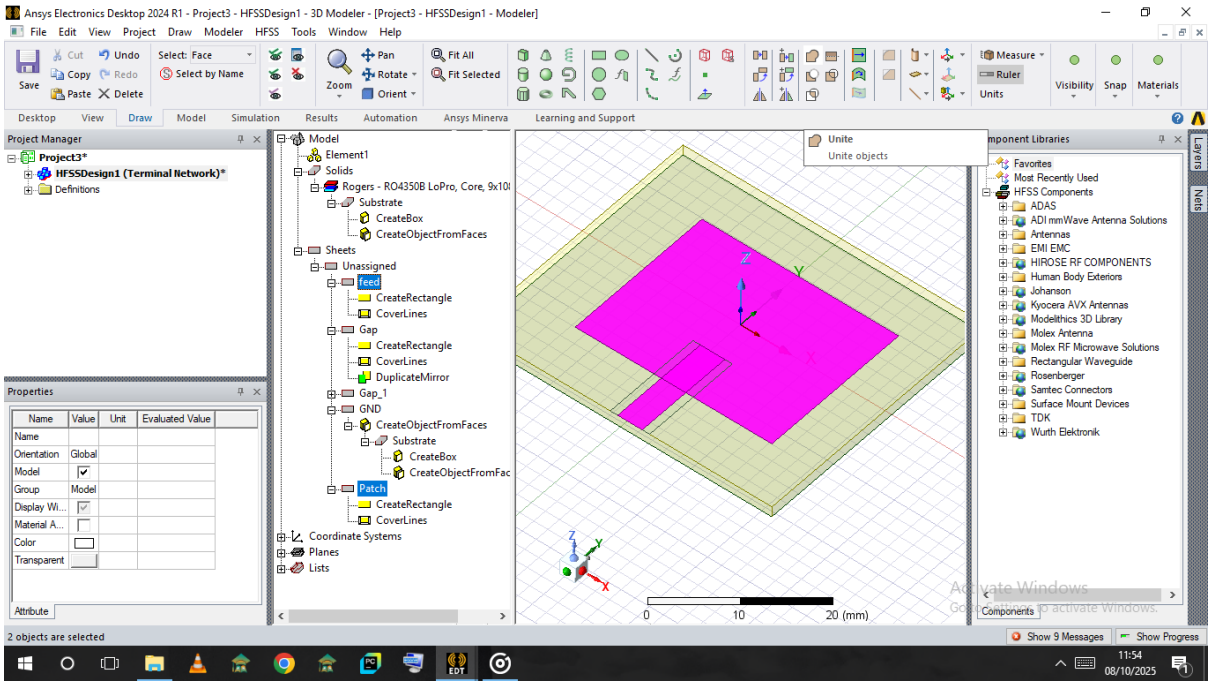

Figure 3.24: Select both the feedline and patch

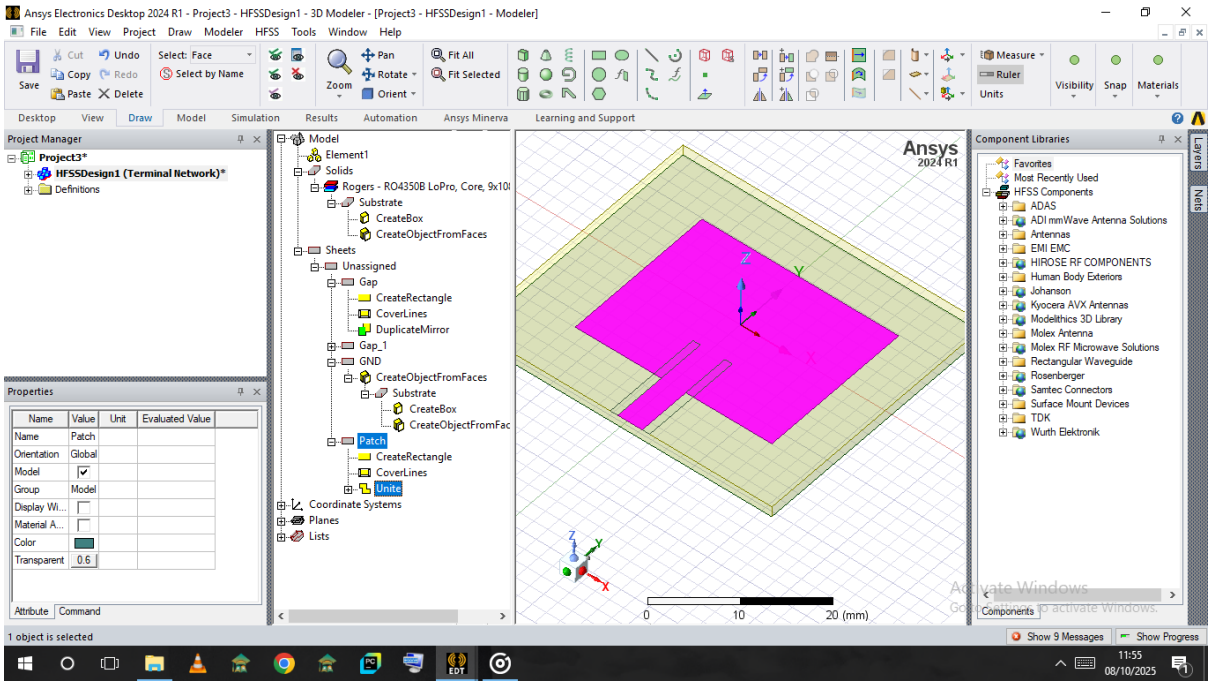

Figure 3.25: Unite the feedline and patch

(g) Select the `patch` and both `Gap` objects, then click the **Subtract** icon to remove the gaps from the patch as shown in figure 3.26.

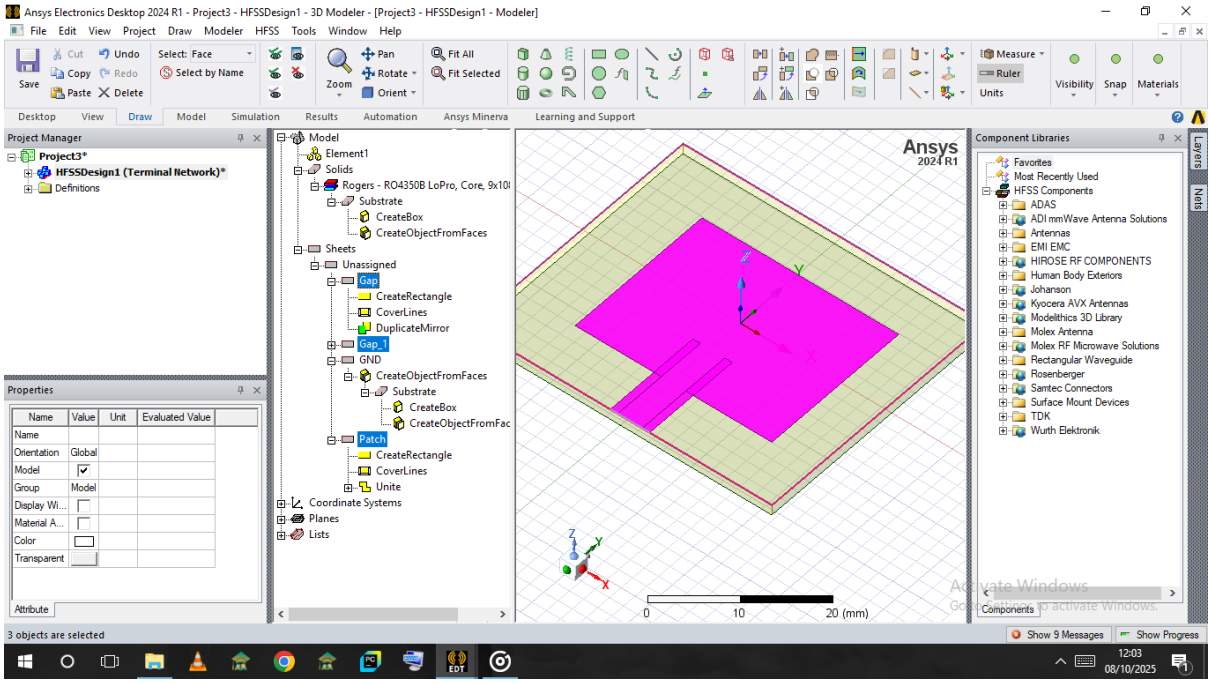

Figure 3.26: Subtract the gaps from the patch

4. **Port and Boundary Assignment**

   (a) To create the Port, select the edge faces of the feed line.

   (b) Go to **Ribbon** → **Create Object from Edge** as shown in figure 3.27.

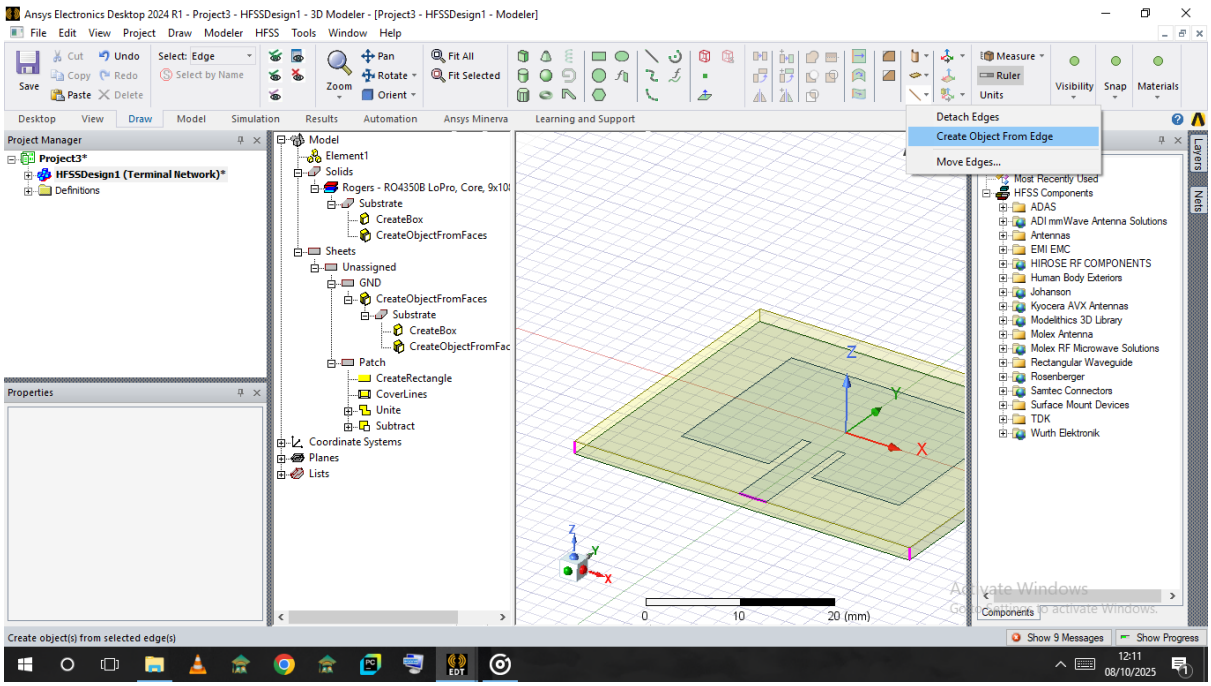

Figure 3.27: Select the edge faces of the feedline and select create object from edge

(c) Select the three created objects and use **Sweep Along Path** to form the Port. Rename it **Port** as shown in figure 3.28 to 3.30.

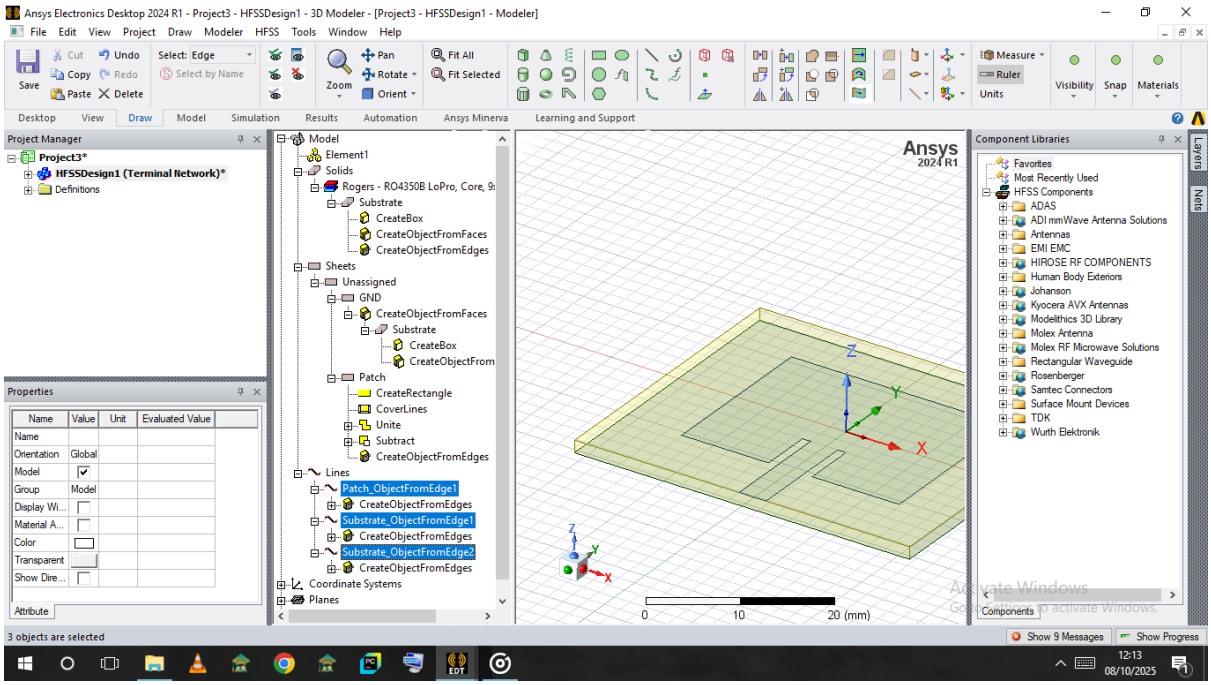

Figure 3.28: Sweep along path

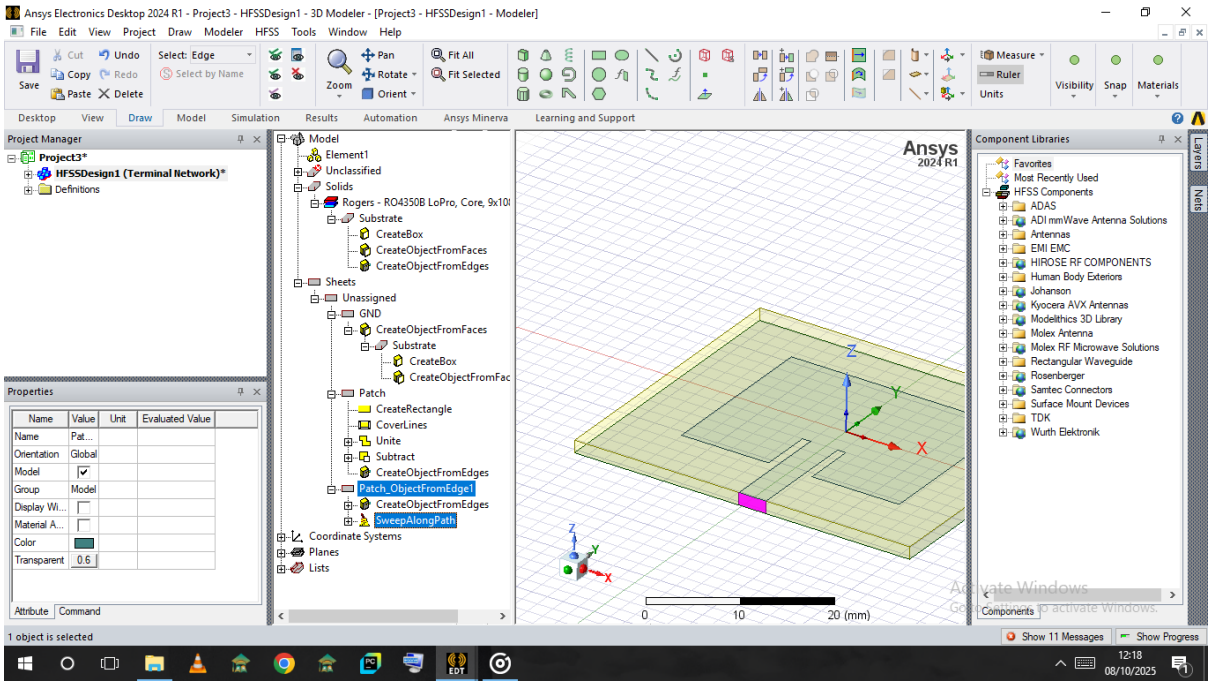

Figure 3.29: The created port

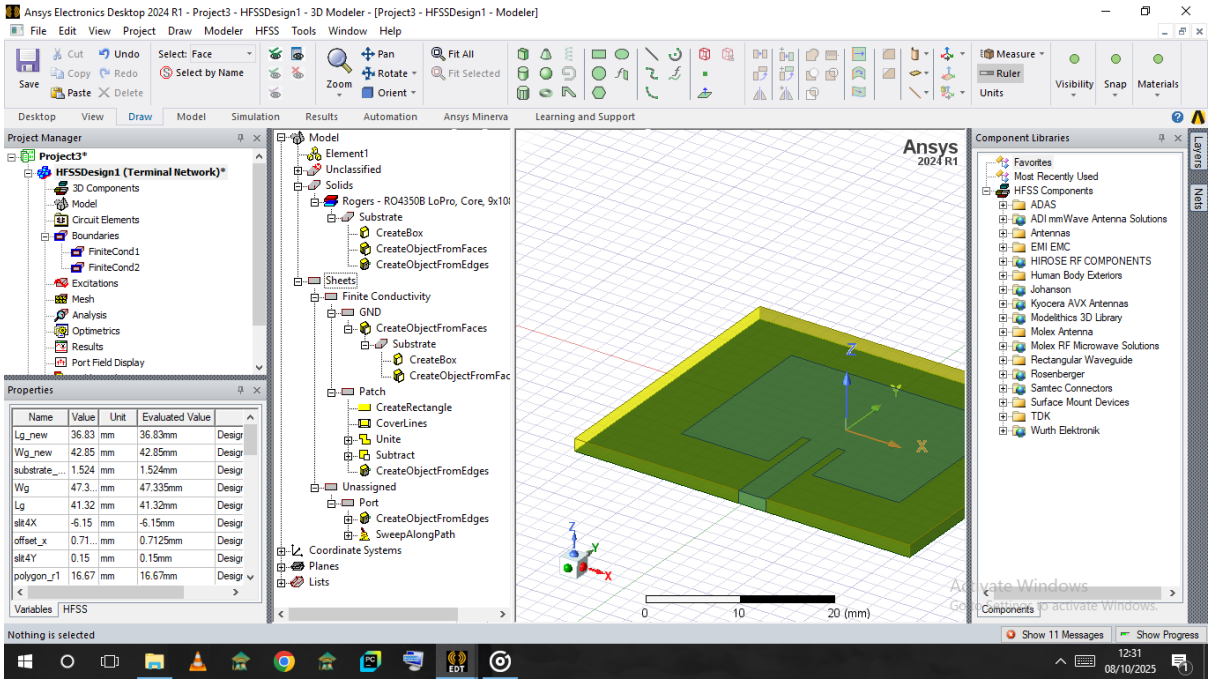

Figure 3.30: Rename the object as port

(d) Assign boundaries by right-clicking `patch` and `GND` and selecting **Assign Boundary → Finite Conductivity** as shown in figure 3.31.

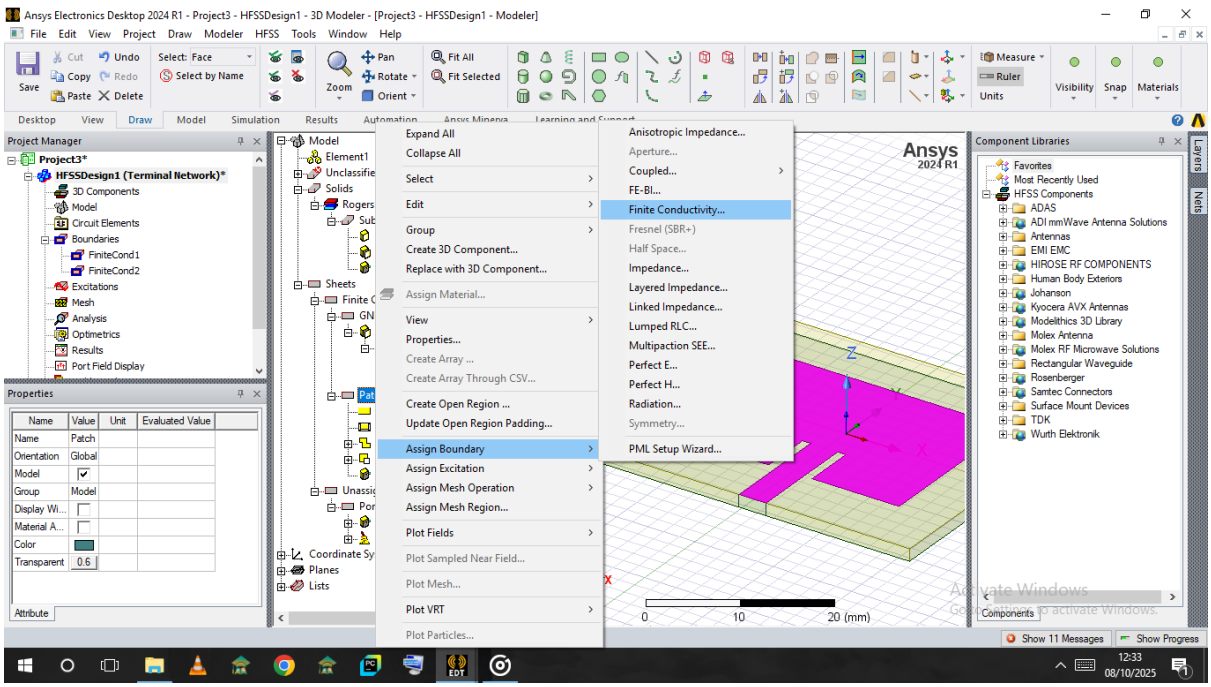

Figure 3.31: Assign finite conductivity boundary to patch and GND

(e) For port excitation, right-click **Port → Assign Excitation → Modal Lumped**

Port as shown in figure 3.32.

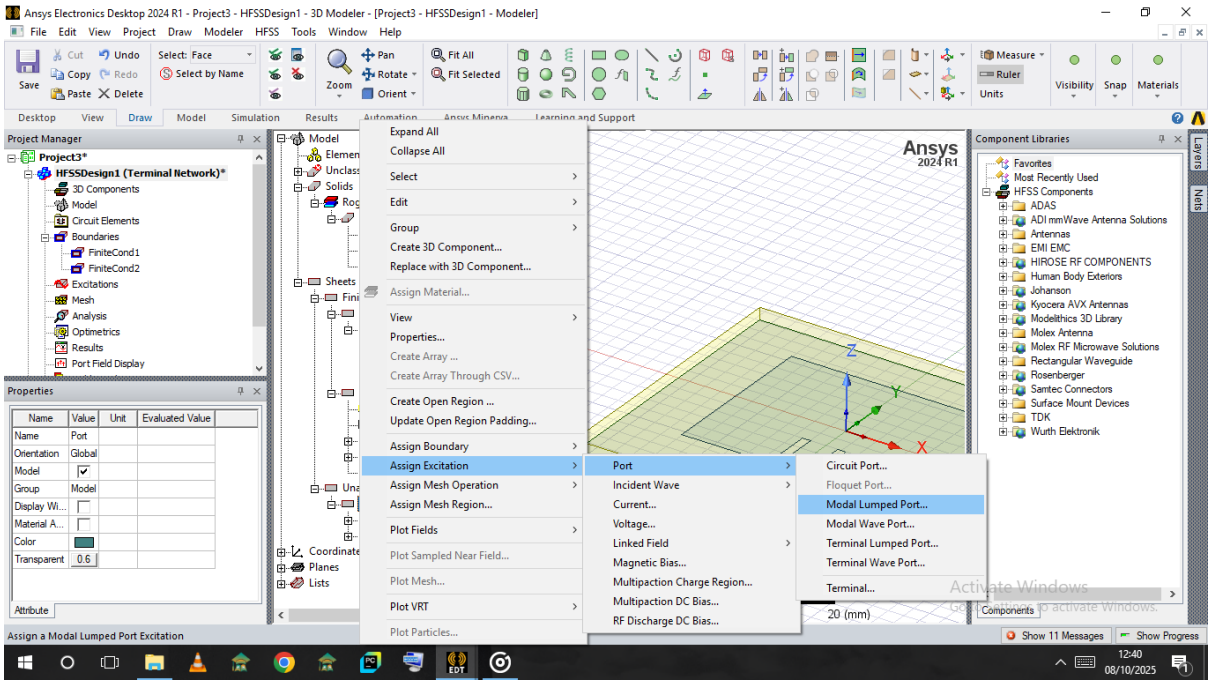

Figure 3.32: Assign port excitation

(f) Click **Next** as shown in figure 3.33

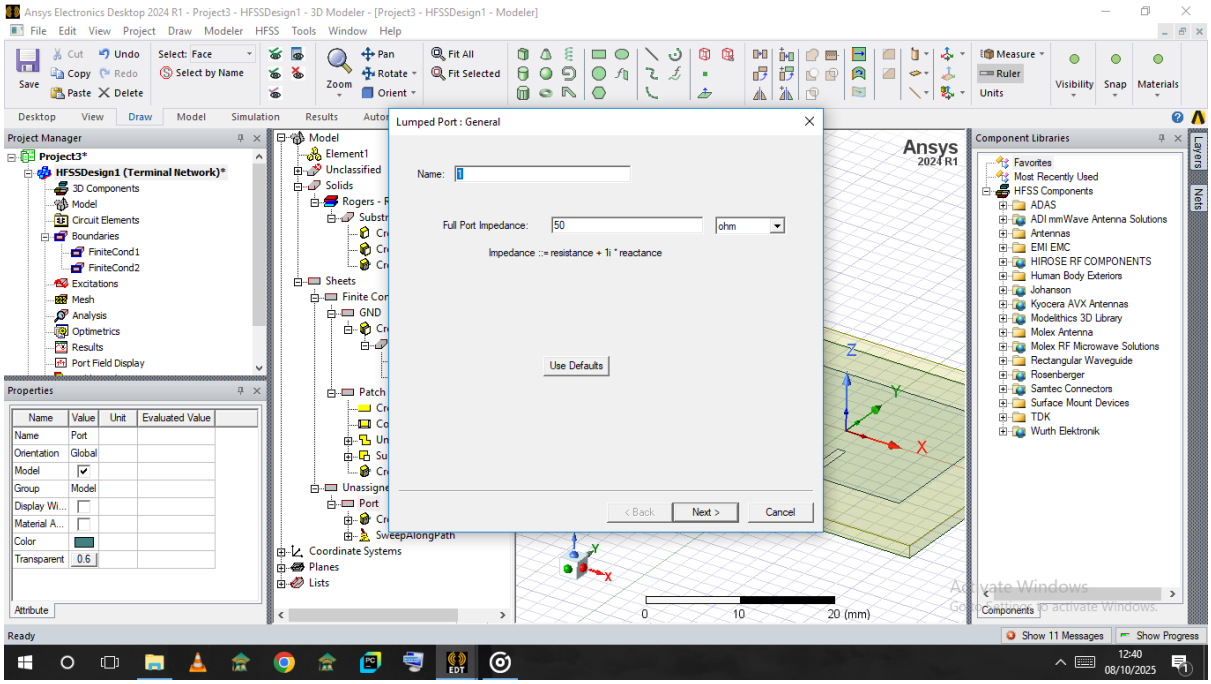

Figure 3.33: Click Next

(g) Click **New Line** as shown in figure 3.34

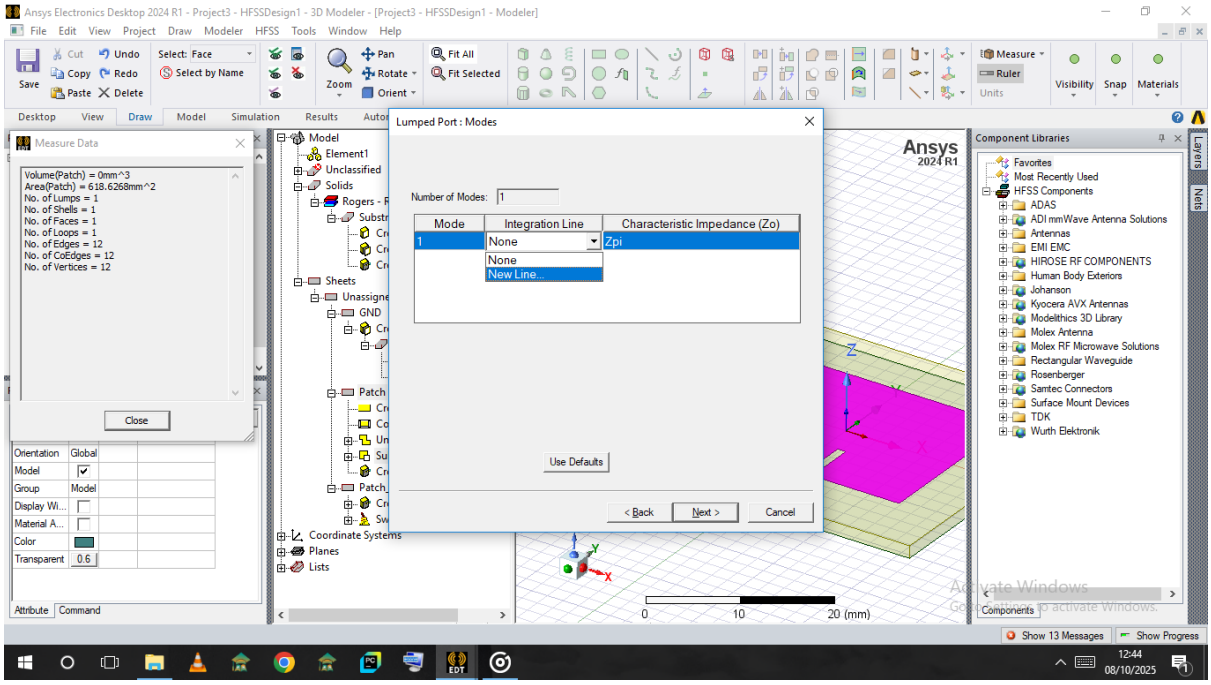

Figure 3.34: Click New Line

(h) Draw the integration line at the midpoint of the port from bottom to top as shown in figure 3.35

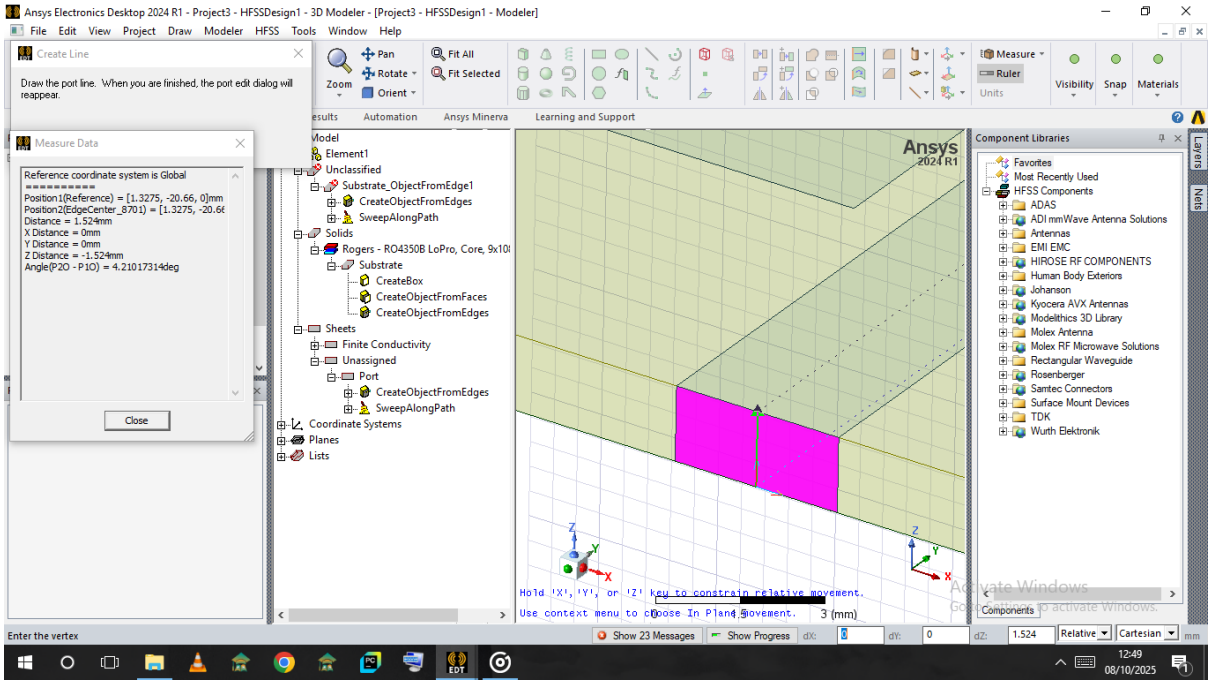

Figure 3.35: Draw the integration line

(i) Make sure the integration line is defined and click Next as shown in figure 3.36

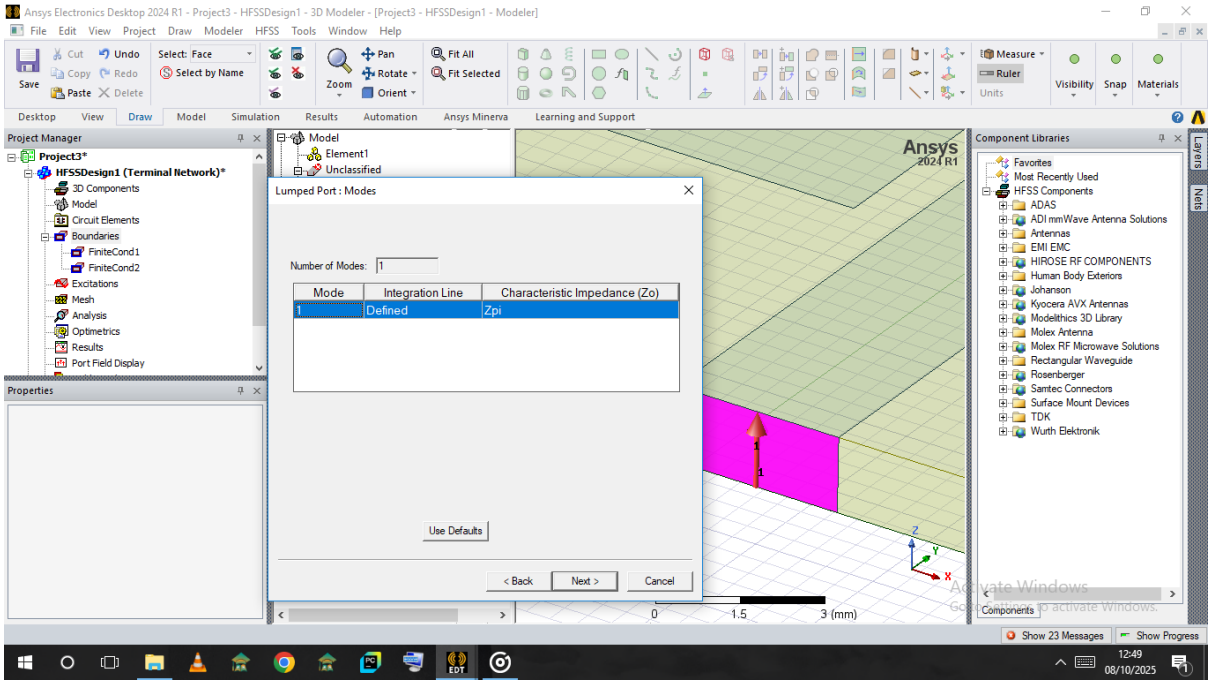

Figure 3.36: Click Next

(j) Click **Finish** as shown in figure 4j

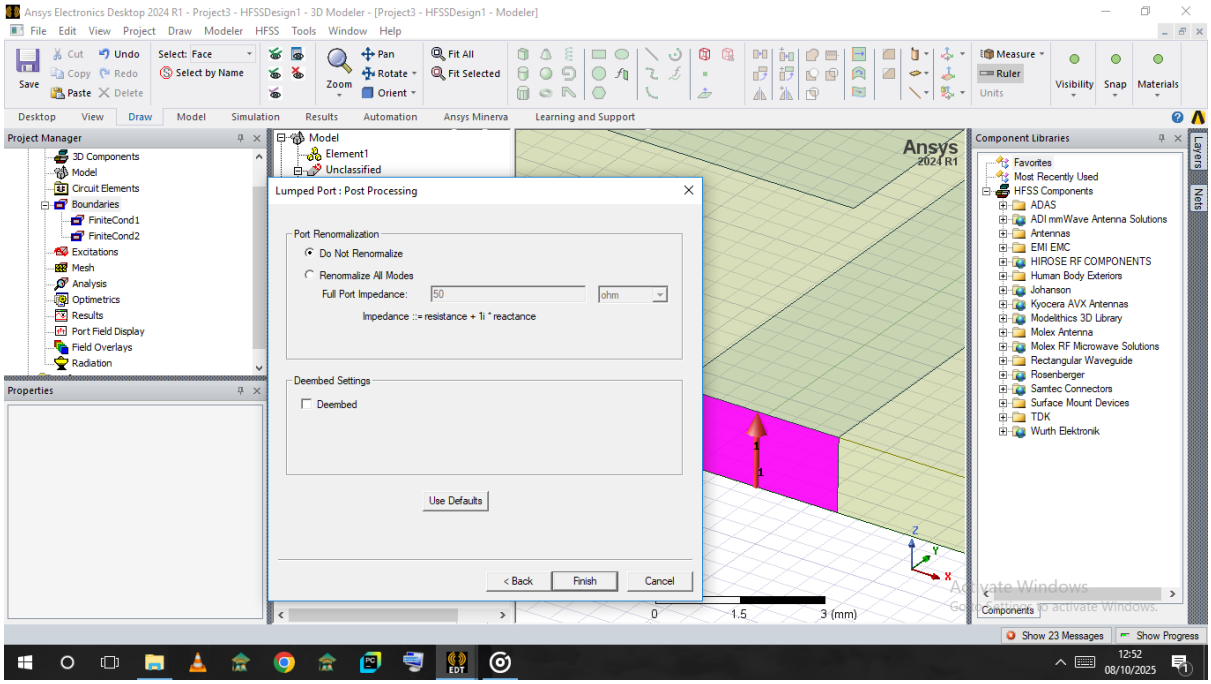

Figure 3.37: Click Finish

(k) The port with assigned excitation as shown in figure 3.38.

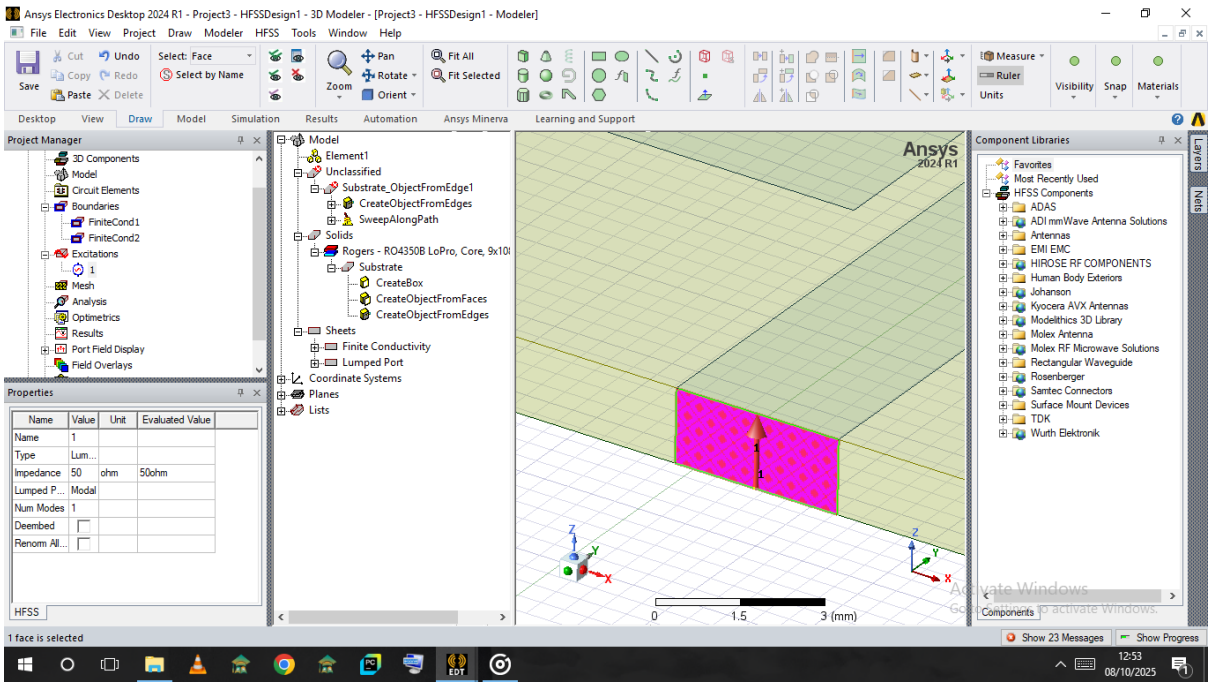

Figure 3.38: Port with assigned excitation

5. Solution Setup and Simulation

(a) In the Project Manager, right-click on **Analysis** → **Add Solutions Setup** → **Advanced** as shown in figure 3.39 and 3.40.

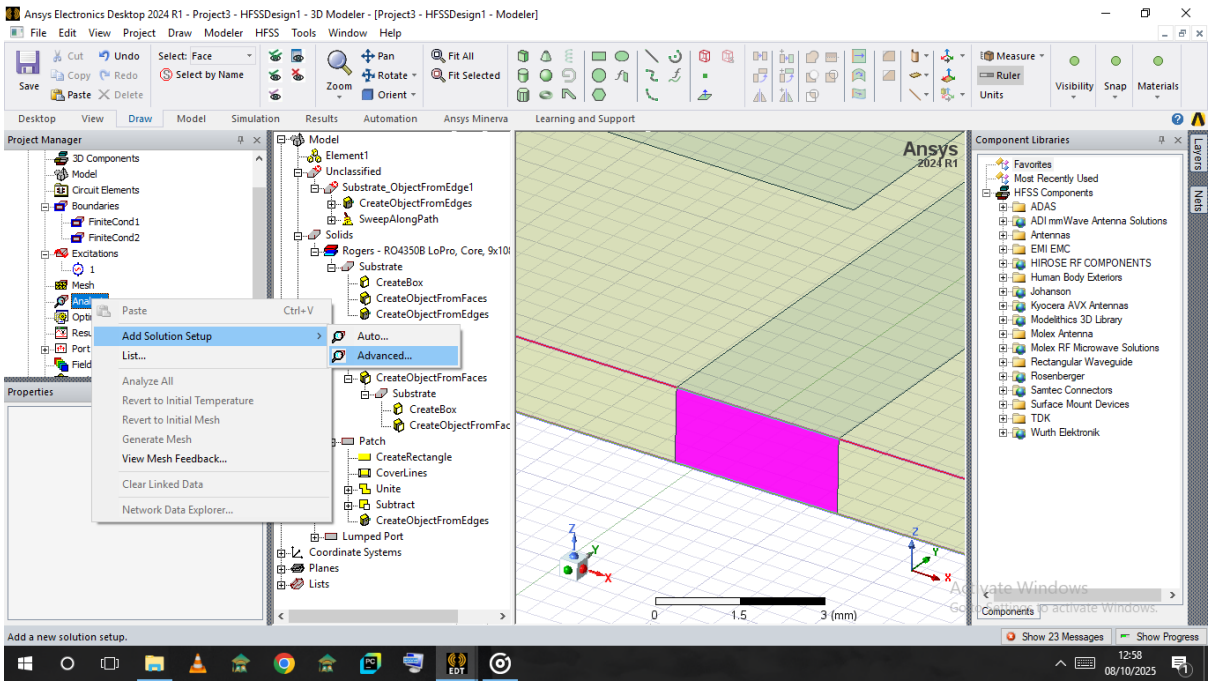

Figure 3.39: Setting up analysis

(b) Set the solution frequency to **3.5 GHz** and the sweep range from **3.3 GHz to 3.8 GHz** as shown in figure 3.41.

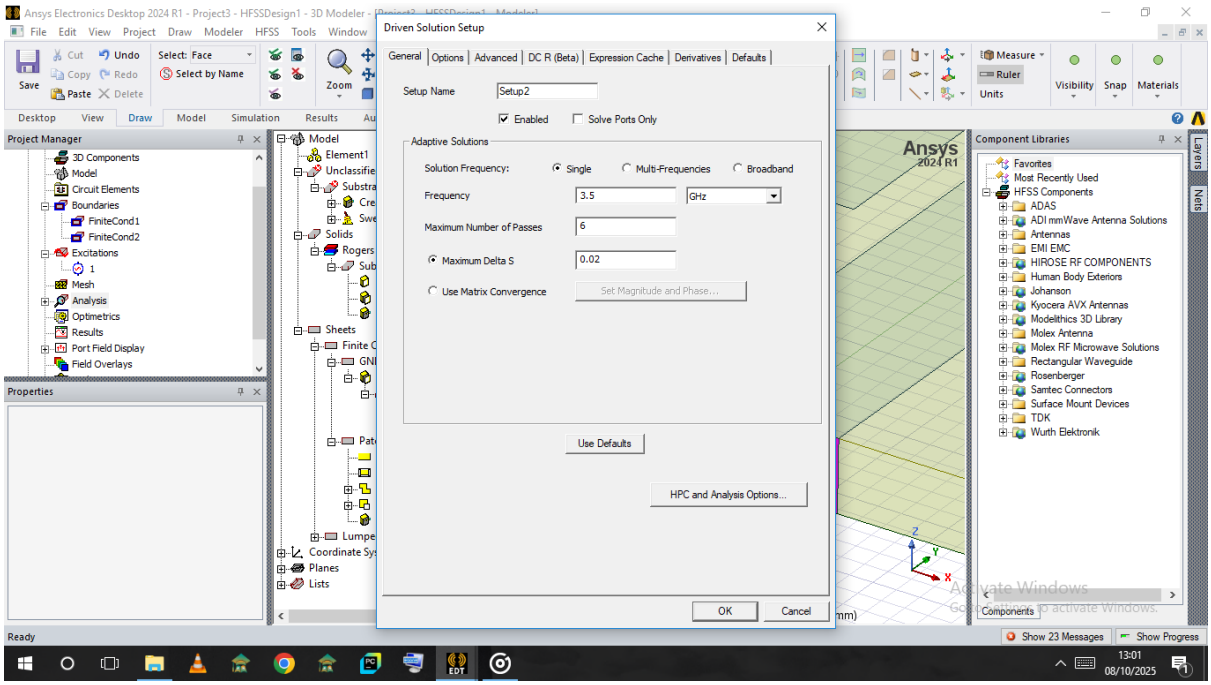

Figure 3.40: Analysis Setup

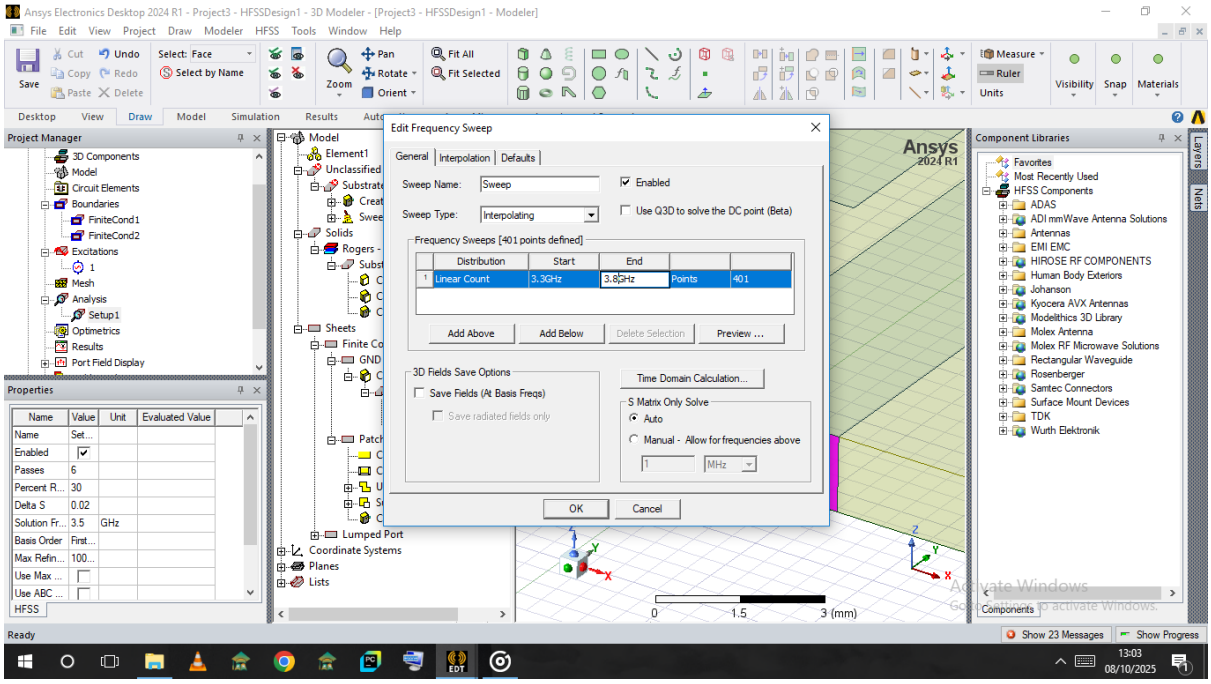

Figure 3.41: Set operating frequency

(c) Define a radiation region by going to **HFSS** → **Model** → **Create Region** as shown in figure 3.43 and 3.44.

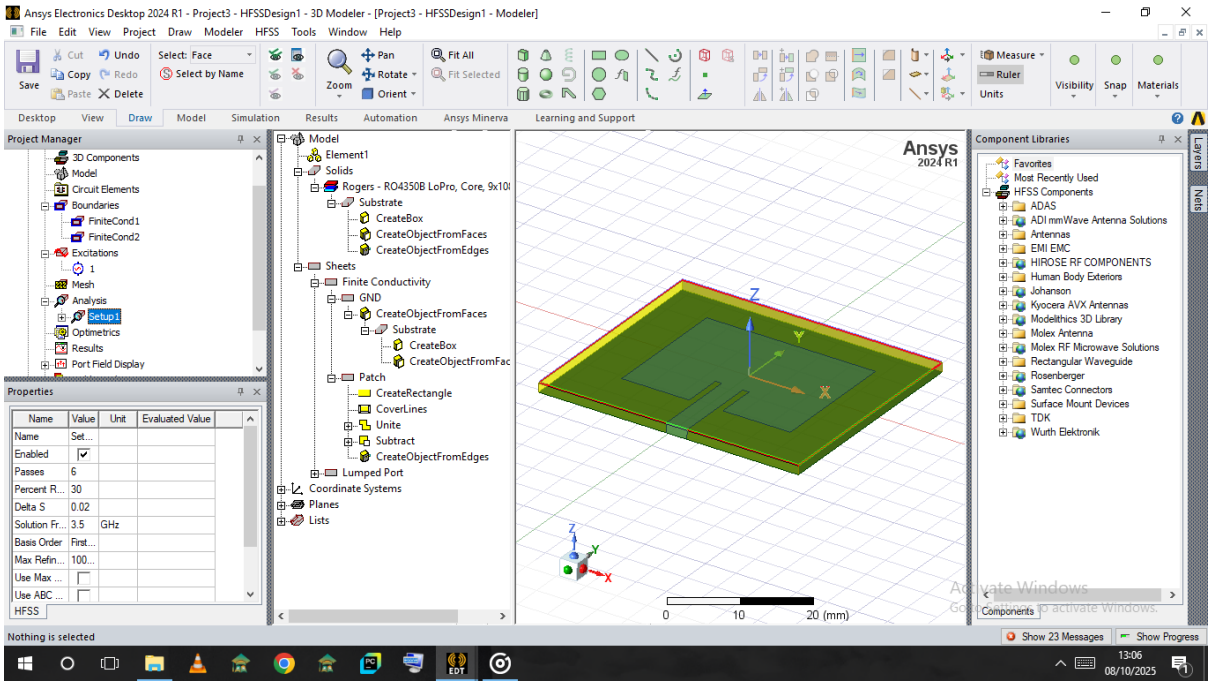

Figure 3.42: Analysis has been setup

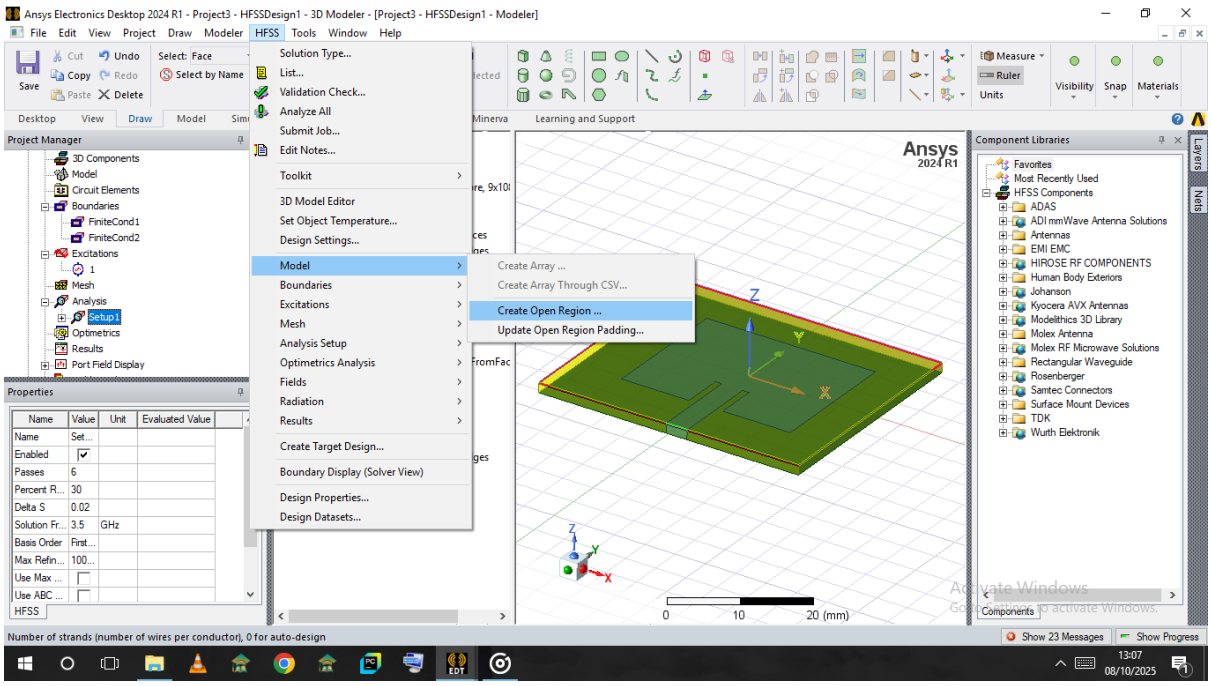

Figure 3.43: Creating Open Region

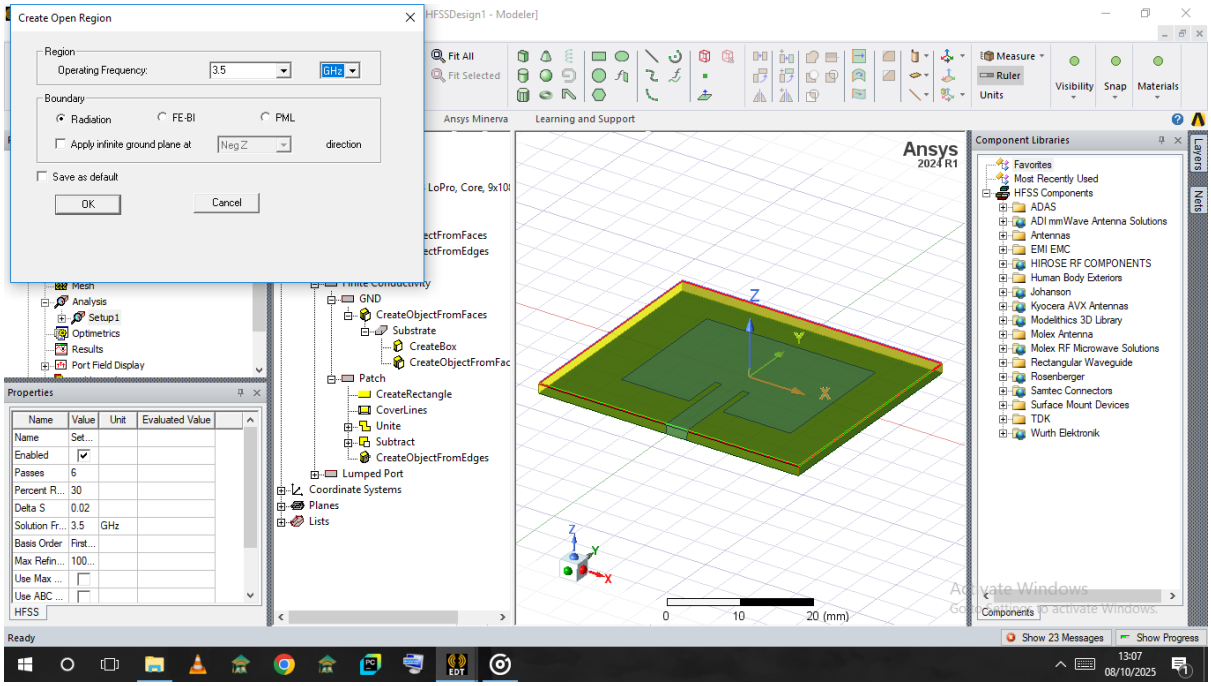

Figure 3.44: Click OK

(d) Validate the design by clicking **Simulation** → **Validate**.

(e) Click **Analyze All** to run the simulation.

(f) To view results, right-click **Results** → **Create Terminal** → **Rectangular Plot** → **New Report** as shown in figure 3.45.

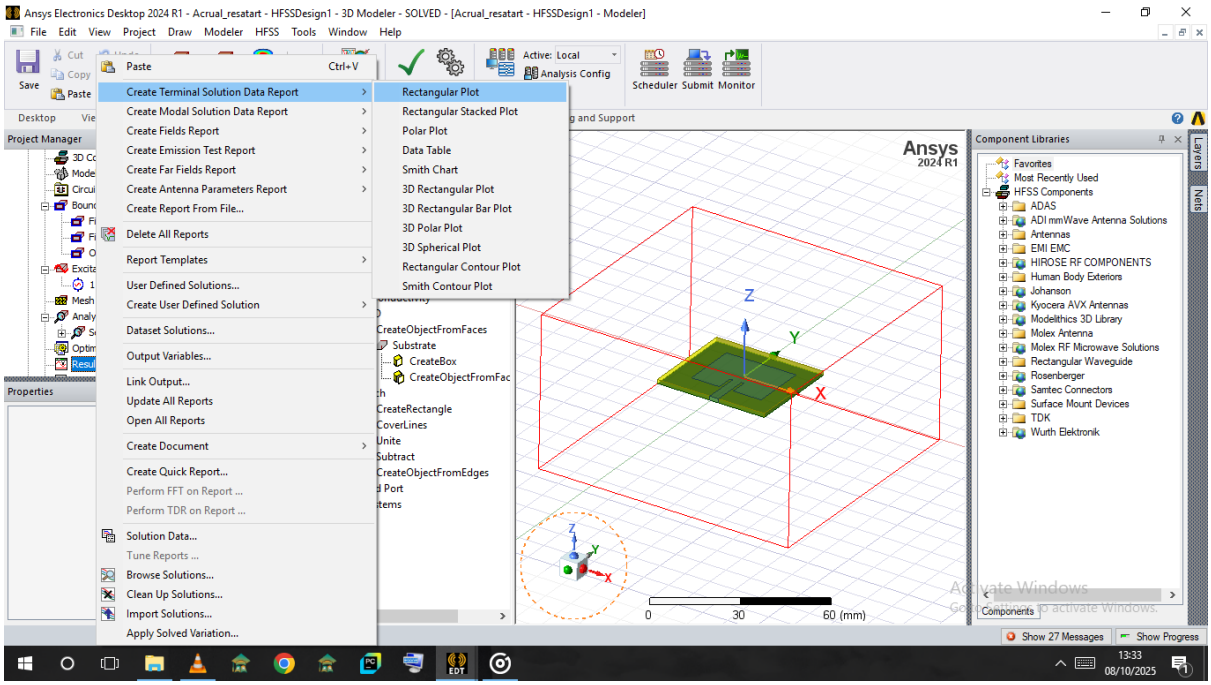

Figure 3.45: Generating Results

(g) For array simulations, change the solution type to **Hybrid with Arrays** by right-clicking the HFSS Design on the project manager as shown in figure 3.46 and 3.47.

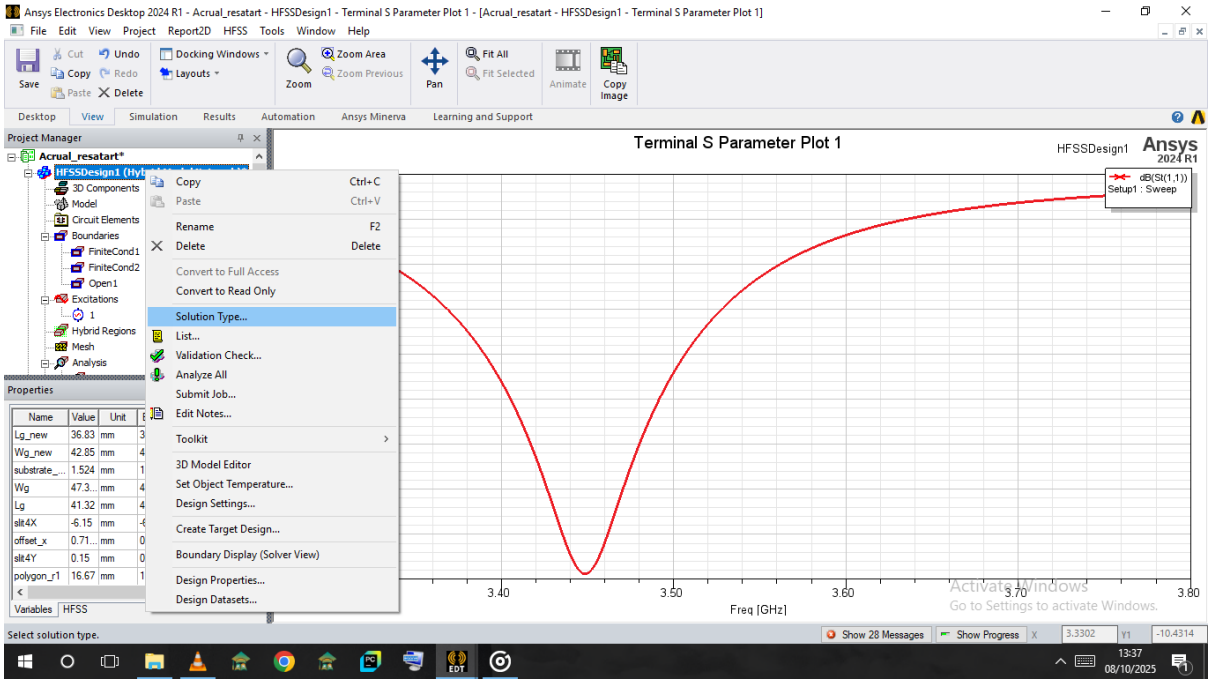

Figure 3.46: Select Solution type

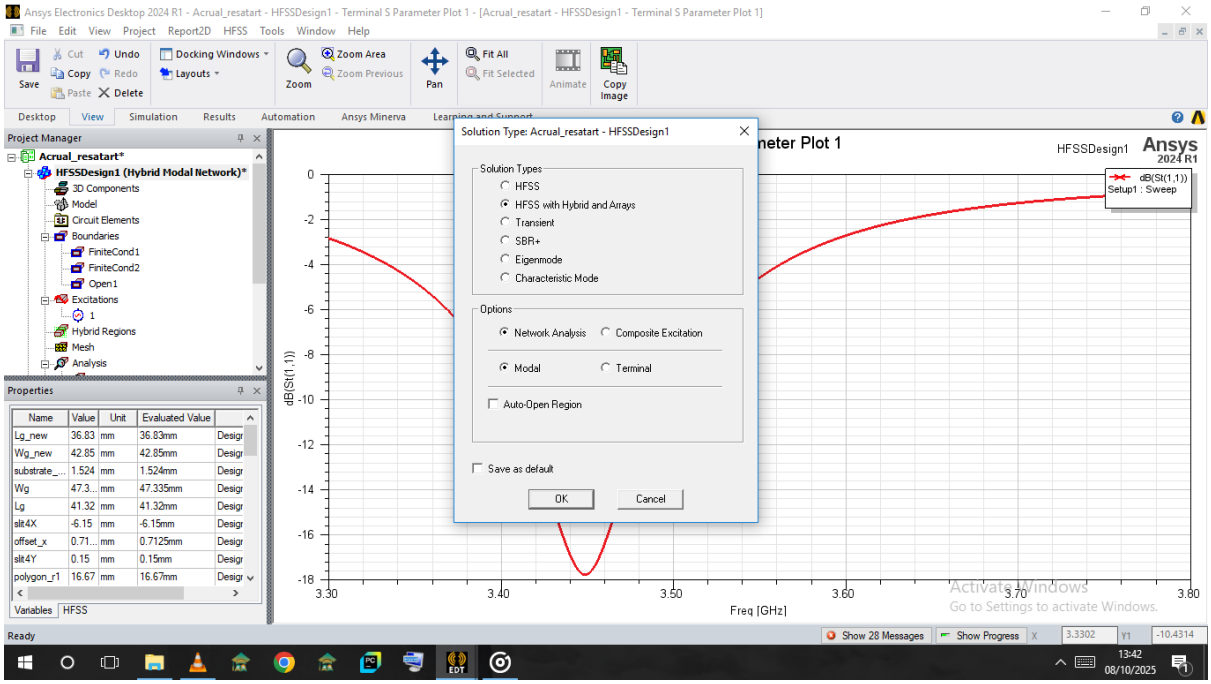

Figure 3.47: Select HFSS with Hybrid Arrays and Modal

3.3.3 Performance Enhancement: Adding Slots and DGS

This phase focuses on improving the performance of a single element.

1. **U-Slot Implementation**

   (a) Draw a box with the specified parameters to create the U-slot as shown in figure 3.48 to 3.51.

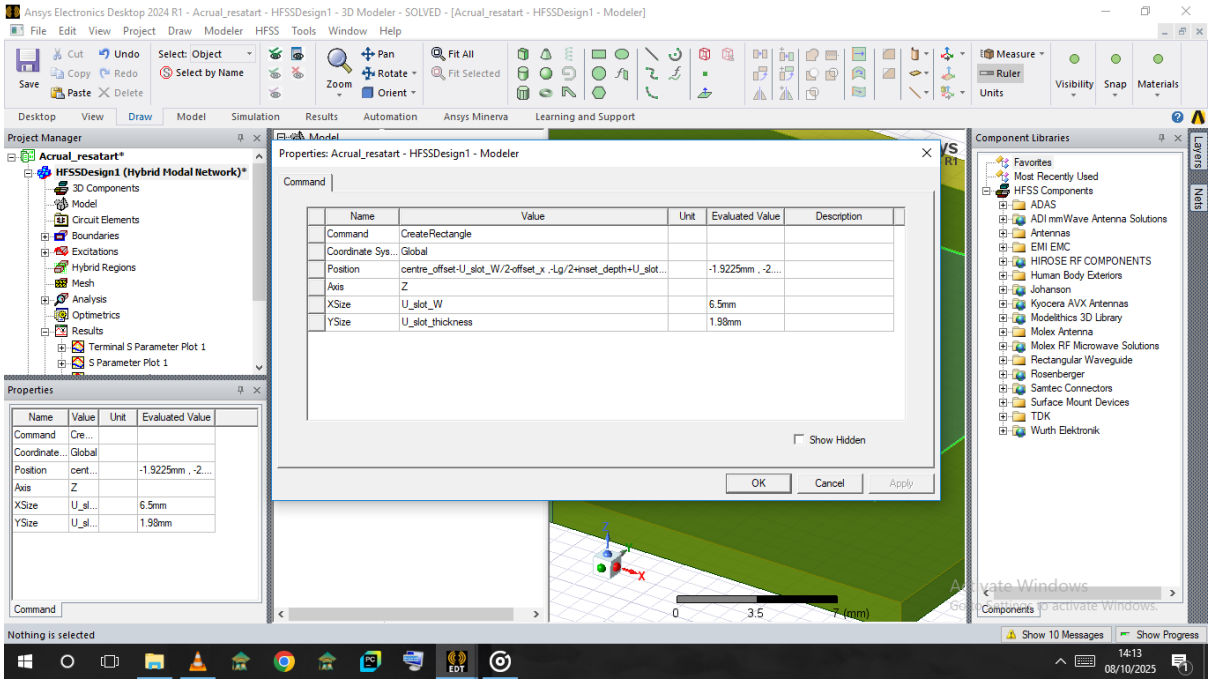

Figure 3.48: U-slot parameters

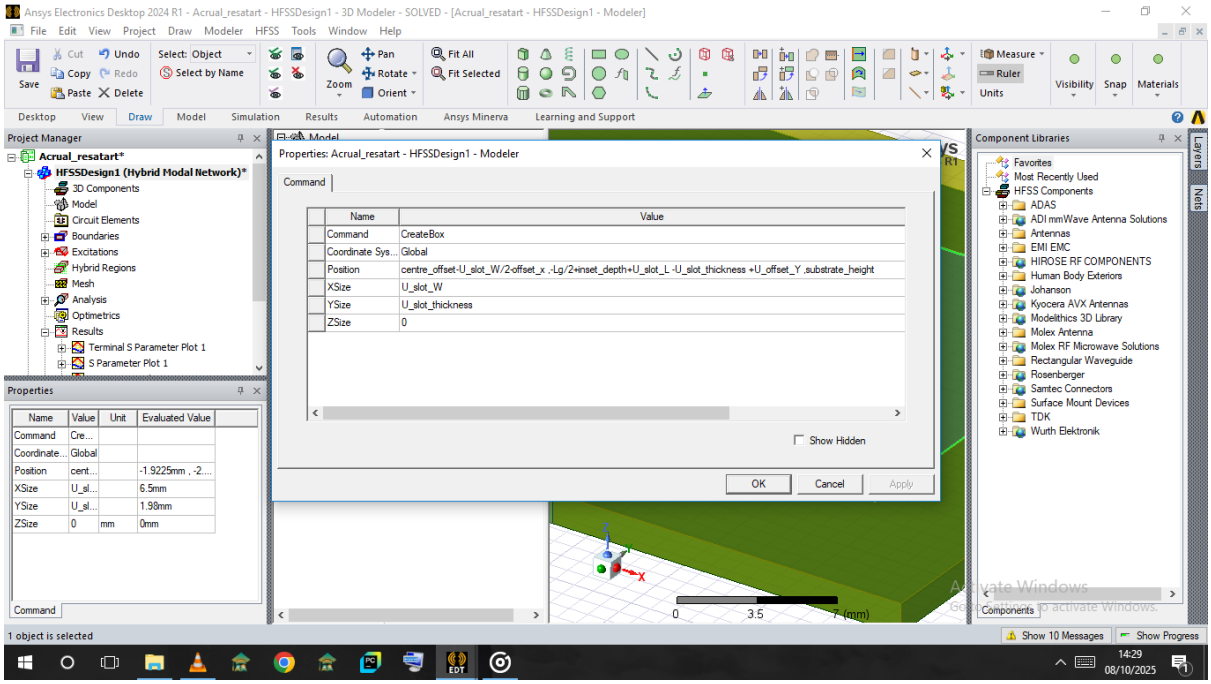

Figure 3.49: Complete U-slot parameters

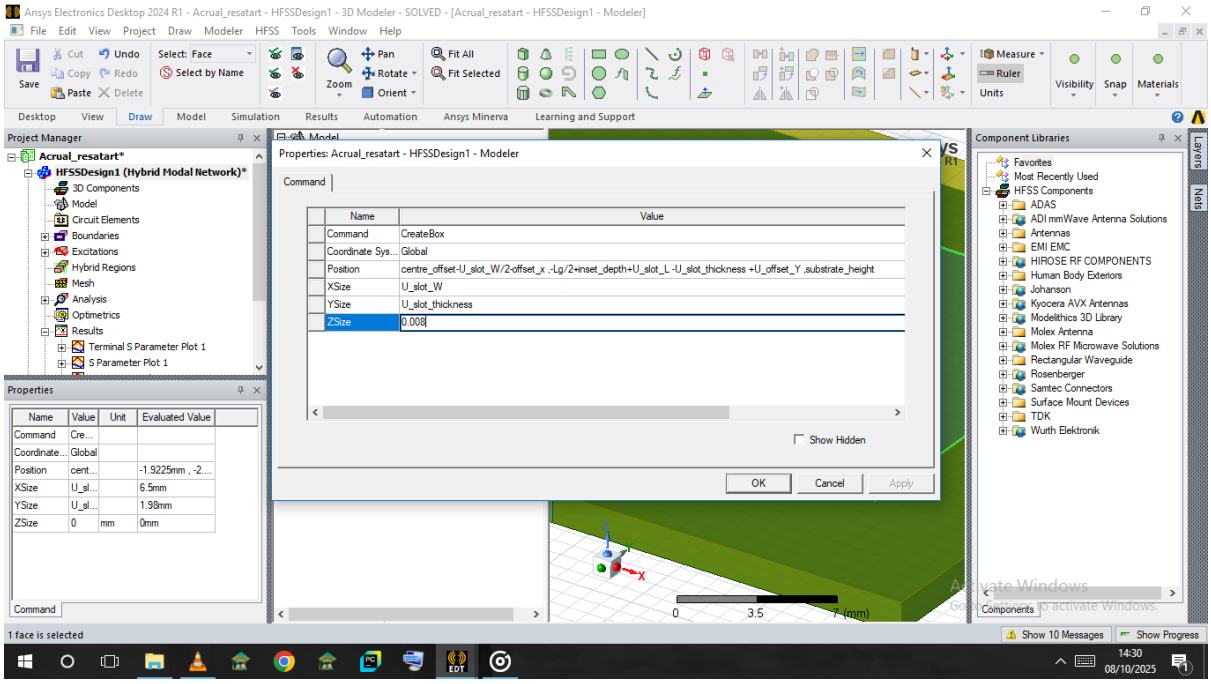

Figure 3.50: Set a vertical height for the U-slot

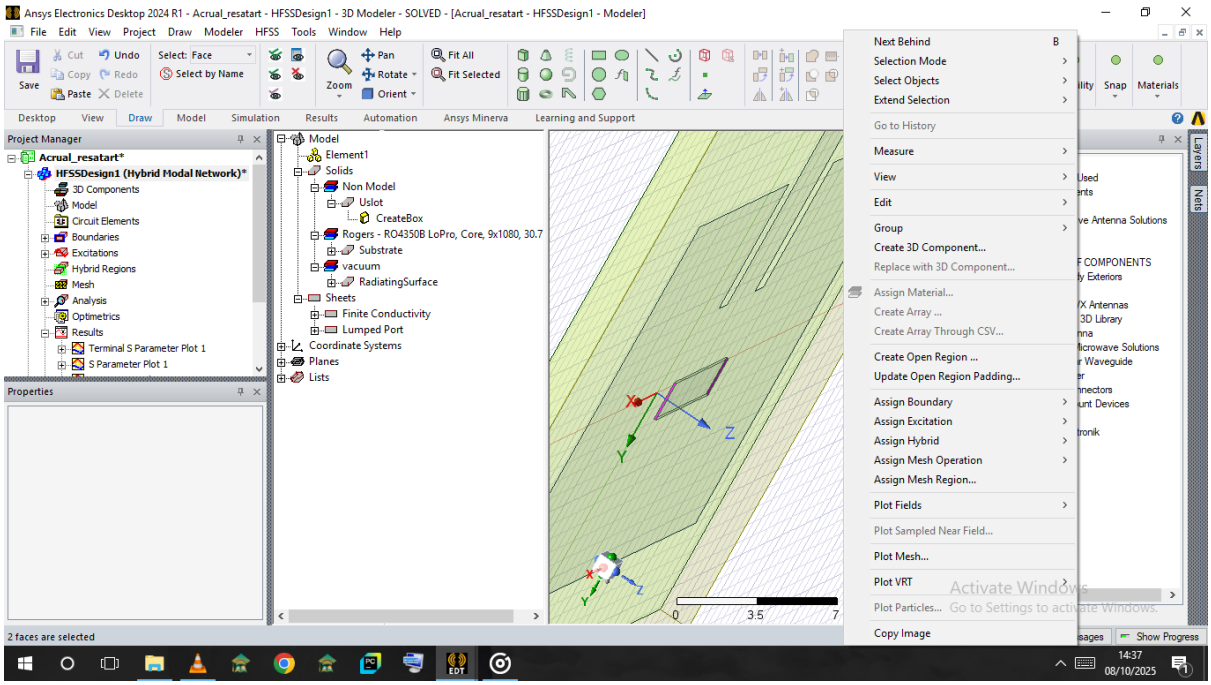

Figure 3.51: Rectangular arm of the U-slot

(b) Select the top edge faces of the box, right-click, and go to **Edit** → **Surface** → **Create Object from Face** as shown in figure 3.52.

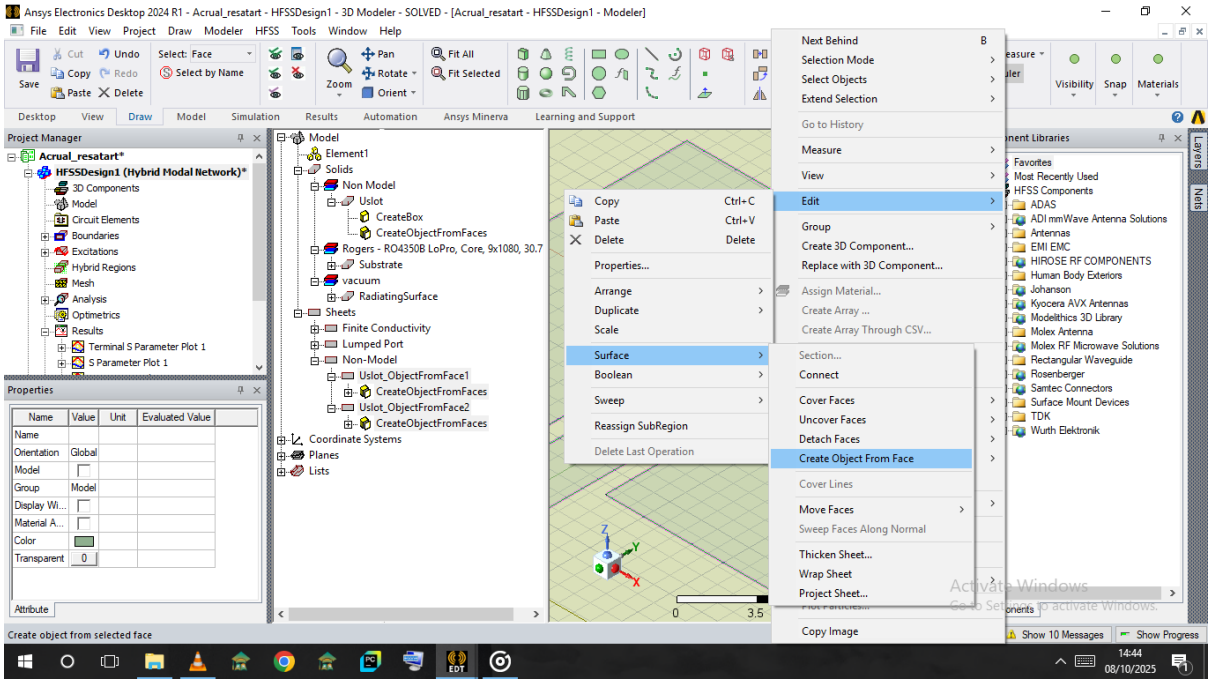

Figure 3.52: Creating object from face

(c) Right-click the new object, go to **Edit** → **Surface** → **Thicken Sheet**, and set the thickness as shown in figure 3.53.

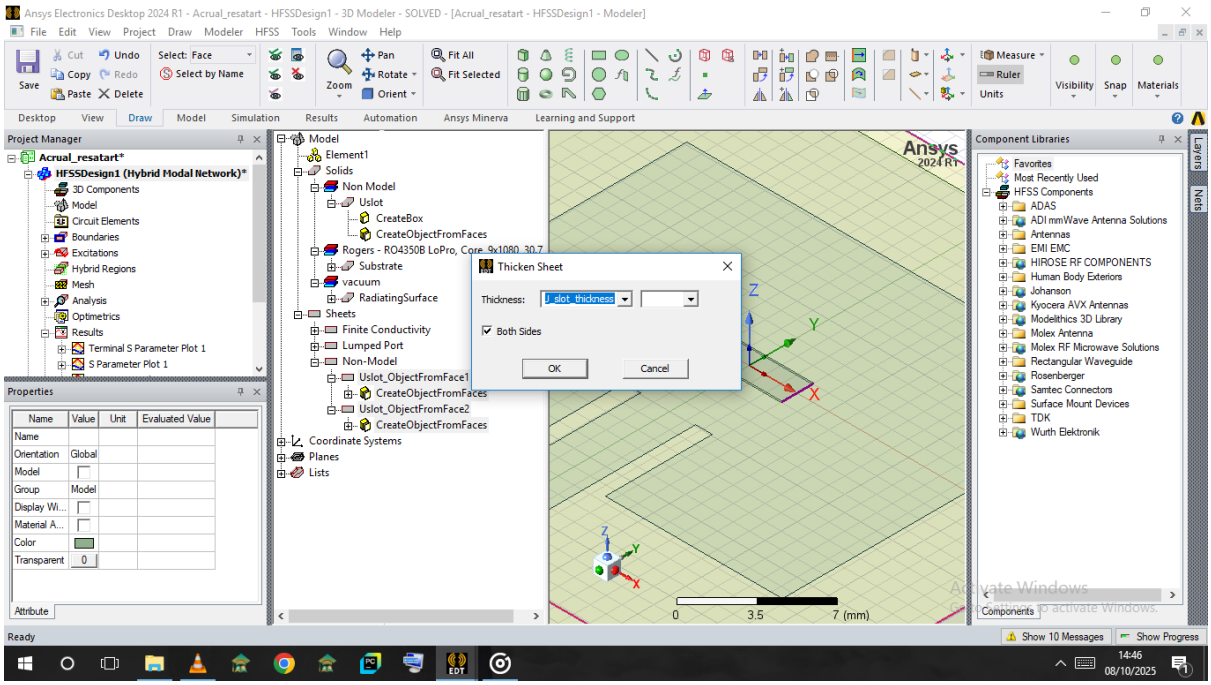

Figure 3.53: Thicken the created object

(d) Select the edge faces, right-click, and use **Move Faces** to move them along

the normal to the specified length as shown in figure 3.54 and 3.55.

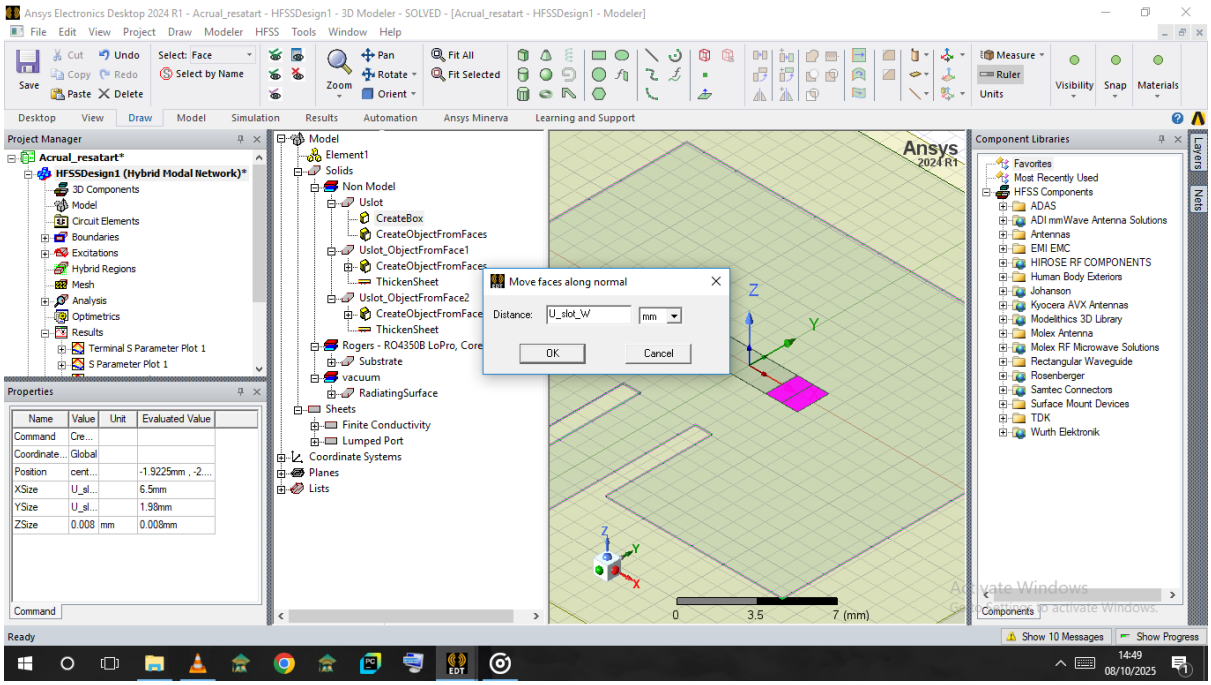

Figure 3.54: Moving faces along normal

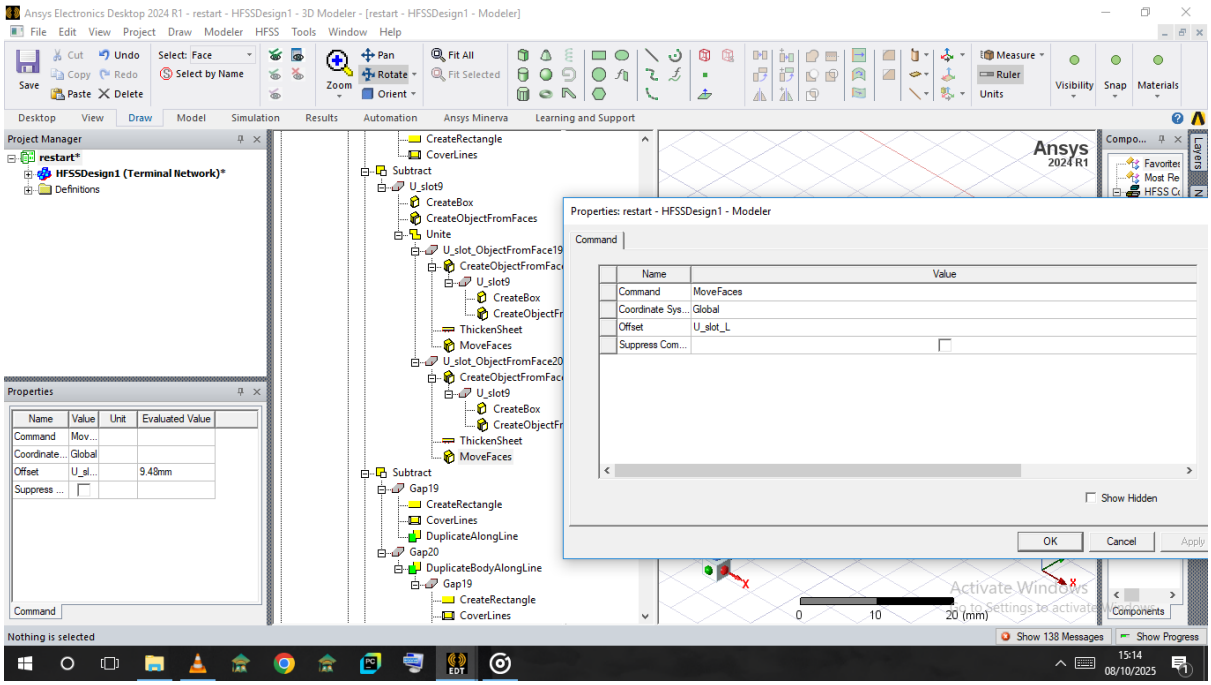

Figure 3.55: Properties window

(e) Unite the U-slot objects and then **Subtract** the unified U-slot from the patch as shown in figure 3.56 and 3.57.

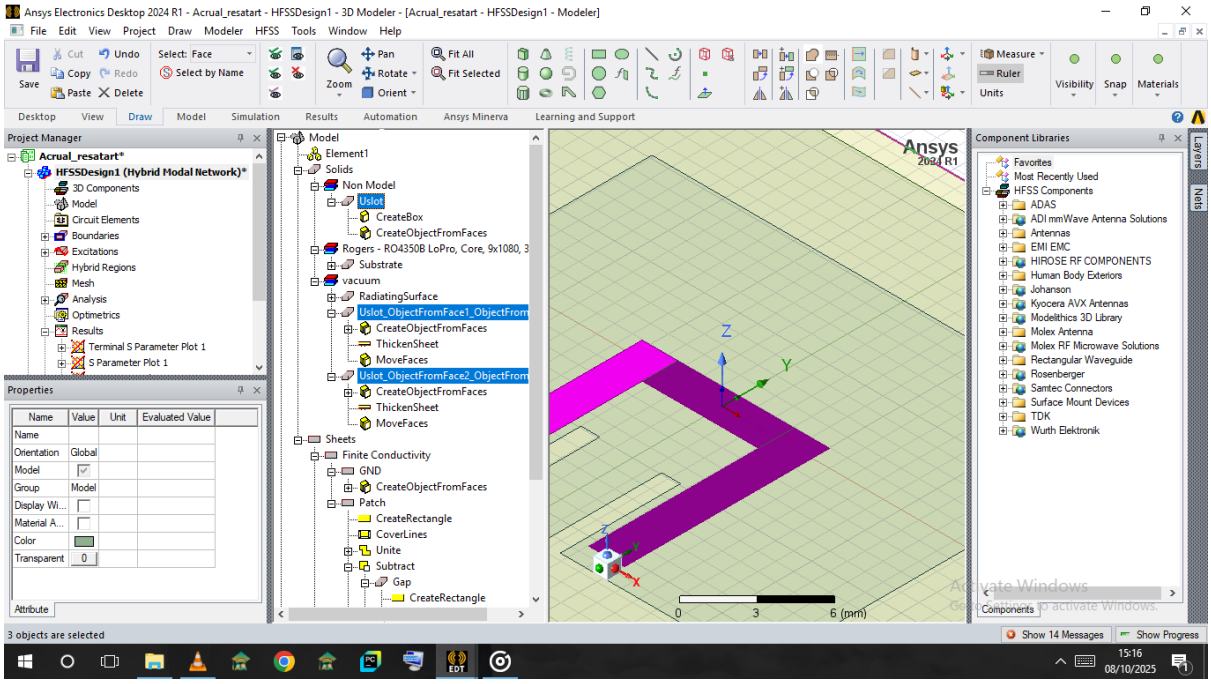

Figure 3.56: Unite U-slot arms

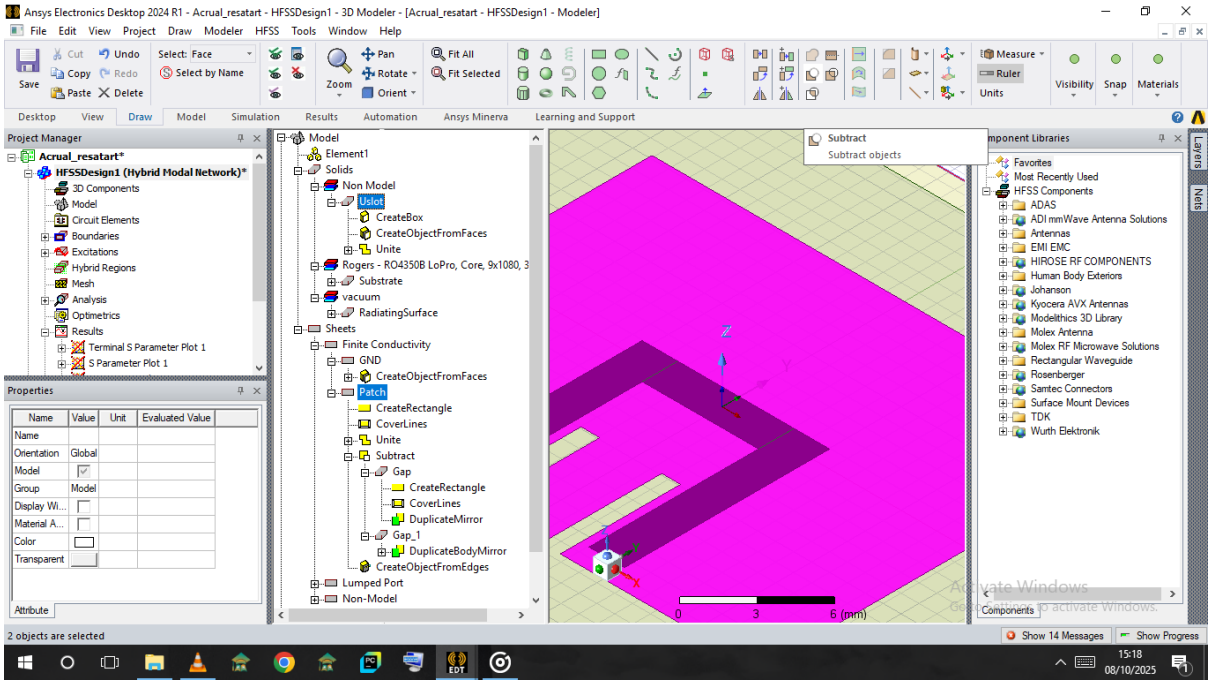

Figure 3.57: Subtracting U-slots from patch

2. DGS (Defected Ground Structure) Implementation

(a) Draw **Polygon 1**, **Polygon 2**, and **Polygon 3** with the specified dimensions as shown in figure 3.58 and 3.59.

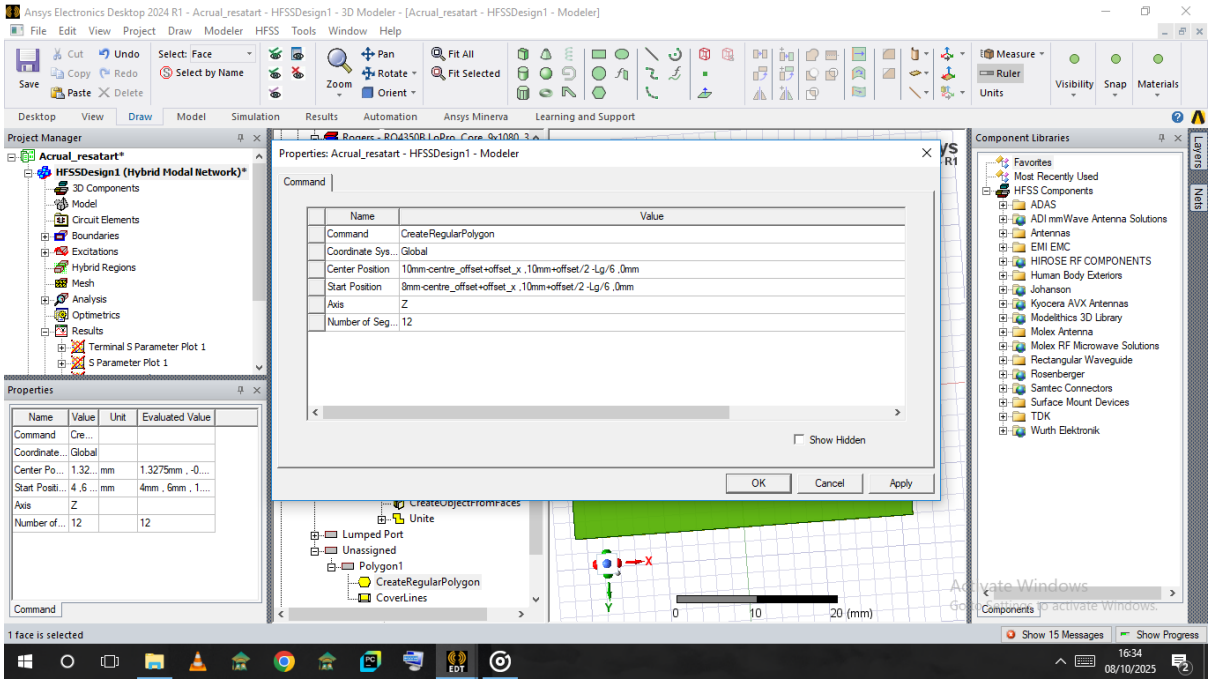

Figure 3.58: Dimensions of polygons

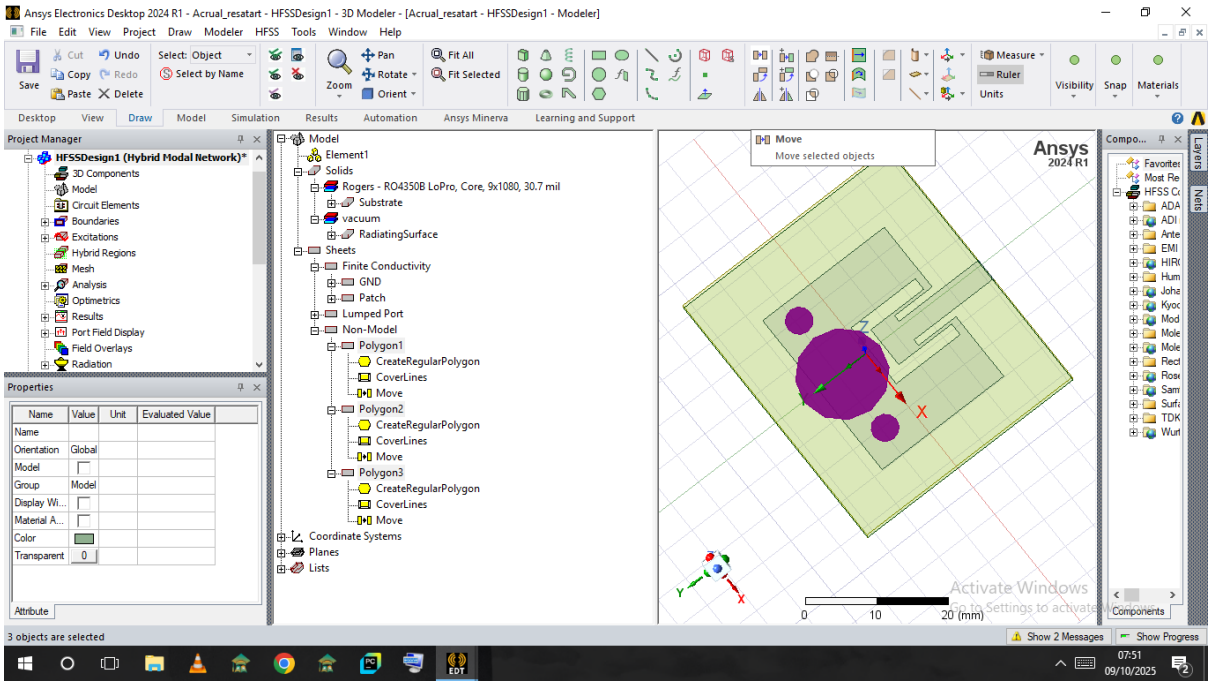

Figure 3.59: Polygons

(b) Subtract these polygons from the ground plane as shown in figure 3.60.

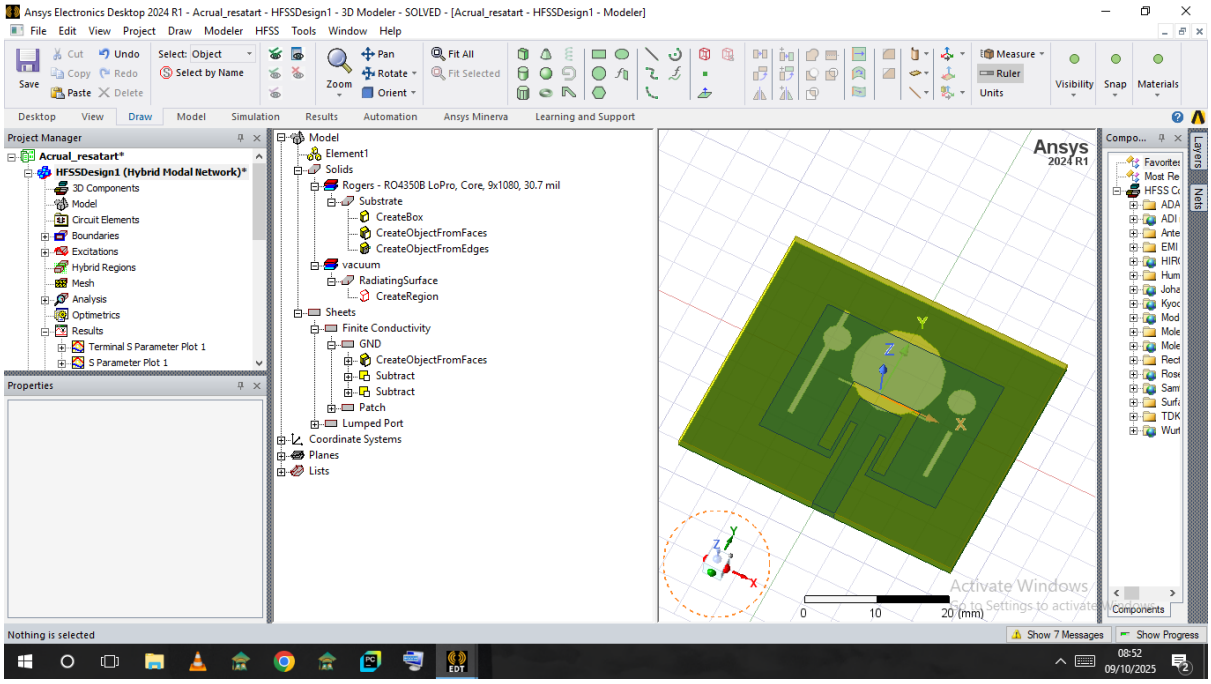

Figure 3.60: Subtracted Polygons from ground plane

(c) Move the three polygons to the specified position and create additional rectangles with defined dimensions as shown in figure 3.61 to 3.70.

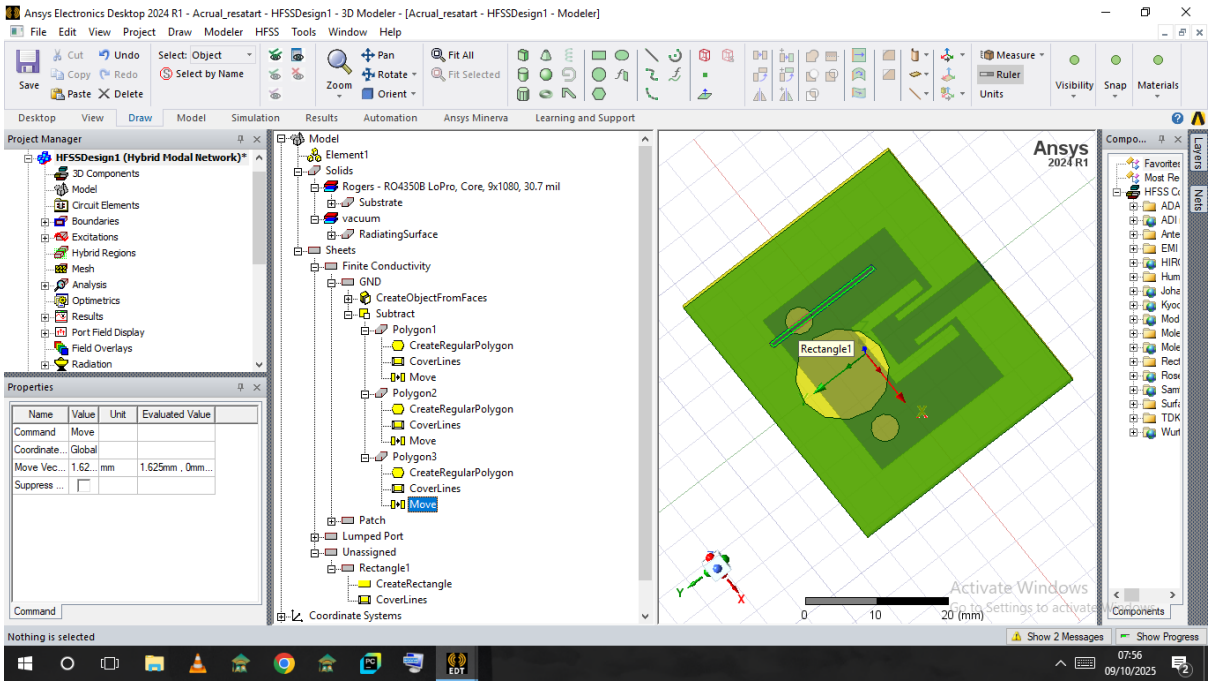

Figure 3.61: Additional Rectangle

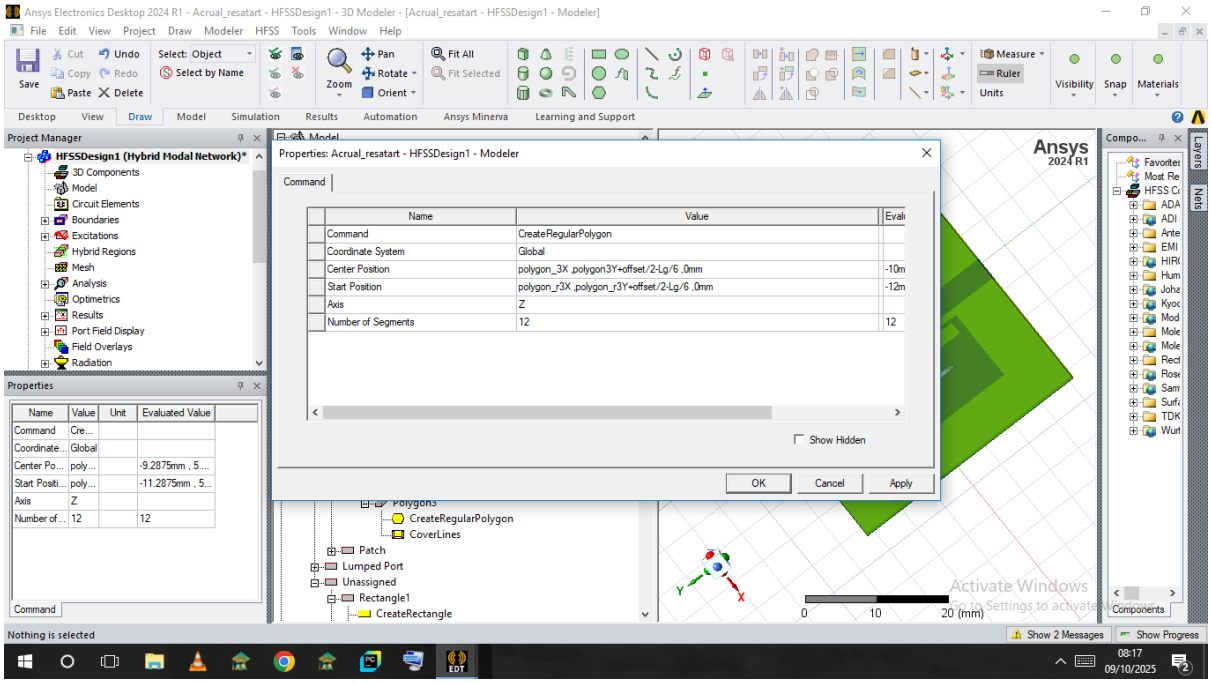

Figure 3.62: Dimensions and position of first polygon

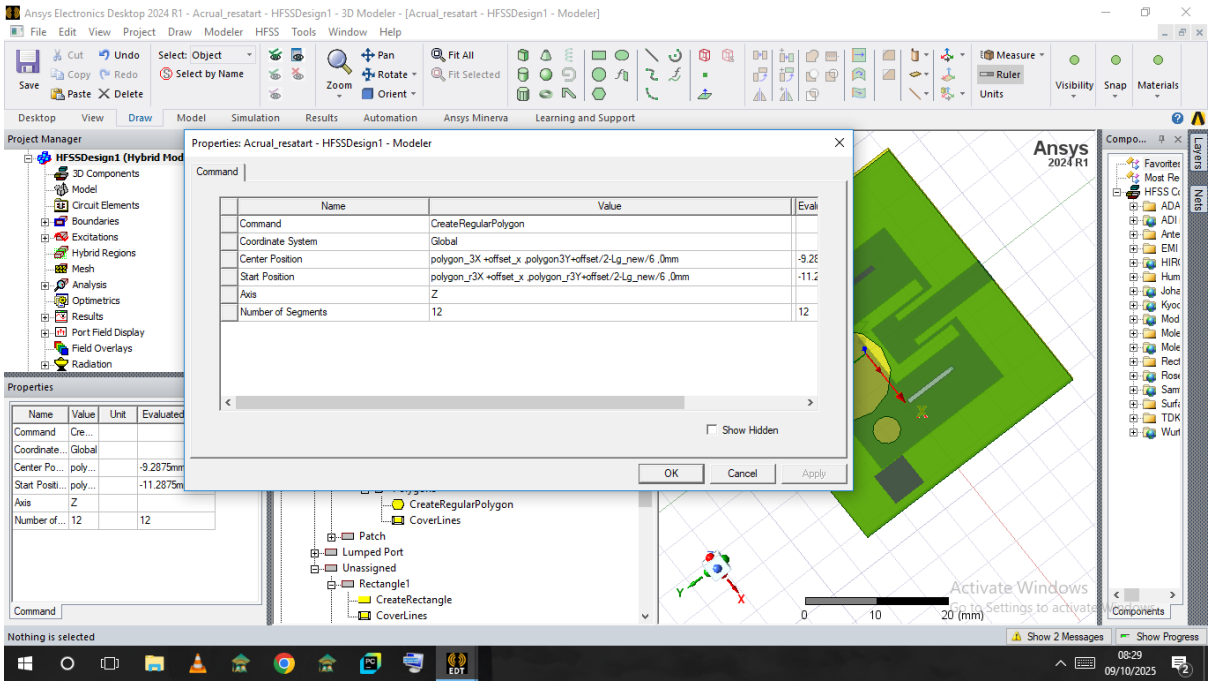

Figure 3.63: Dimensions and position of second polygon

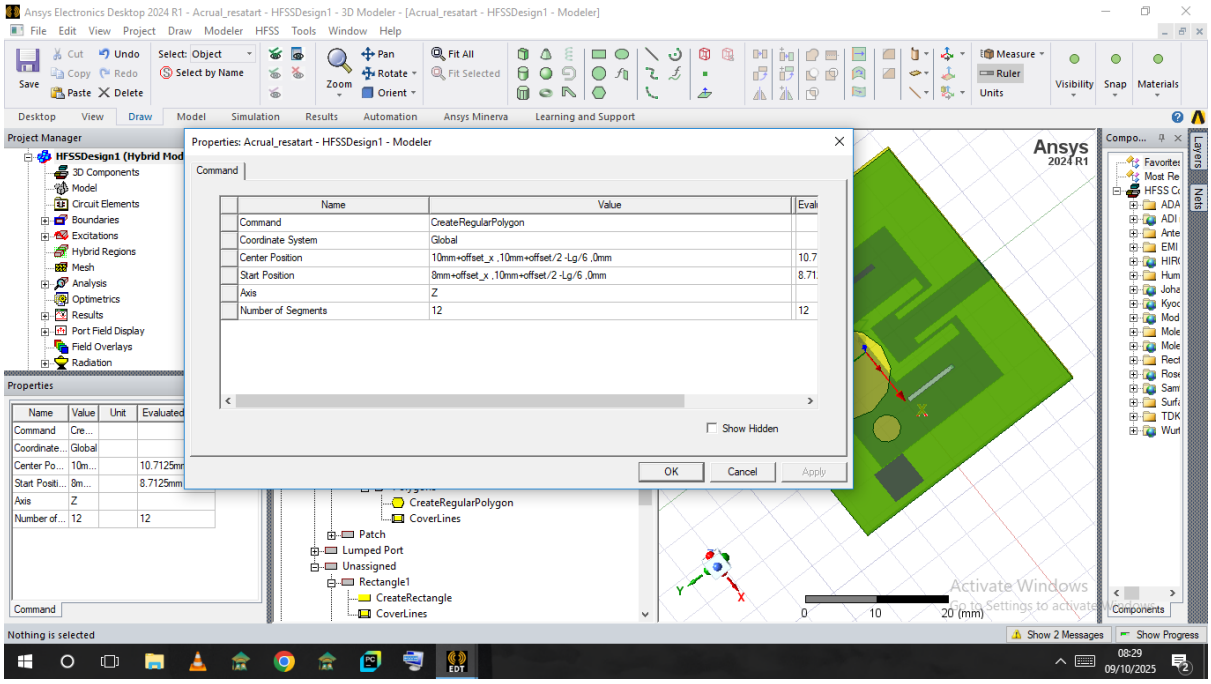

Figure 3.64: Dimensions and position of third polygon

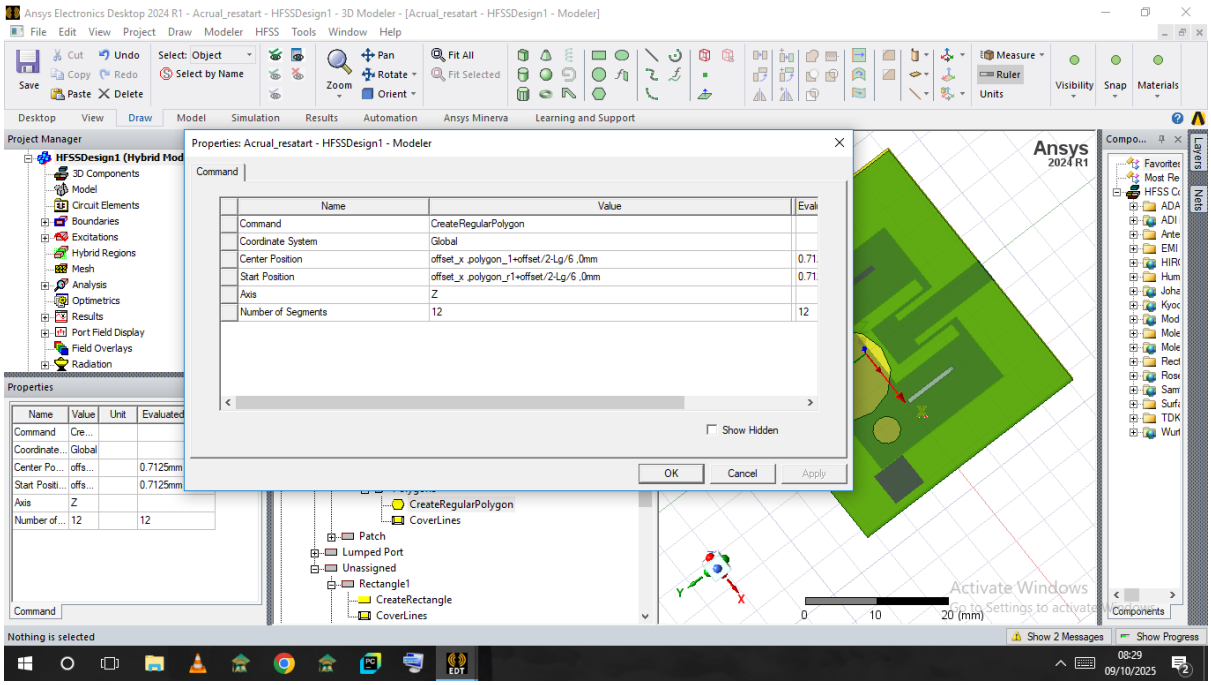

Figure 3.65: Dimensions and position of fourth polygon

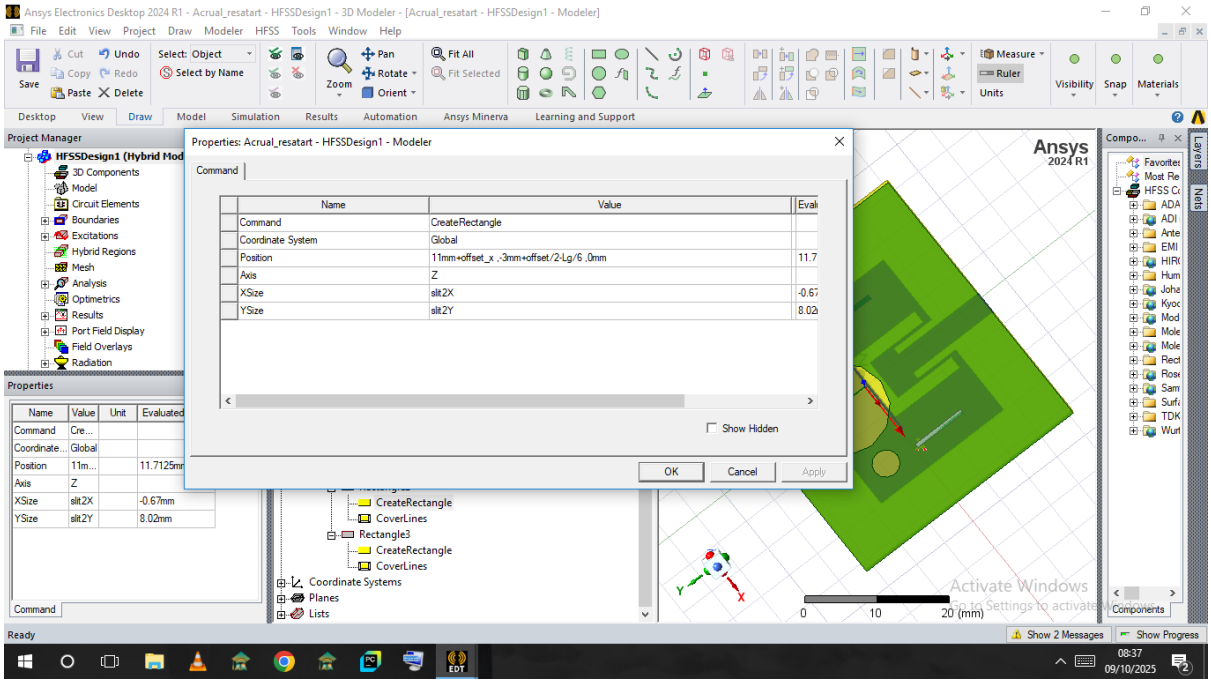

Figure 3.66: Dimensions and position of first rectangle

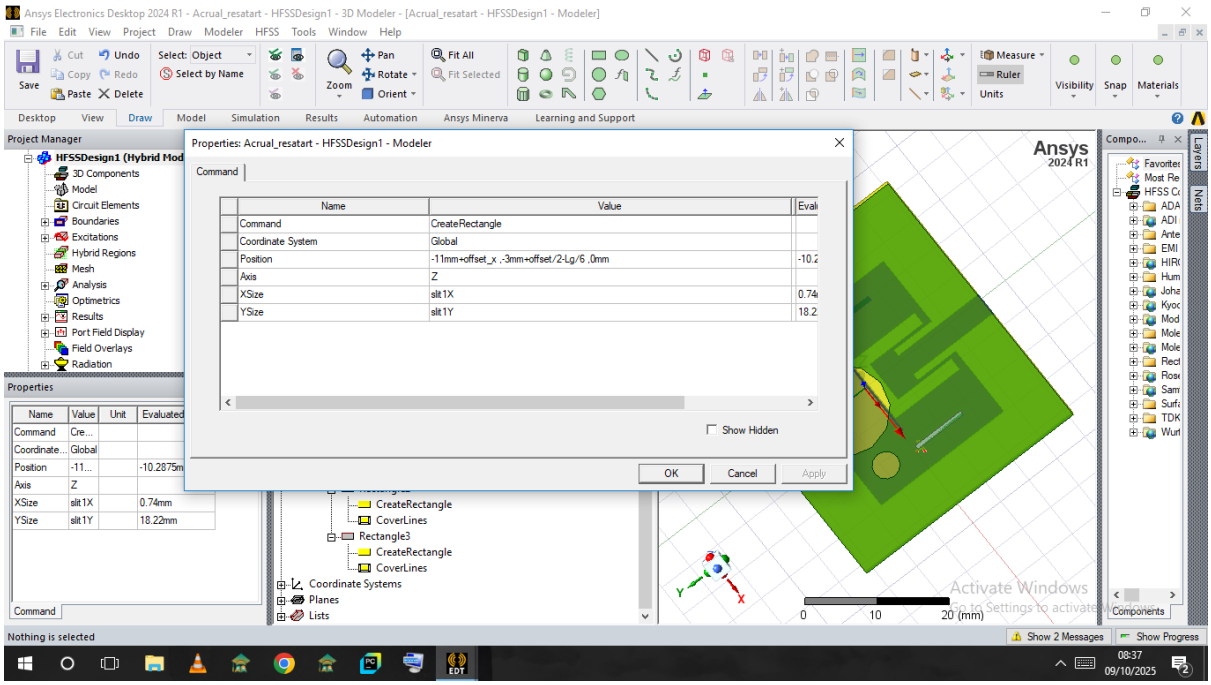

Figure 3.67: Dimensions and position of second rectangle

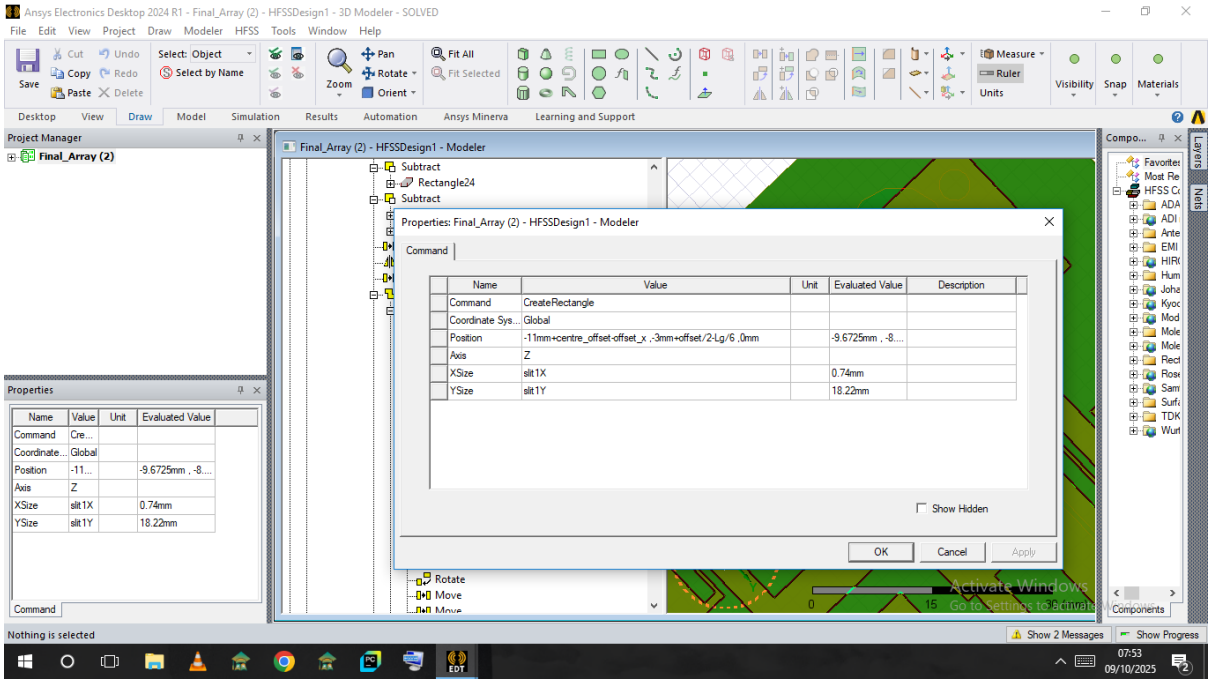

Figure 3.68: Dimensions and position of third rectangle

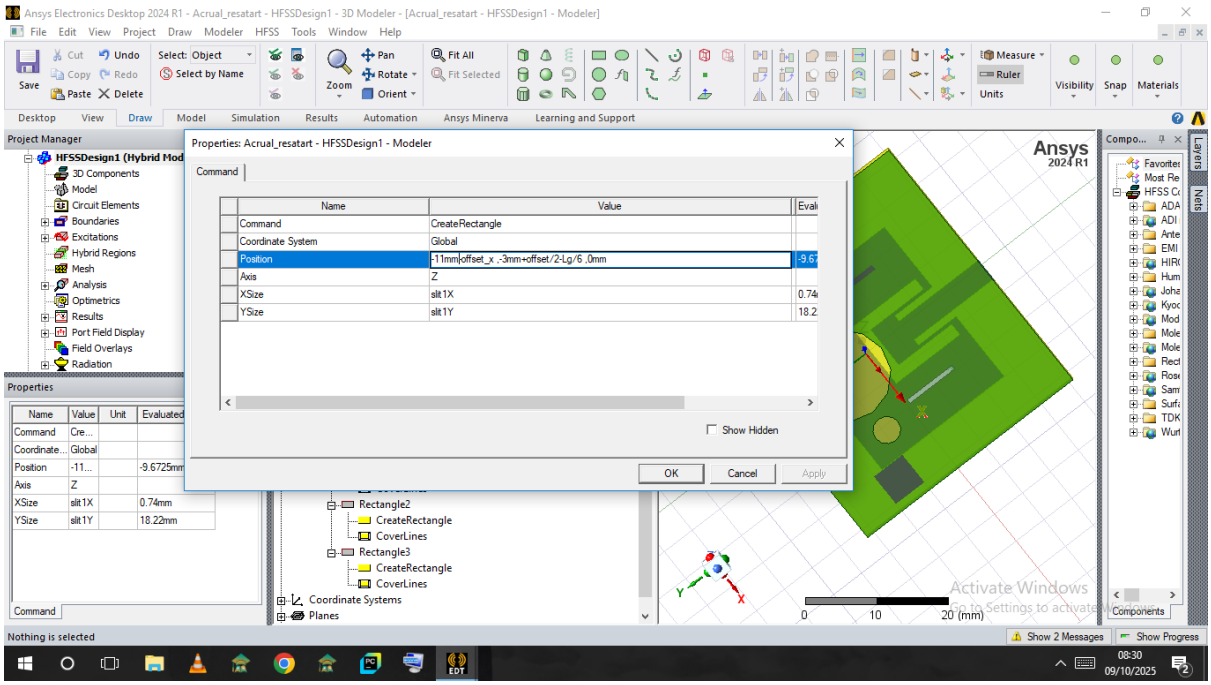

Figure 3.69: Dimensions and position of fourth rectangle

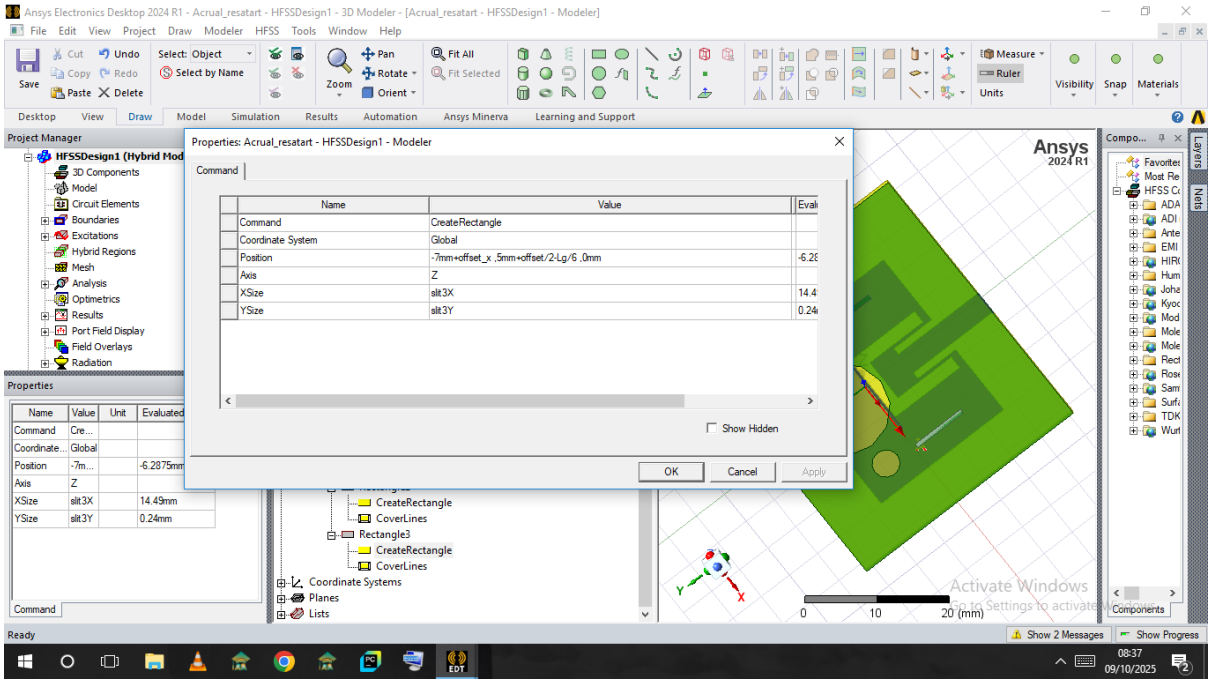

Figure 3.70: Dimensions and position of fifth rectangle

(d) Subtract these rectangles from the ground plane as shown in figure 3.71.

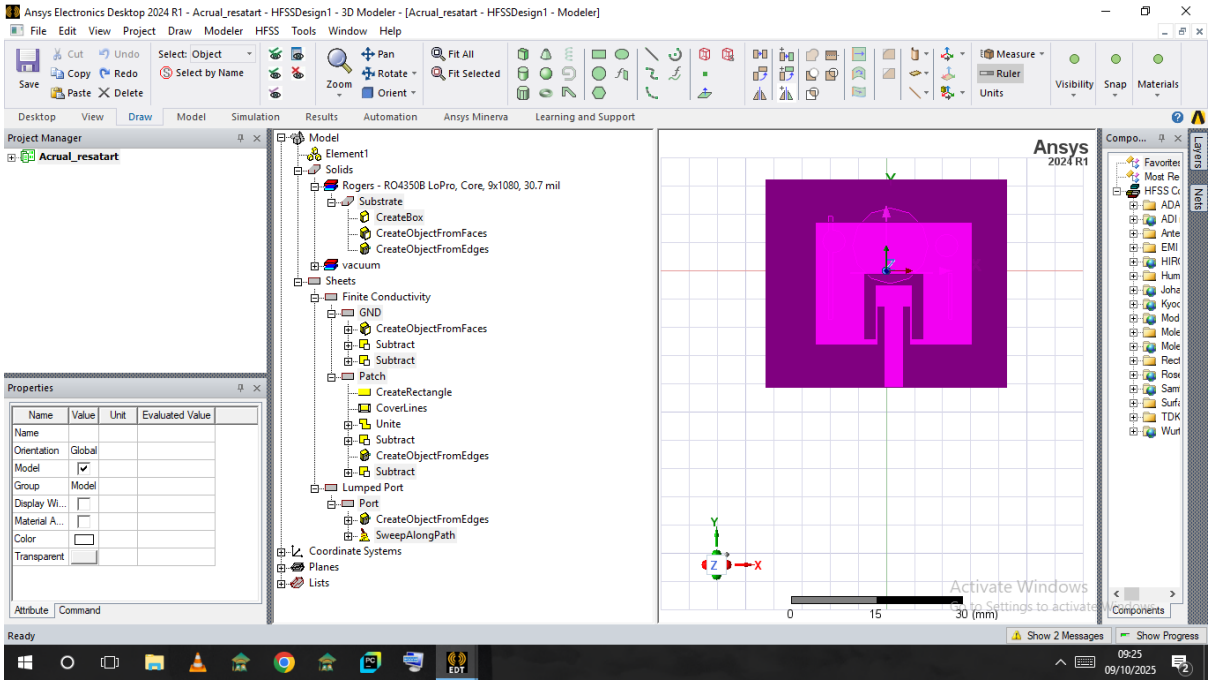

Figure 3.71: Complete DGS

(e) **Validate** and **Analyse** the new design.

3.3.4 Array Construction and Final Simulation

This final phase details the assembly and final analysis of the full array.

1. Select all components of the optimized single patch by pressing **Ctrl + A**.
2. Click on **Duplicate and Mirror** and set the angle to 180° to create a **2x1 array** as shown in figure 3.72.

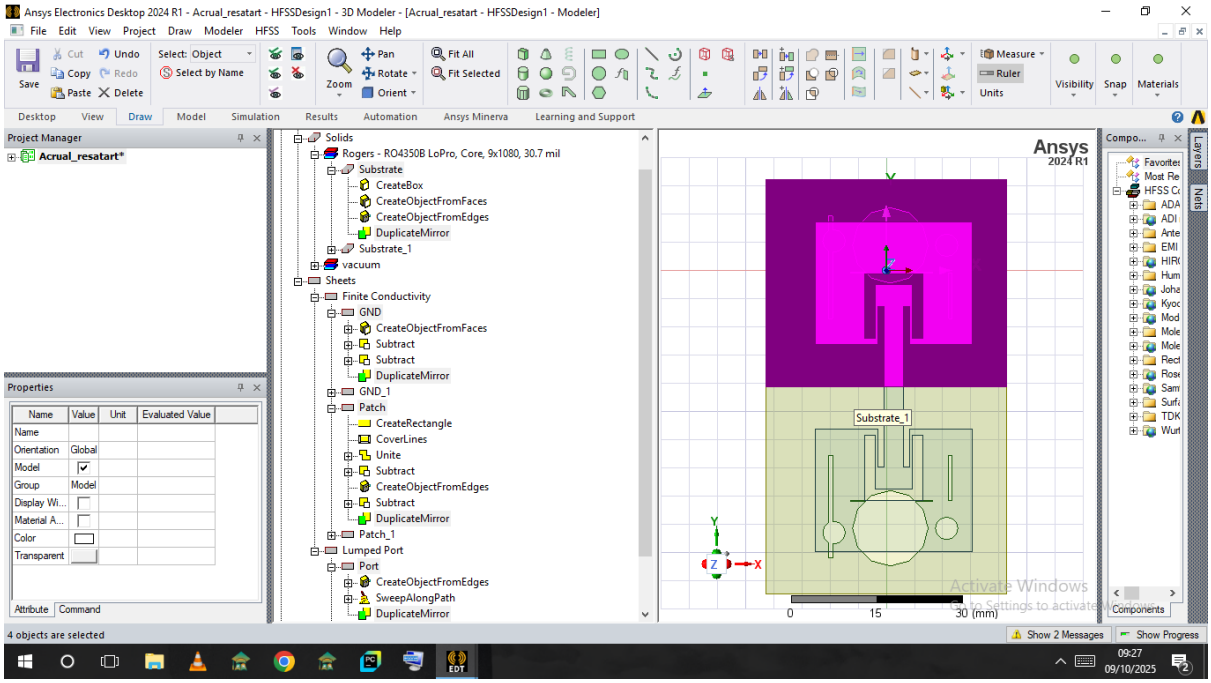

Figure 3.72: Duplicate and mirror the single patch

3. Create rectangular feed lines and unite them with the adjacent patches as shown in figure 3.73 to 3.75.

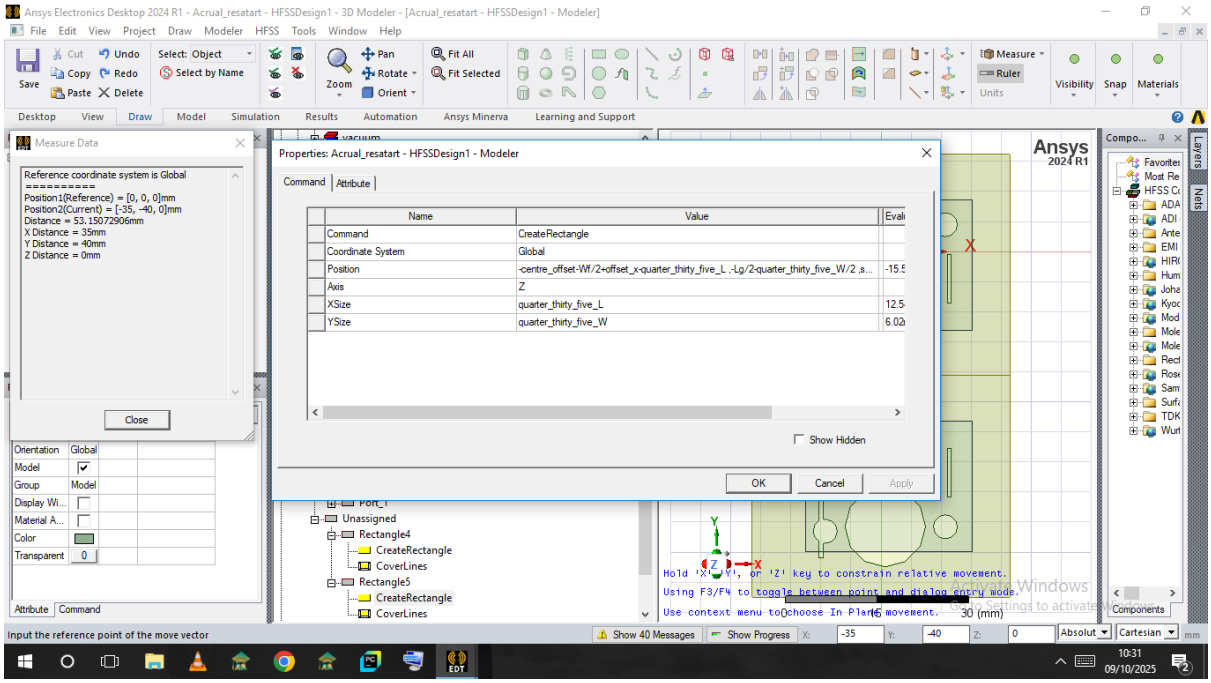

Figure 3.73: Dimensions and position of feedlines

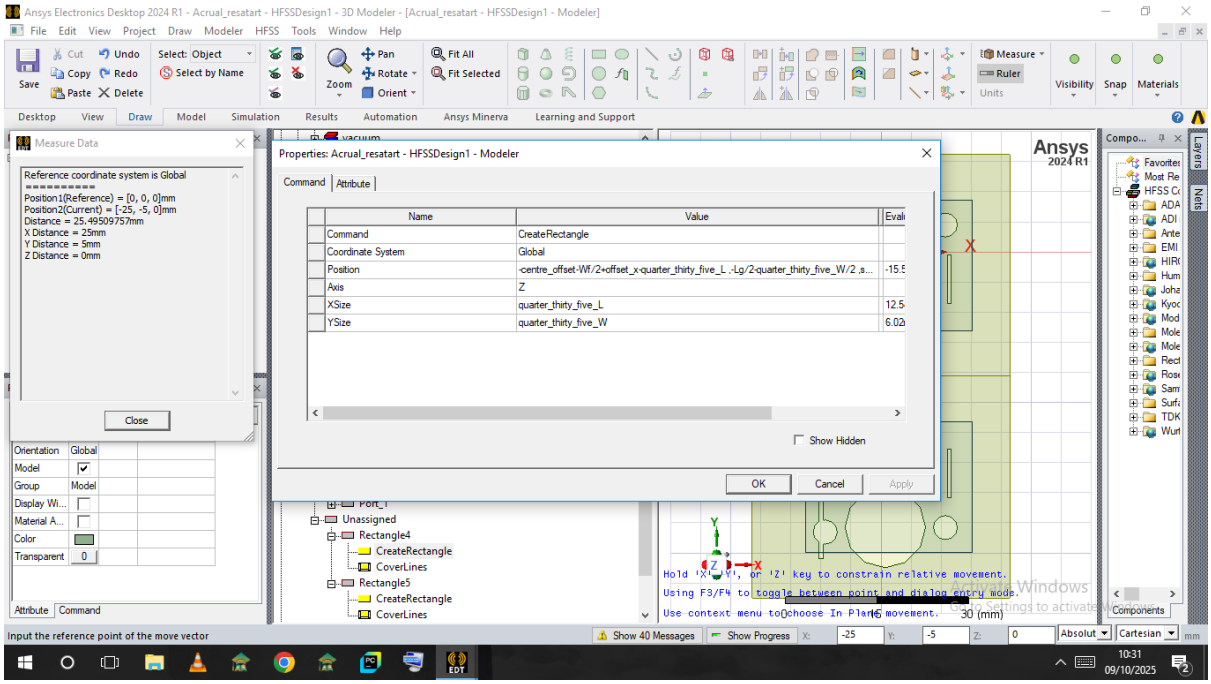

Figure 3.74: Dimensions and position of feedlines

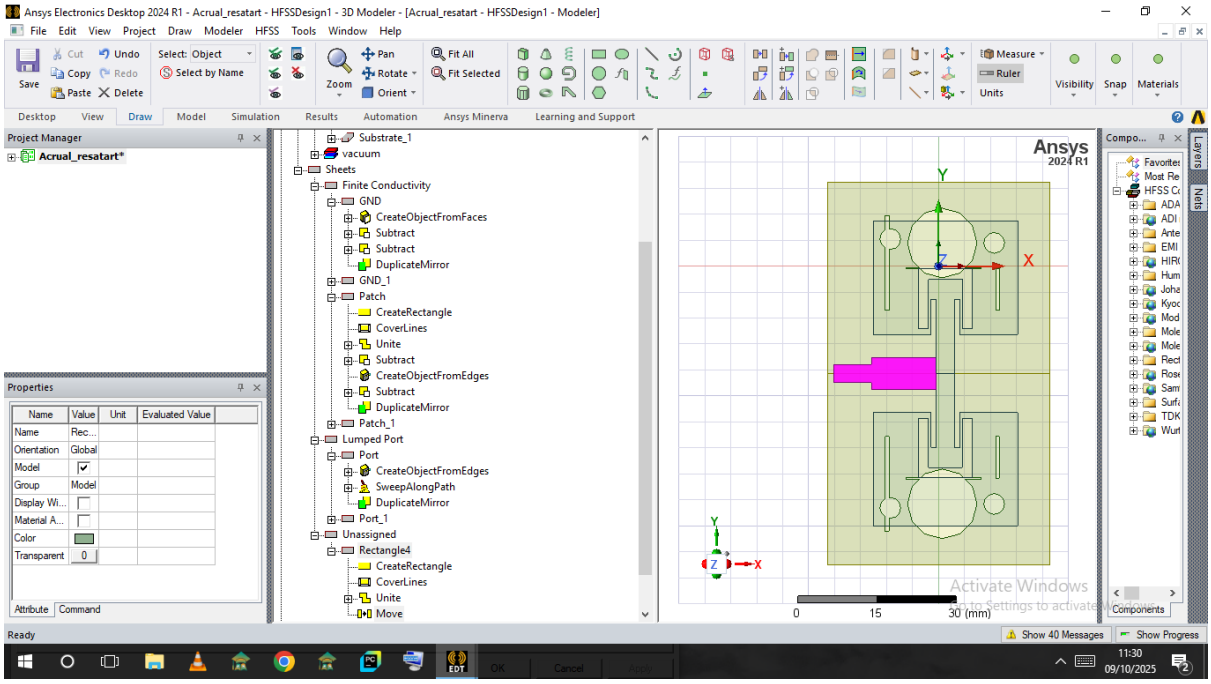

Figure 3.75: 2×1 array with feedlines

4. Select the entire **2x1 array** and use **Duplicate and Mirror** to create a **2x2 array**, then repeat to create the full **4x4 array** as shown in figure 3.76 to 3.83.

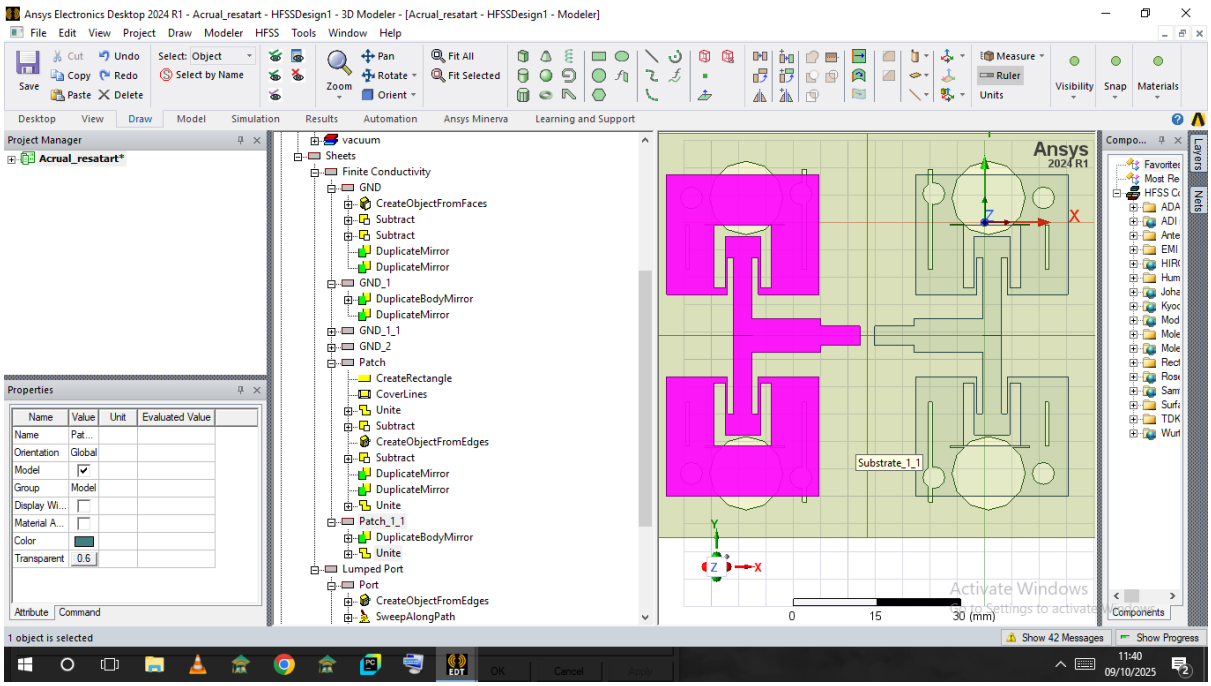

Figure 3.76: Duplicate and mirror the 2×1 array

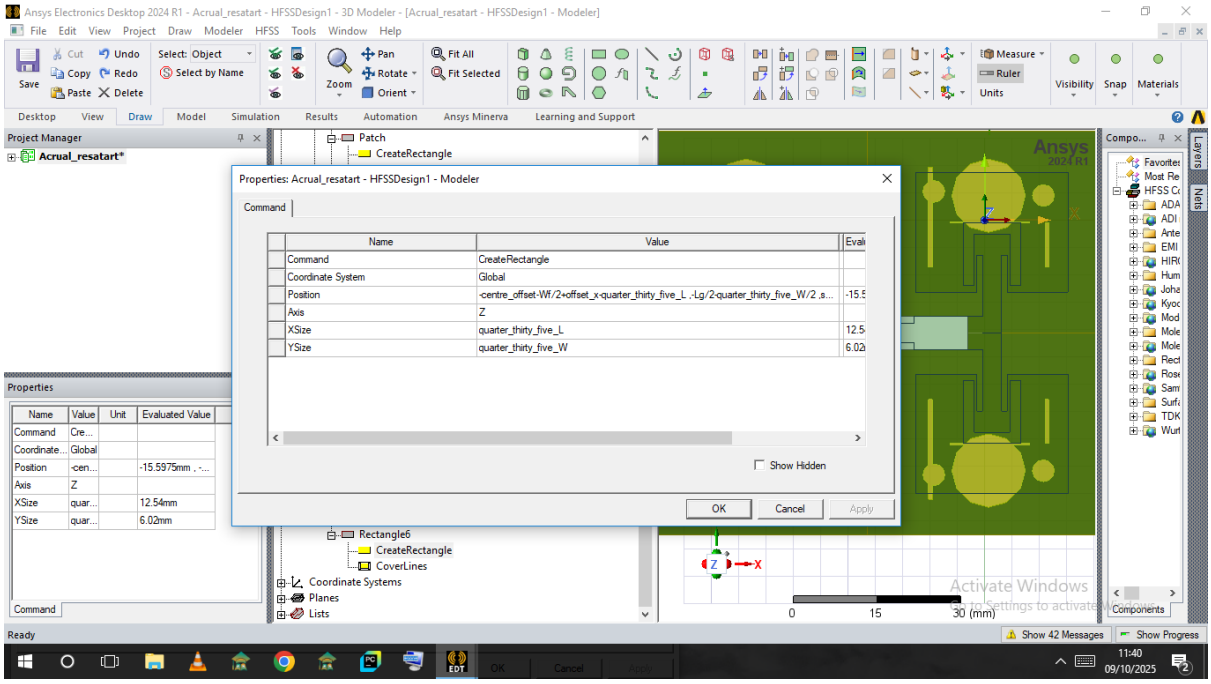

Figure 3.77: Dimensions and position of feedlines

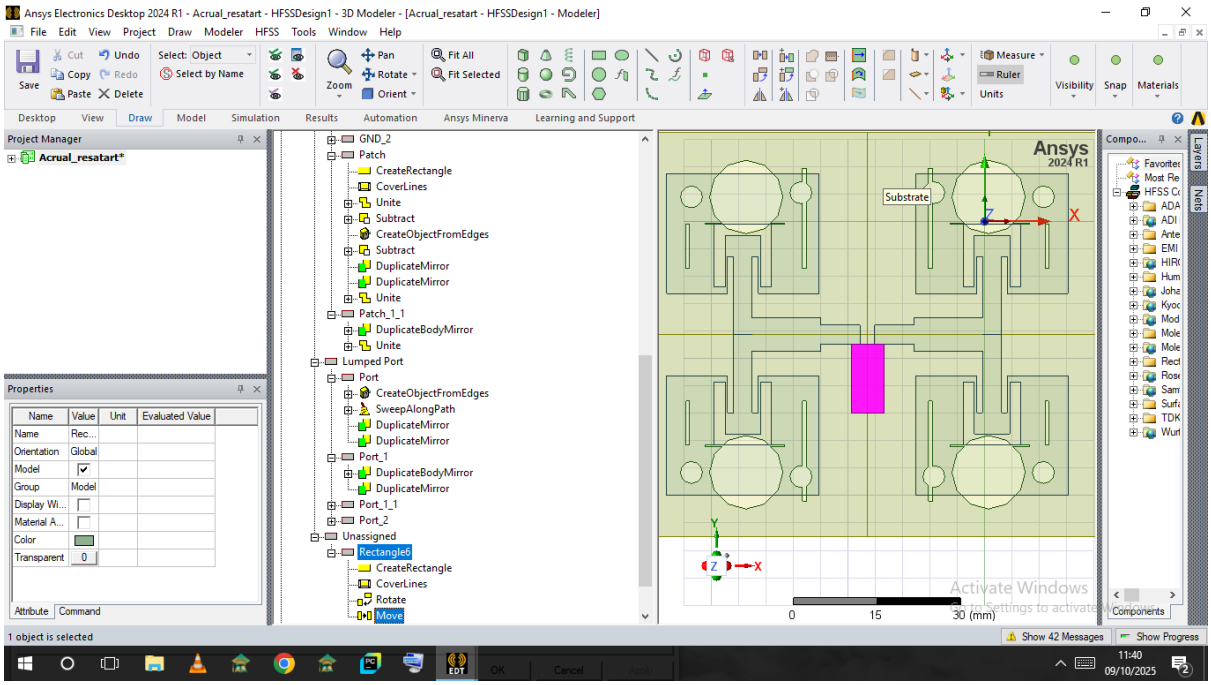

Figure 3.78: Feedlines

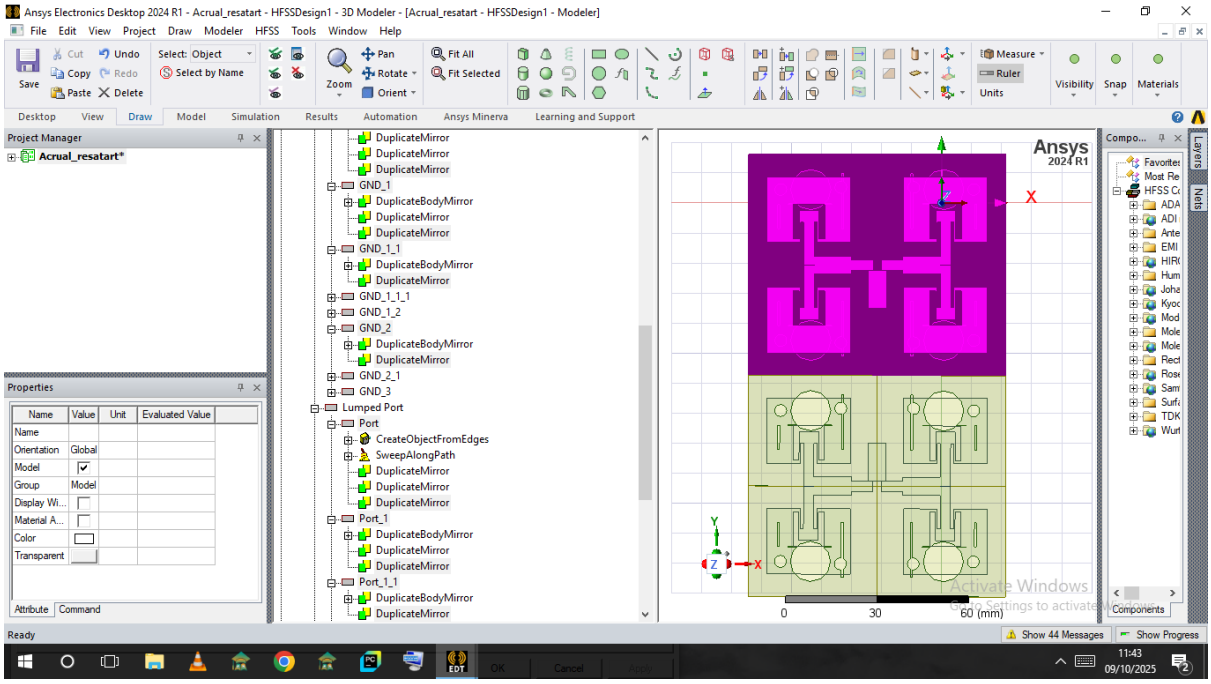

Figure 3.79: Duplicate and mirror the 2×2 array

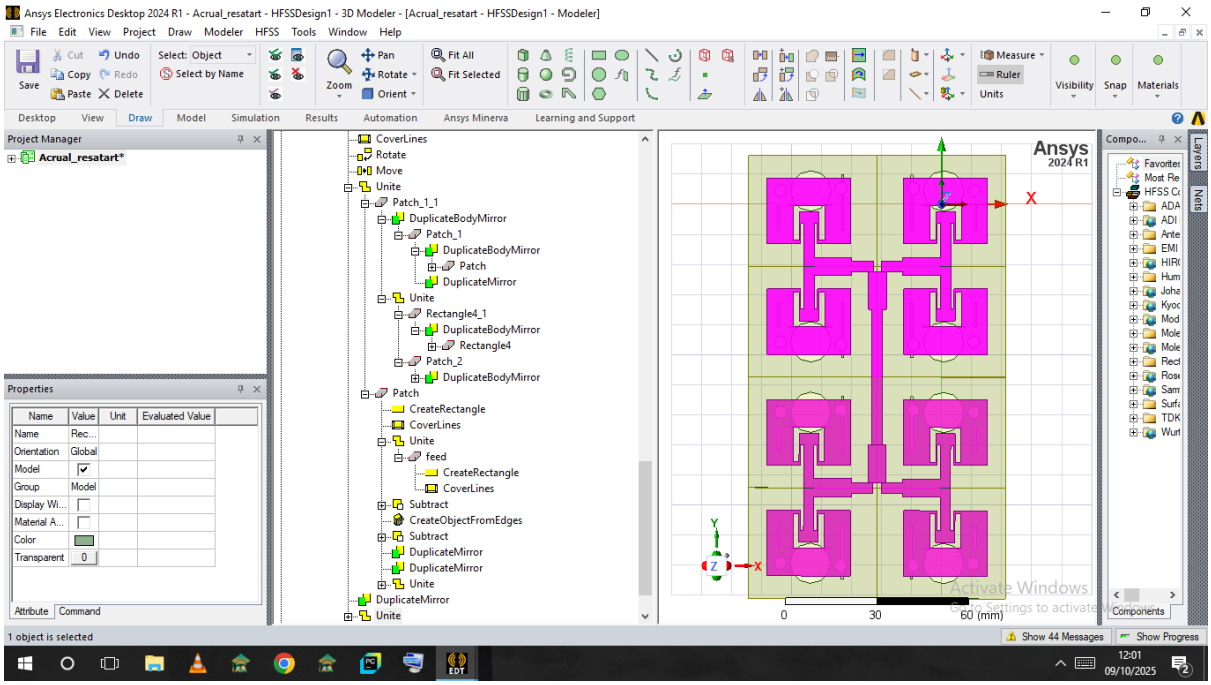

Figure 3.80: 4×2 array

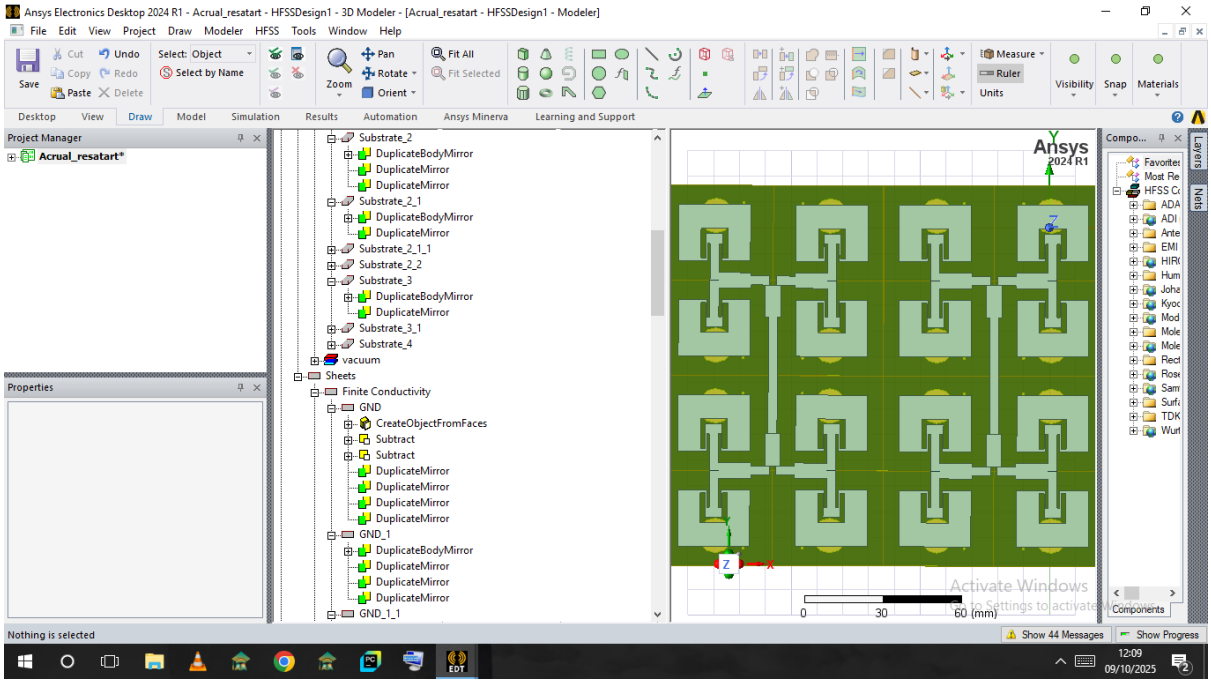

Figure 3.81: Duplicate and mirror the 4 × 2 array

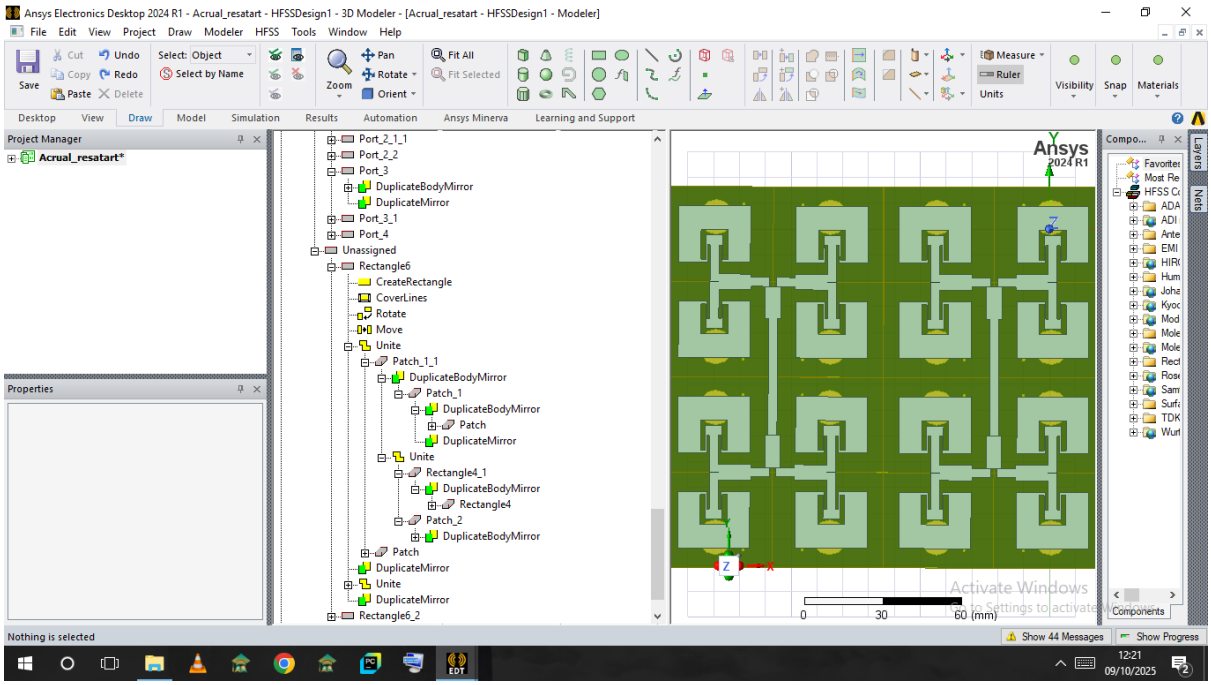

Figure 3.82: 4 × 4 array

5. Join the feed lines as shown in the reference layout as shown in figure 3.83.

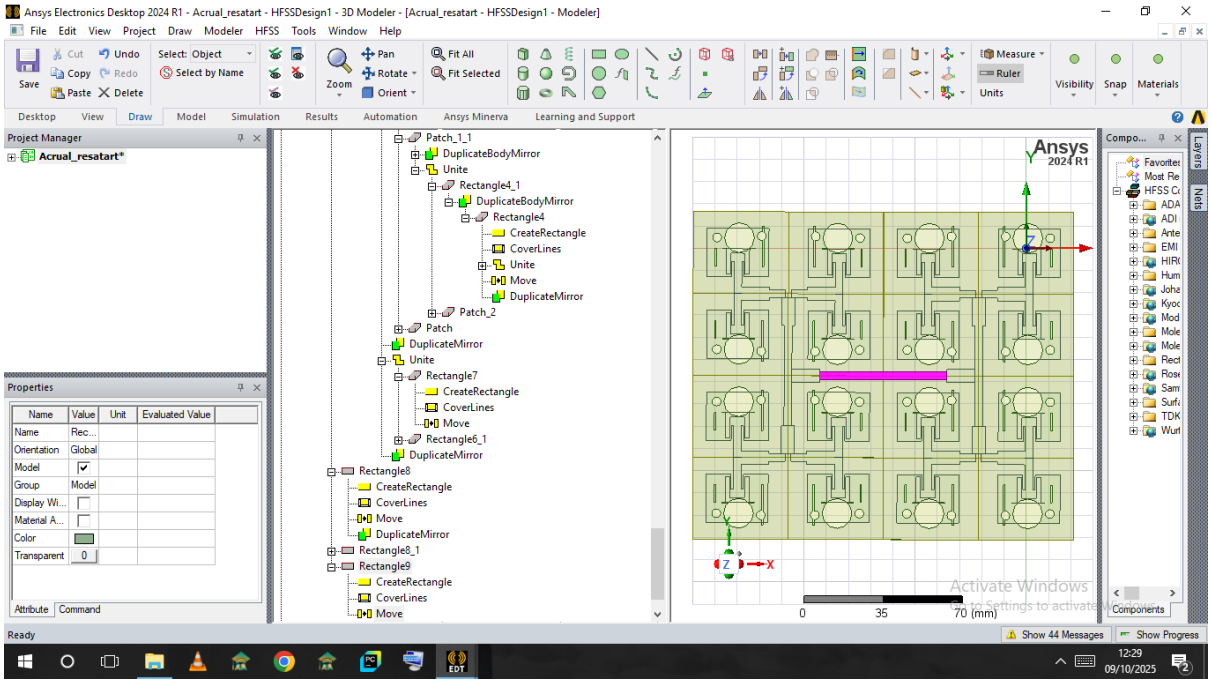

Figure 3.83: Join the feedlines

6. Unite all substrates, all ground planes, and all adjacent patches as shown in figure 3.84.

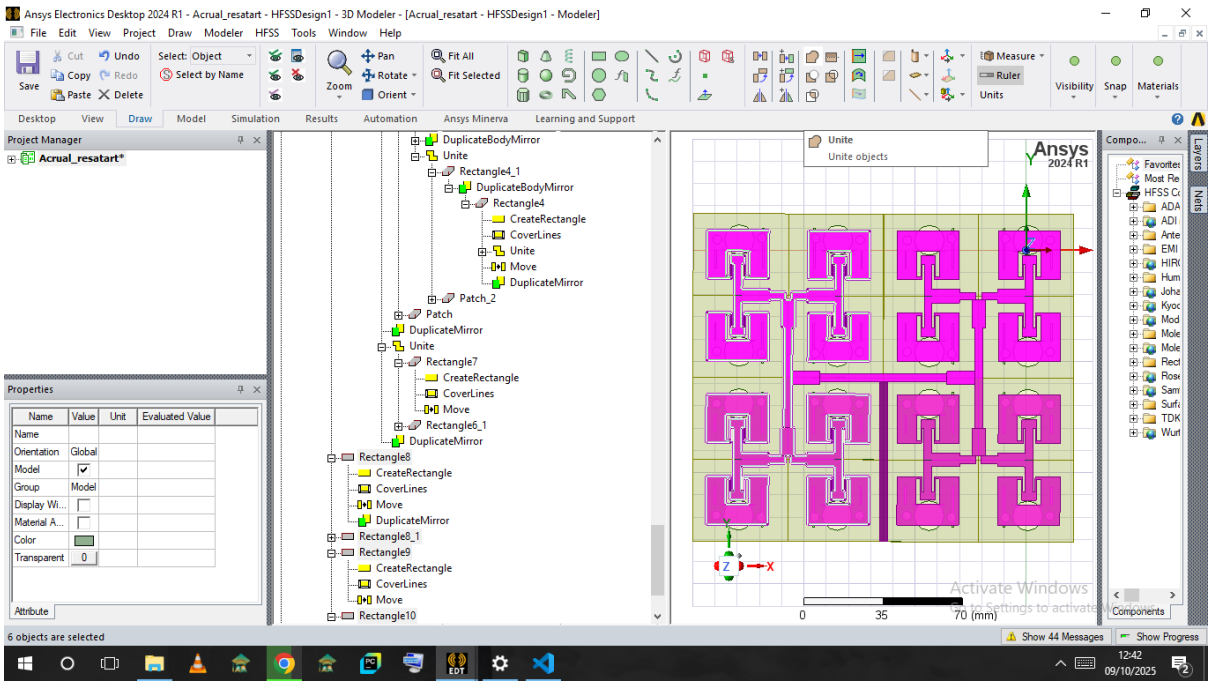

Figure 3.84: Unite all patches and ground planes

7. Delete any old ports and boundaries.

8. Right-click `patch` and `GND`, and assign **Finite Conductivity** boundaries.

9. Create a new port and define an open region as shown in figure 3.85 to 3.87.

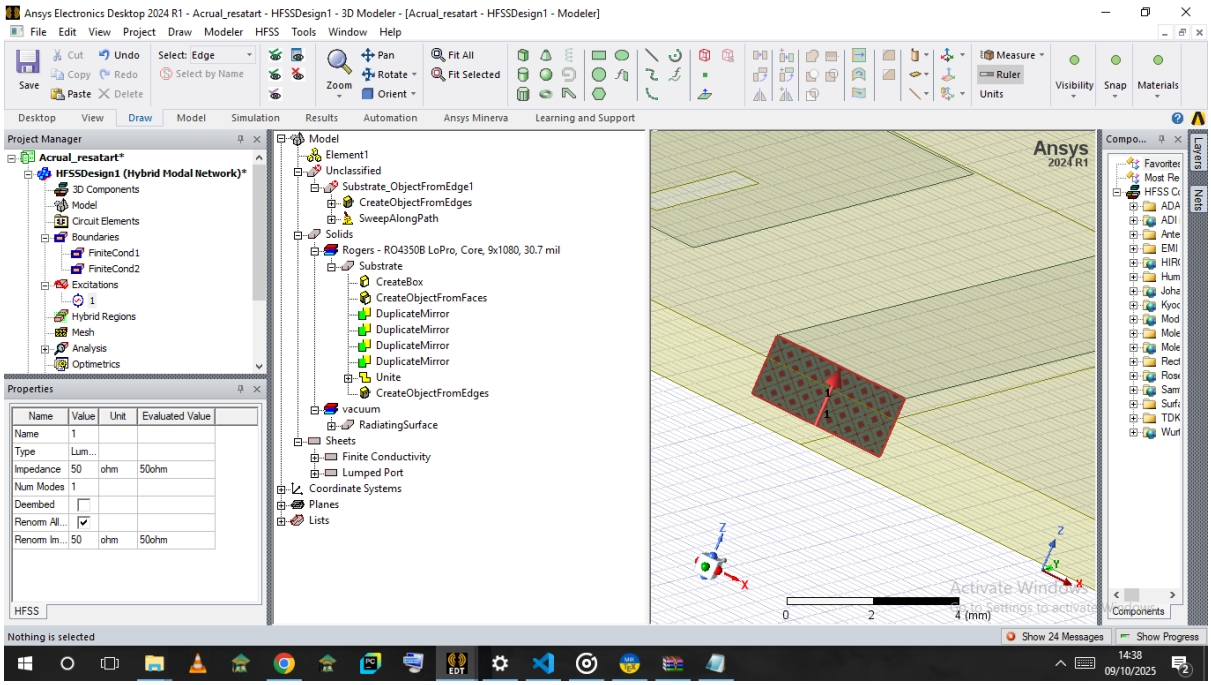

Figure 3.85: Create a new port

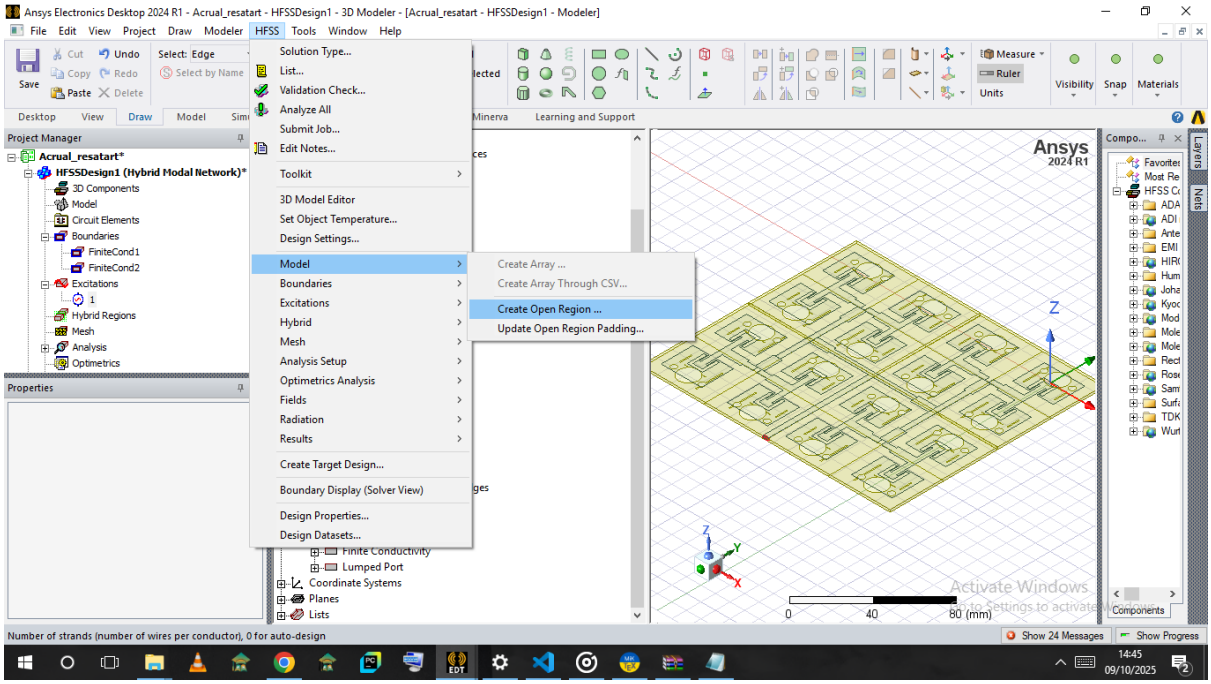

Figure 3.86: Create open region

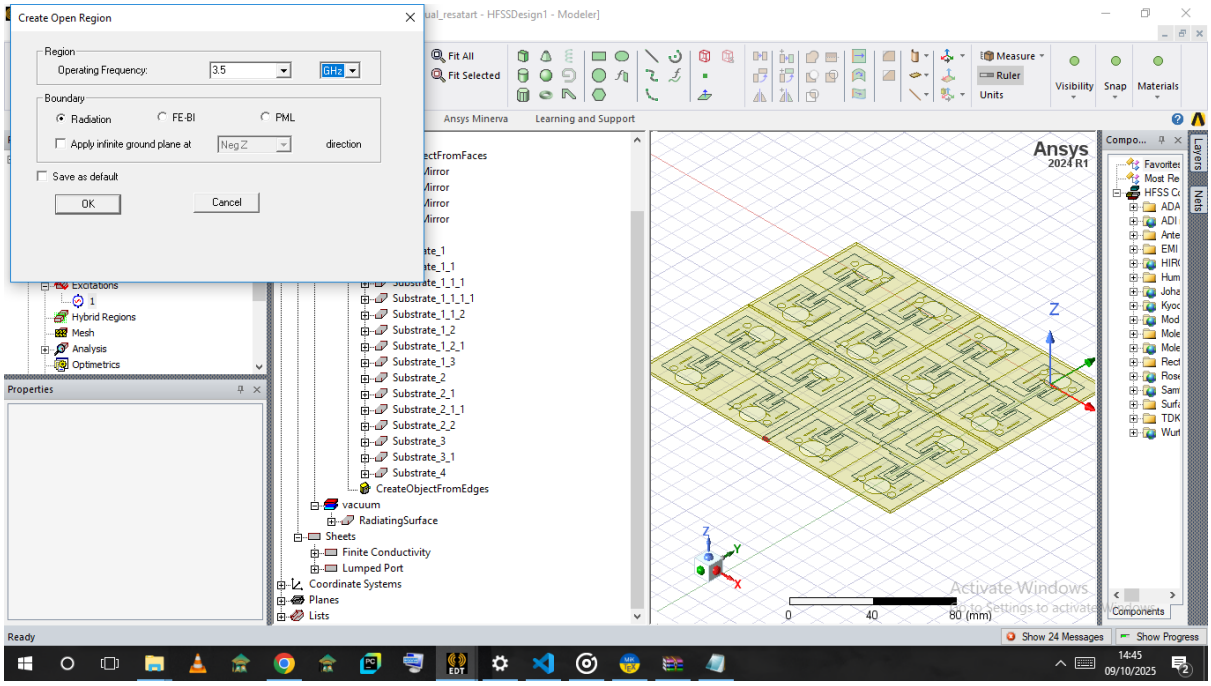

Figure 3.87: Click OK

10. **Validate** and **Analyse** the complete **4x4 array design**.

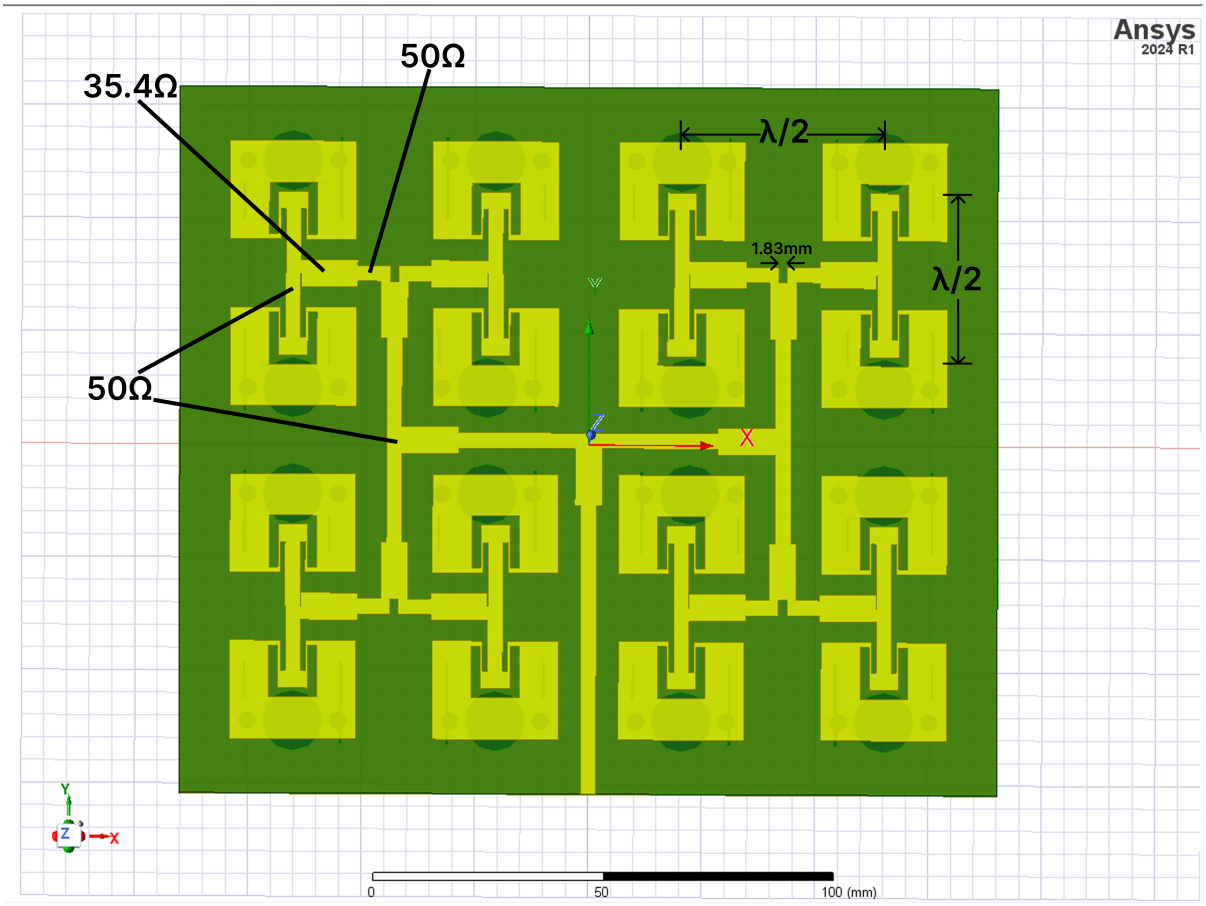

Figure 3.88: Final Array

Chapter FOUR

OUTCOMES AND DISCUSSION

4.1 Introduction

This section outlines and examines our simulated outcomes based on the design of a 4×4 microstrip patch antenna configuration featuring U-slots and a Defected Ground Structure (DGS) for sub-6 GHz 5G applications, utilizing ANSYS HFSS. The addition of U-slots in the radiating components was focused on expanding the frequency response range, while the implementation of DGS on the ground plane was intended to enhance impedance matching, mitigate surface waves, and enhance overall radiation performance. The primary performance metrics of this evaluated antenna includes return loss (S_{11}), Voltage Standing Wave Ratio (VSWR), gain, bandwidth, radiation pattern, surface current distribution, and radiation efficiency.

4.2 Simulation Results Overview

The individual microstrip patch antenna (MPA) and the 4×4 MPA array featuring U-slots and DGS were created, simulated, and fine-tuned using ANSYS HFSS. The findings generated from the simulations are presented in Table 4.1, highlighting the significant performance improvement achieved in the array configuration.

Table 4.1: Overview of modeled antenna performance metrics

Parameter	**Symbol**	**Simulated Value**
Resonant Frequency	f_r	3.5 GHz
Return Loss	S_{11}	–19.96 dB
Bandwidth (at –10 dB)	B_w	180 MHz
Gain	G	10.64 dBi
VSWR	—	1.22
Radiation Efficiency	η	72.3%

4.3 Return Loss (S_{11})

Figure 4.1 shows the modeled return loss for the individual MPA, exhibiting a minimum S_{11} of –17.44 dB and a –10 dB impedance bandwidth of approximately 57.5 MHz.

As illustrated in Figure 4.2, the 4×4 MPA array with U-slots and DGS demonstrates a significantly improved return loss of -19.96 dB and a wider bandwidth of 180 MHz at 3.5 GHz. This improvement can be attributed to the combined effect of the U-slots and DGS, which improve impedance matching and decrease surface wave losses.

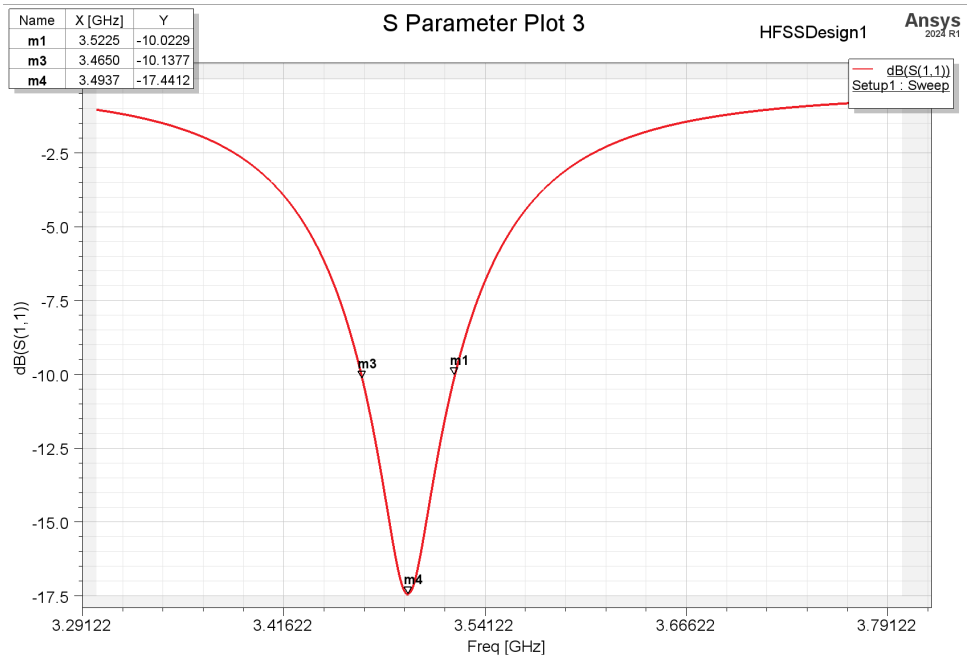

Figure 4.1: Modeled return loss (S_{11}) for the single MPA.

4.4 Voltage Standing Wave Ratio (VSWR)

The VSWR of the designed array is shown in Figure 4.3. At the resonant frequency of 3.5 GHz, the VSWR is approximately 1.22, showing effective impedance matching between the feed line and the antenna. This value satisfies the standard condition for efficient power transfer, where VSWR ≤ 2.

4.5 Radiation Pattern and Gain

Figures 4.5a and 4.5b display the 2D and 3D radiation patterns for the single MPA, which demonstrates a peak gain of 5.79 dBi. The radiation is mainly oriented perpendicular to the patch surface, aligning with expectations for the fundamental TM_{10} mode.

For the 4×4 array with U-slots and DGS, the radiation characteristics shown in Figures 4.5a and 4.5b reveal a peak gain of 10.64 dBi, demonstrating a substantial enhancement due to array directivity and reduced surface wave interference. The main lobe is well-defined, showing significant constructive interference among the array components.

4.6 Surface Current Distribution

Figure 4.8 demonstrates the surface current distribution on the 4×4 MPA array at the resonant frequency of 3.5 GHz. It is noticeable that the surface currents are primarily concentrated along the edges of the patches and the feeding lines, highlighting significant

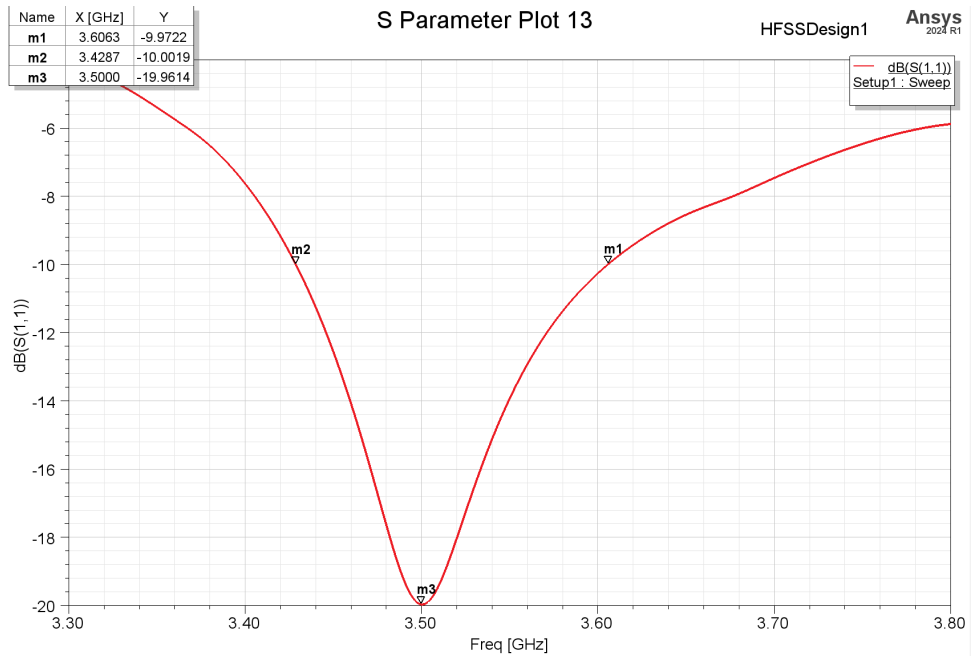

Figure 4.2: Simulated return loss (S_{11}) for the 4×4 MPA array with U-slots and DGS.

coupling and efficient radiation. The presence of U-slots alters the current path, effectively lengthening it and thereby enhancing bandwidth, while the DGS modifies the ground-plane current distribution, improving impedance matching.

4.7 Discussion

The integration of U-slots and a DGS significantly improved the antenna's overall performance compared to the conventional patch structure. The U-slots enhanced the effective current path and bandwidth, while the DGS reduced surface wave losses and improved impedance characteristics. The array configuration resulted in higher gain and directivity, suitable for sub-6 GHz 5G communication systems. The simulated outcomes confirm that the designed 4×4 MPA array offers a good compromise among compactness, gain, and bandwidth, making it a viable candidate for 5G base-station or end-user applications.

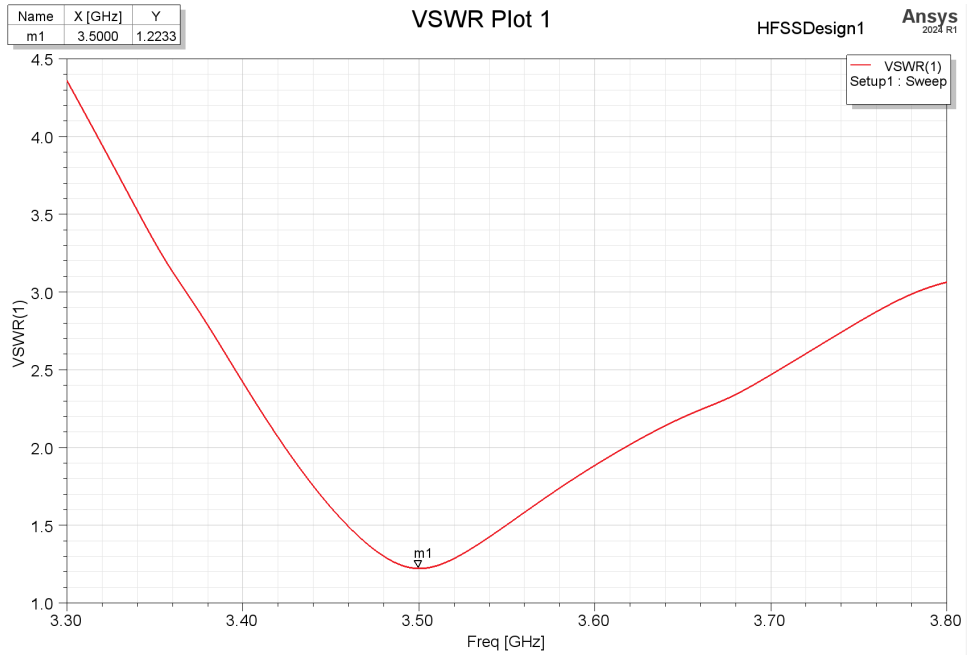

Figure 4.3: VSWR plot for the 4×4 MPA array with U-slots and DGS.

4.8 Comparative Performance Evaluation

To validate the improvement achieved through the U-slot and DGS designs, Table 4.2 contrasts the modelled array with comparable studies documented in existing literature.

Table 4.2: Comparison of the suggested antenna with existing 5G array configurations

Reference	**Configuration**	**Gain (dBi)**	**Bandwidth (MHz)**
Proposed Design	4×4 U-slot + DGS	10.64	180
Irfansyah et al. (2021)	1×2 conventional array	5.5	66.5
Jiménez et al. (2023)	4×4 slot Array	8.03	80
Reynalda et al. (2011)	4×4 high gain Array	16.02	150
Aswoyo et al. (2021)	4×4 high gain Array	12.15	61.7
Hossain et al. (2023)	Slotted patch antenna + DGS	6.463	69.2

From Table 4.2, it is evident that although some reported works, such as those by Reynalda et al. (2011) and Aswoyo et al. (2021), achieved higher peak gains of 16.02 dBi and 12.15 dBi respectively, their corresponding impedance bandwidths remain relatively narrow, typically below 150 MHz. In contrast, the proposed 4×4 U-slot patch array with DGS achieved a measured gain of 10.64 dBi while maintaining a significantly broader bandwidth of 180 MHz.

The enhancement in bandwidth serves as a direct confirmation of the intended design goal of improving impedance matching and frequency stability throughout the sub-6 GHz range. By incorporating U-slots within the radiating elements and utilizing a defected ground structure, the resonant modes have been effectively expanded, allowing the antenna to accommodate a broader operational frequency range suitable for the new 5G

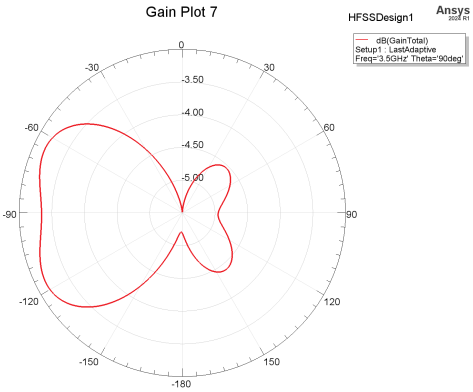

Figure 4.4: (a) 2D radiation pattern of the single MPA.

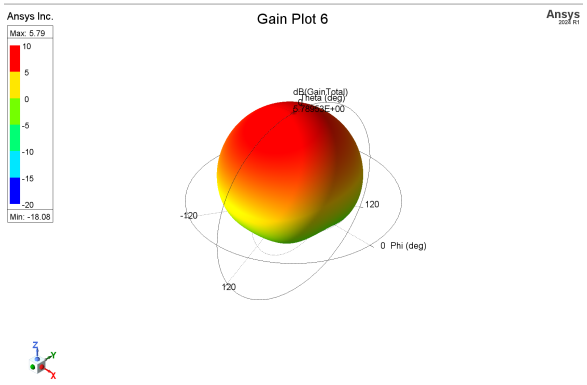

Figure 4.5: (b) 3D radiation pattern of the single MPA.

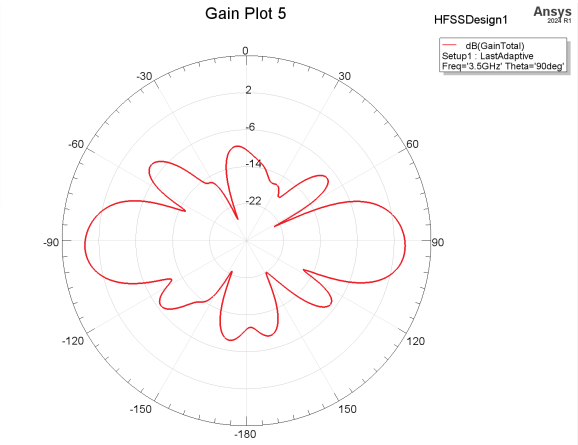

Figure 4.6: (a) 2D radiation pattern of the 4×4 MPA array.

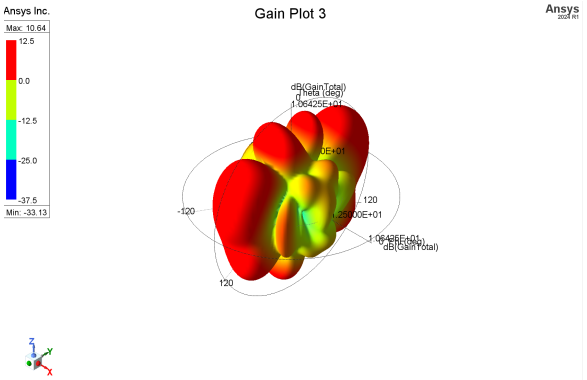

Figure 4.7: (b) 3D radiation pattern of the 4×4 MPA array.

NR bands (such as n77/n78).

While the gain is somewhat lower compared to certain high-gain designs documented in previous studies, the proposed configuration presents a better balance between bandwidth, compactness, and ease of fabrication. Additionally, higher-gain designs typically necessitate intricate feeding networks, extra parasitic layers, or larger physical sizes, which can elevate costs and limit integration capabilities.

Consequently, the proposed design is particularly relevant for applications in 5G base stations and user terminals, where wideband coverage, a low profile, and integration ease are prioritized over slight gain advantages.

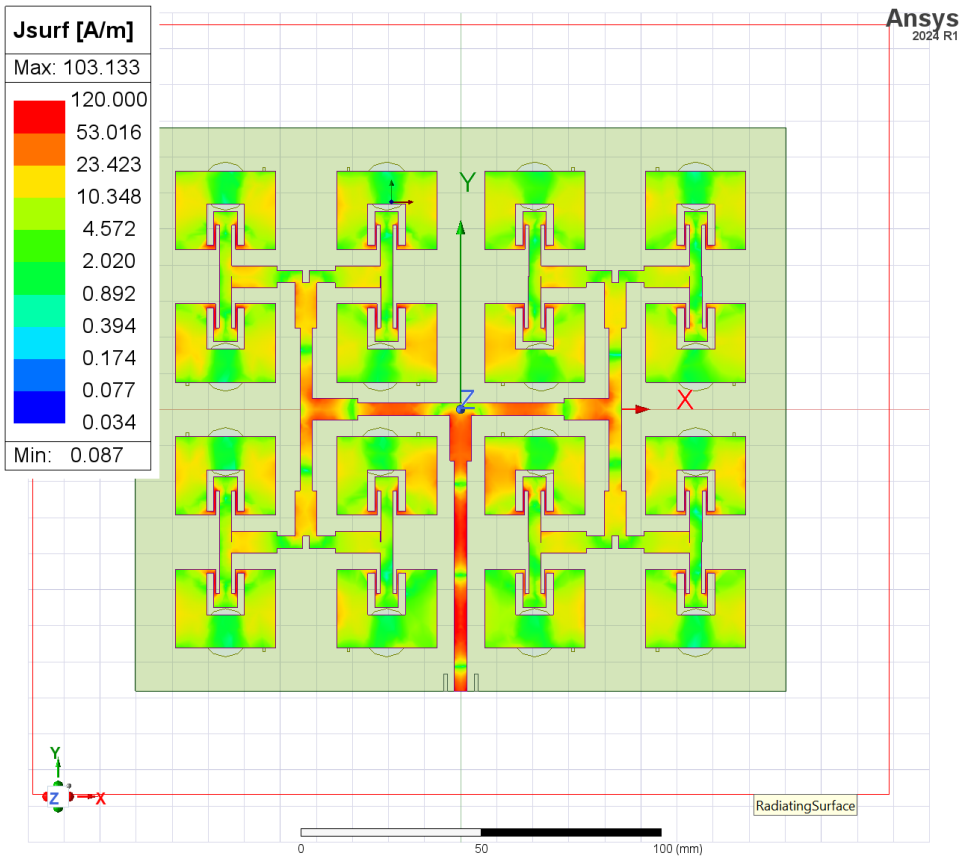

Figure 4.8: Surface current distribution on the 4×4 MPA array with U-slots and DGS.

4.9 Discussion of Results

This segment provides a comprehensive examination of how incorporating U-slots and Defected Ground Structure (DGS) in the proposed 4×4 microstrip patch antenna array affects its performance for sub-6 GHz 5G applications. The design evolution is examined in three stages: (i) conventional array without U-slots and DGS, (ii) array with U-slots only, and (iii) array incorporating both U-slots and DGS.

4.9.1 Conventional 4×4 Array without U-Slots and DGS

Figure 4.9 shows the layout of the conventional 4×4 patch array without any structural modification. The modelled reflection coefficient (S_{11}) of this design is presented in Figure 4.10.

As shown in Figure 4.10, the reflection coefficient at the target frequency of 3.5 GHz is above the -10 dB threshold, indicating poor impedance matching and the absence of a well-defined resonance. Consequently, the array exhibits negligible effective bandwidth and limited radiation efficiency.

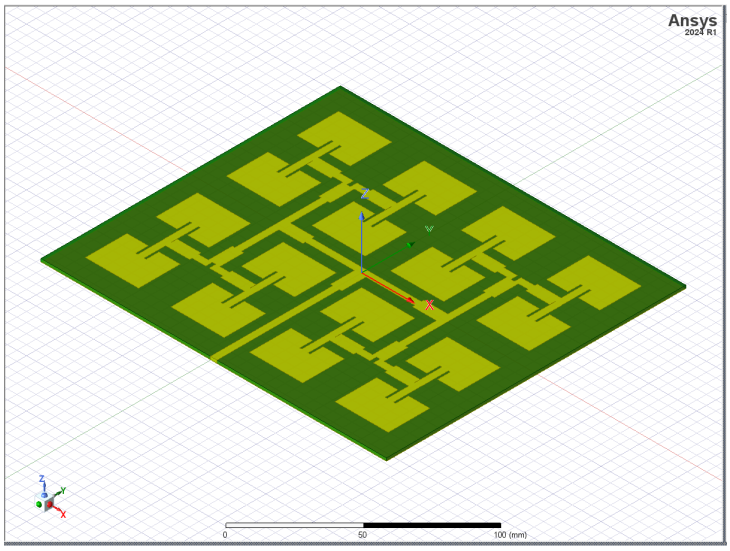

Figure 4.9: 4×4 array without U-slots and DGS.

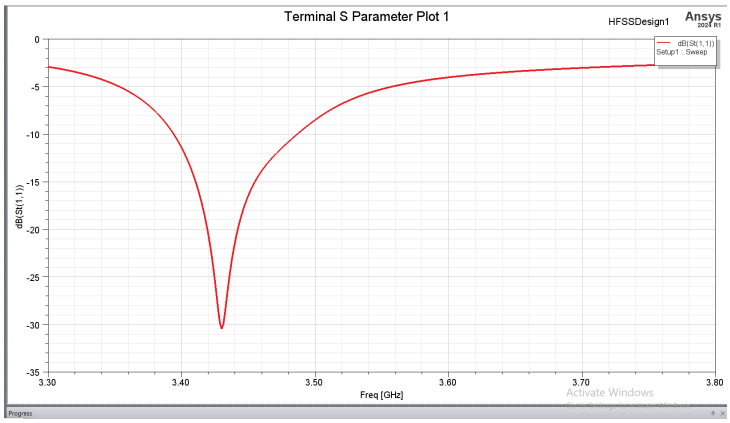

Figure 4.10: Simulated S_{11} parameter of 4×4 array without U-slots and DGS.

4.9.2 4×4 Array with U-Slots Only

To improve impedance matching and bandwidth, U-slots were introduced on each patch element, as illustrated in Figure 4.11. The corresponding S_{11} response is shown in Figure 4.12.

From Figure 4.12, the incorporation of U-slots resulted in a noticeable improvement in impedance matching, achieving a bandwidth of approximately 67.4 MHz. The U-slots introduced additional surface-current paths, effectively generating multiple resonant modes that led to a modest improvement in bandwidth in comparison to the traditional design.

4.9.3 4×4 Array with Combined U-Slots and DGS

Further enhancement was achieved by introducing a Defected Ground Structure (DGS) beneath the radiating patches. The ultimate setup of the suggested array is illustrated in

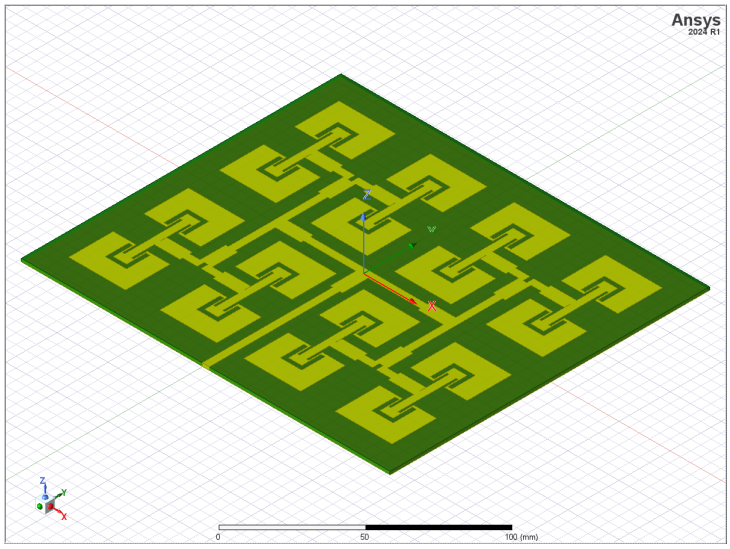

Figure 4.11: 4×4 array with U-slots only.

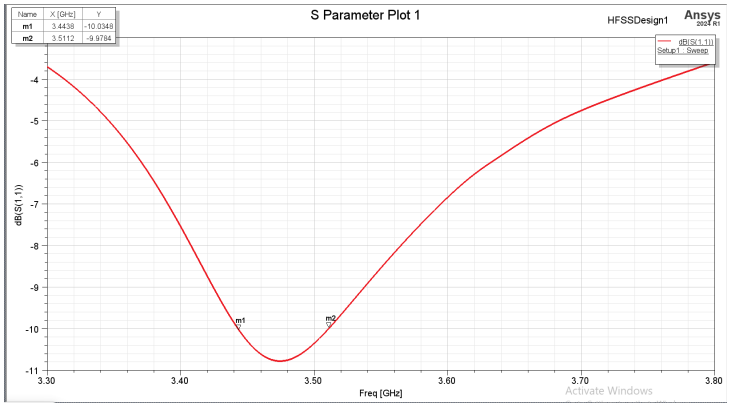

Figure 4.12: Simulated S_{11} parameter of 4×4 array with U-slots only.

Figure 4.13, while the associated reflection coefficient graph is displayed in Figure 4.14.

The introduction of DGS effectively suppressed surface wave propagation and improved the uniformity of current distribution. As observed in Figure 4.14, the array achieved a significantly wider impedance bandwidth of approximately 180 MHz, extending across the 3.4025-3.5875 GHz range. The combined use of U-slots and DGS produced a synergistic effect—U-slots enhanced multi-resonance behavior, while DGS improved impedance matching and gain stability.

4.9.4 Performance Analysis and Key Observations

Based on the simulation outcomes, the following observations were made:

- The inclusion of U-slots broadened the impedance bandwidth by introducing additional resonant paths.
- The DGS reduced surface wave losses, thereby improving impedance matching and

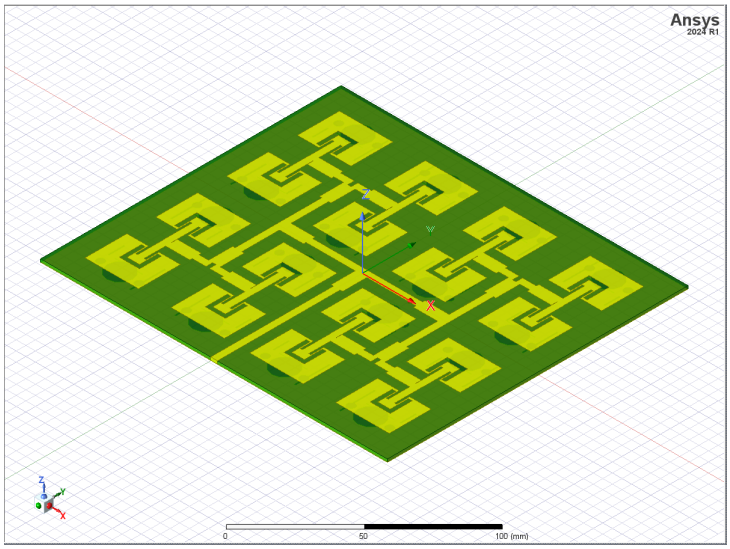

Figure 4.13: 4×4 array with U-slots and DGS.

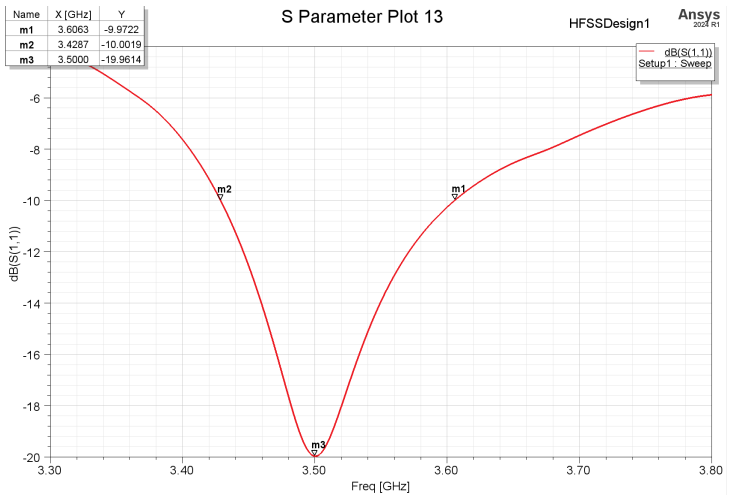

Figure 4.14: Simulated S_{11} parameter of 4×4 array with U-slots and DGS.

radiation efficiency.

- The integration of U-shaped slots and DGS led to a compact, high-efficiency, and broad-bandwidth array design ideal for sub-6 GHz 5G applications.

In general, the suggested design attained a reflection coefficient lower than $-10\,\text{dB}$ throughout the target frequency range, a peak gain of 10.64 dBi, and a total bandwidth of 180 MHz—showing a significant enhancement compared to the traditional configuration.

4.10 Overview

This chapter provided a comprehensive analysis of simulations and assessed the performance of the proposed 4×4 U-slot and DGS-integrated microstrip patch antenna array. Through systematic design modification and performance comparison, it was established

that integrating U-slots and DGS significantly enhances impedance matching, bandwidth, and radiation characteristics without substantially increasing the array size or complexity.

The findings validate that the suggested antenna is highly appropriate for sub-6 GHz 5G communication systems, where broad bandwidth functionality, a compact design, and effective radiation are essential. The following chapter will discuss the general conclusions of the study and provide suggestions for future research.

Chapter FIVE

CONCLUSION AND RECOMMENDATIONS

5.1 Project Overview

This study outlined the design, simulation, and evaluation of a 4×4 microstrip patch antenna array featuring U-slot and Defected Ground Structure (DGS) aimed at sub-6 GHz 5G communication applications. The design process consisted of multiple optimization phases, starting with a standard rectangular patch array and gradually integrating U-slots and DGS to enhance impedance bandwidth, gain, and radiation efficiency.

Using ANSYS HFSS, each design iteration was simulated to evaluate key performance parameters, including the reflection coefficient (S_{11}), bandwidth, and gain. The ultimate suggested configuration attained a recorded bandwidth of 180 MHz and a gain of 10.64 dBi, indicating significant improvement over the conventional configuration. The enhanced bandwidth performance validates the effectiveness of U-slot and DGS integration for 5G sub-6 GHz systems.

5.2 Conclusion

According to the outcomes of the simulation and analysis, the following deductions can be made:

1. The implementation of U-slots in the radiating patches effectively created several resonant modes, which in turn expanded the impedance bandwidth.

2. The inclusion of a Defected Ground Structure (DGS) minimized surface wave effects, improved impedance matching, and contributed to higher radiation efficiency.

3. The integrated utilization of U-slots and DGS offered an efficient balance between size, bandwidth, and gain, rendering the suggested antenna appropriate for sub-6 GHz 5G applications, including bands n77 (3.3–4.2 GHz) and n78 (3.3–3.8 GHz).

4. The simulation outcomes demonstrate that bandwidth enhancement can be achieved without significantly increasing the array's physical dimensions or fabrication complexity.

5.3 Impact of the Research

This study advances the domain of antenna engineering in several significant ways:

- It demonstrates a systematic approach to combining U-slot and DGS techniques to enhance bandwidth in compact sub-6 GHz 5G antenna arrays.

- It provides a parametric understanding of how structural modifications affect impedance matching and radiation performance.
- It offers a design methodology that balances gain, bandwidth, and manufacturability—key considerations in practical antenna implementation.

5.4 Limitations

Although the proposed antenna exhibited satisfactory performance in simulation, several limitations were identified during the design and analysis process:

- The study was limited to numerical simulations; experimental fabrication and measurements were not conducted due to time and equipment constraints.
- The feeding network used in the simulation was idealized and did not account for real-world losses, impedance mismatches, or fabrication tolerances.
- Mutual coupling effects among array elements were reduced but not fully optimized, which may affect array isolation and overall radiation performance.
- The sub-6 GHz frequency spectrum inherently offers limited fractional bandwidth, making it challenging to achieve wideband operation using conventional microstrip techniques.
- There is no universally defined analytical formula for determining the optimal geometry of DGS, inset feed, or U-slot structures; hence, extensive optimization through simulation software is often required.
- The ANSYS HFSS software, though highly accurate, is complex and computationally intensive, leading to longer design and simulation cycles.
- Efficient operation of HFSS requires high-performance computing resources, which may not be readily available to all researchers, resulting in slower simulation speeds on standard systems.

5.5 Recommendations for Future Study

To enhance and validate the proposed design, the following recommendations are suggested:

- Fabricate the designed antenna array and perform experimental validation using a Vector Network Analyzer (VNA) to compare measured and simulated results.

- Investigate alternative slot geometries, DGS patterns, or hybrid configurations to achieve even broader bandwidth or improved gain–bandwidth trade-offs.
- Explore the implementation of beamforming networks or phase-shifting mechanisms to enable directional control and electronic beam steering capabilities.
- Integrate the proposed antenna array with 5G transceiver front-end modules to evaluate system-level performance under real-world conditions.
- Conduct parametric and tolerance analysis to study the effects of substrate variation, feedline losses, and manufacturing inaccuracies on antenna performance.
- Think about utilizing alternative electromagnetic simulation software or optimization methods (such as genetic algorithms or particle swarm optimization) to minimize computational demands and enhance design convergence.

5.6 Closing Remarks

The proposed 4×4 U-slot and DGS-integrated microstrip patch antenna array demonstrates a balanced performance suitable for sub-6 GHz 5G communication.Its improved bandwidth, strong gain, and compact design position it as a suitable option for advanced wireless communication devices and base station uses.

REFERENCES

Abdulhamed, A. (2019). "Surface wave mitigation techniques in patch antennas". In: *Antenna Systems Journal*.

Ahmed, M. and S. Raza (2024). "Advancements in antenna array design for 5G communication networks: A comprehensive review". In: *International Journal of Scientific Research in Modern Science and Technology* 10.2, pp. 45–52. URL: https://ijsrmst.com/index.php/ijsrmst/article/view/181.

Akbar, A. et al. (2021). "Design Of Microstrip Antenna With DGS Slot For Satellite Applications". In: *2021 IEEE International Conference on Aerospace Electronics and Remote Sensing Technology (ICARES)*. IEEE, pp. 1–5. DOI: 10.1109/ICARES53960.2021.9665176.

Alsaif, H. and M. Eleiwa (2021). "Compact design of 2×2 MIMO antenna with super-wide bandwidth for millimeters wavelength systems". In: *Symmetry* 13.2, p. 233. DOI: 10.3390/sym13020233.

Andrews, J. G. et al. (2016). "What will 5G be?" In: *IEEE Journal on Selected Areas in Communications* 32.6, pp. 1065–1082. DOI: 10.1109/JSAC.2016.2550338.

ANSYS, Inc. (n.d.). *ANSYS HFSS*. https://www.ansys.com/products/electronics/ansys-hfss. Accessed 2025.

Aswoyo, B. and A. H. Putra (2021). "High gain microstrip square patch array antenna 4×4 element 2.3 GHz for 5G communication in Indonesia". In: *Proceedings of the 2021 International Electronics Symposium (IES)*, pp. 102–107. DOI: 10.1109/IES53407.2021.9593290. URL: https://doi.org/10.1109/IES53407.2021.9593290.

Balanis, C. A. (2016). *Antenna theory: Analysis and design*. 4th ed. John Wiley & Sons, Inc.

Balanis, C. A. and P. Ioannides (2007). *Introduction to smart antennas*. Vol. 2. 1. Synthesis Lectures on Antennas, pp. 1–175. DOI: 10.2200/S00026ED1V01Y200611ANT003.

Barnardo, H. S. (2024). *Electromagnetic modeling of microstrip patch antennas for 5G applications*.

Chen, T. et al. (2024). "A Rectangular Microstrip Patch Antenna with Multiple Slits and Slots for Sub-6 GHz 5G Applications". In: *IEEE Access*. URL: https://www.researchgate.net/publication/393994800.

Chen, Z. N. (2017). "Antennas for 5G mobile devices". In: *Proceedings of IEEE International Workshop on Antenna Technology*. IEEE.

Chowdhury, Mehdi et al. (June 2019). "Single Feed Circularly Polarized Crescent-Cut and Extended Corner Square Microstrip Antennas for Wireless Biotelemetry". In: *International Journal of Electrical and Computer Engineering* 9. DOI: 10.11591/ijece.v9i3.pp1902-1909.

Dange, S. A. et al. (2021). "A Review on 5G Technology: Evolution, Features and Challenges". In: *Asian Journal of Science and Applied Technology* 10.2, pp. 15–21. DOI:

10.51983/ajsat-2021.10.2.3044. URL: https://doi.org/10.51983/ajsat-2021.10.2.3044.

Davuluri, A. J. and P. Siddaiah (2021). "Design of wide band slotted microstrip patch antenna with defective ground structure for ku band". In: *International Journal of Electrical and Computer Engineering (IJECE)* 11.2, pp. 1337–1345.

De, Asok et al. (2010). "Effect of different substrates on Compact stacked square Microstrip Antenna". In: DOI: 10.48550/arXiv.1002.3337.

Didi, S.-E. et al. (2022). "Design of a microstrip antenna patch with a rectangular slot for 5G applications operating at 28 GHz". In: *TELKOMNIKA (Telecommunication Computing Electronics and Control)* 20.3, pp. 527–534. DOI: 10.12928/telkomnika.v20i3.23159.

Dubey, Anil Kumar (July 2021). "Substrate material selection and design optimization of patch antenna". In: *IOP Conference Series: Materials Science and Engineering* 1168.1, p. 012025. DOI: 10.1088/1757-899X/1168/1/012025. URL: https://dx.doi.org/10.1088/1757-899X/1168/1/012025.

Farahbakhsh, A., D. Zarifi, and A. U. Zaman (2017). "60-GHz Groove Gap Waveguide Based Wideband *H*-Plane Power Dividers and Transitions: For Use in High-Gain Slot Array Antenna". In: *IEEE Microwave Theory and Techniques Society*. DOI: 10.1109/tmtt.2017.2699680.

Fistum, E. (2017). "Aperture coupled feed analysis for patch antennas". In: *RF Design Journal*.

Fubara, E. A., P. P. Gyang, and F. P. Olubodun (2023). "Full-wave numerical analysis of dual-band E-patch antenna and reactive loading technique to ascertain the impedance driving point function". In: *International Journal of Wireless and Microwave Technologies* 13.3, pp. 26–38. DOI: 10.5815/ijwmt.2023.03.03.

Fubara, Edmund Alfred-Abam, P. P. Gyang, and F. P. Olubodun (2023). "Full-Wave Numerical Analysis of Dual-Band E-Patch Antenna and Reactive Loading Technique to Ascertain the Impedance Driving Point Function". In: *International Journal of Wireless and Microwave Technologies* 13.3, pp. 26–38. DOI: 10.5815/ijwmt.2023.03.03. URL: https://doi.org/10.5815/ijwmt.2023.03.03.

Gaid, A. S. A. et al. (2024). "Design and analysis of a low profile, high gain rectangular microstrip patch antenna for 28 GHz applications". In: *Cogent Engineering* 11.1.

Ganatra, A. N. (2017). "Developments of 5G Technology". All Student Theses and Dissertations, 104. Master's thesis. Governors State University. URL: https://opus.govst.edu/theses/104.

Gao, Steven (2019). "Compact MIMO antennas for mobile terminals in 5G". In: pp. 1–1. DOI: 10.1109/ConTEL.2019.8848534.

Gemeda, M. et al. (2021). "Design and analysis of a 28 GHz microstrip patch antenna for 5G communication systems". In: *International Journal of Emerging Technology and Advanced Engineering* 8, pp. 881–886.

Ghimire, J. et al. (2021). "Vivaldi Antenna Arrays Feed by Frequency-Independent Phase Shifter for High Directivity and Gain Used in Microwave Sensing and Communication Applications". In: *Italian National Conference on Sensors*. DOI: 10.3390/s21186091.

Gupta, A. et al. (2023). "Design and Analysis of a Sub-6 GHz Antenna Array with High Gain for 5G Mobile Phone Applications". In: *IEEE Access*. URL: https://www.researchgate.net/publication/386304222.

Gupta, P. and V. Gupta (2022). "Linear 1×4 microstrip antenna array using slotted circular patch for 5G communication applications". In: *Wireless Personal Communications*, pp. 1–17. DOI: 10.1007/s11277-022-09896-4.

Hemalatha, T. et al. (2023). "Substrate selection criteria for microstrip patch antennas". In: *Journal of Antenna Design*.

Hossain, M., D. Das, and M. A. Hossain (2024). "A 5G beam-steering microstrip array antenna using both-sided microwave integrated circuit technology". In: *International Journal of Electrical and Computer Engineering (IJECE)* 14.1, pp. 457–468. DOI: 10.11591/ijece.v14i1.pp457-468.

Hossain, M. et al. (2023). "Design and performance analysis of defected ground slotted patch antenna for sub-6 GHz 5G applications". In: *Journal of Engineering Advancements* 4.4, pp. 130–140. DOI: 10.38032/jea.2023.04.004. URL: https://doi.org/10.38032/jea.2023.04.004.

Huang, Z. Y., B. Y. Liu, and Y. Jiang (2021). "T-Junction Power Divider Based on Rectangular Microcoaxial Structure in W-band". In: *Applied Computational Electromagnetics Society Journal* 39.1, pp. 1279–1286.

Huseien, G. F. and K. W. Shah (2021). "Potential applications of 5G network technology for climate change control: A scoping review of Singapore". In: *Sustainability* 13.17, p. 9720. DOI: 10.3390/su13179720.

Ibrahim, M. et al. (2024). "Sub-6 GHz Ultrawideband Gain Enhanced Antenna for IoT Applications". In: *IEEE Sensors Journal*. URL: https://www.researchgate.net/publication/393997531.

Irfansyah, A., B. H. Harianto, and N. Pambudiyatno (2021). "Design of rectangular microstrip antenna 1×2 array for 5G communication". In: *Journal of Physics: Conference Series* 2117, p. 012028. DOI: 10.1088/1742-6596/2117/1/012028.

Ismam, S. et al. (2023). "Design and Performance Analysis of 28 GHz two-port MIMO Rectangular Microstrip Patch Antenna Array for 5G Applications". In: *None*. DOI: 10.69955/ajoeee.2023.v3i2.51.

Jabeen, S. and G. Hemalatha (2023). "Microstrip Fed PI-Slot Patch Antenna with T-Slot DGS for UWB Applications". In: *The Electromagnetics Academy*. DOI: 10.2528/pierc22112804.

Jamshidi, M. B. et al. (2021). "Size reduction and performance improvement of a microstrip Wilkinson power divider using a hybrid design technique". In: *Scientific Reports* 11, p. 7773.

Jiménez, D. et al. (2023). "Design of 4×4 low-profile antenna array for CubeSat applications". In: *Micromachines* 14.1, p. 180. DOI: 10.3390/mi14010180. URL: https://doi.org/10.3390/mi14010180.

Joshi, R. (2018). "Dielectric materials for high-frequency antenna applications". In: *IEEE Transactions on Dielectrics*.

Kanniyappan, S. (2017). "Proximity coupled feeding techniques for microstrip antennas". In: *Microwave Engineering Letters*.

Karimi, Armin and Joachim Oberhammer (2022). "Design of an Amplitude-Tapered Corporate-Feed Slot Array Antenna with Reduced Side-Lobe Level for Silicon Micromachining". In: *2022 16th European Conference on Antennas and Propagation (EuCAP)*, pp. 1–5. DOI: 10.23919/EuCAP53622.2022.9769103.

Kaur, N. and N. Sharma (2017). "Designing of Slotted Microstrip Patch Antenna Using Inset Cut Line Feed For S, C And X Band Applications". In: *International Journal of Engineering Research & Technology (IJERT)* 6.7, pp. 965–968.

Khan, F. et al. (2020). "A Novel Design of a Compact Wideband Patch Antenna for Sub-6 GHz Fifth-Generation Mobile Systems". In: *Electronics*. URL: https://www.researchgate.net/publication/343676628.

Khan, Imran et al. (Sept. 2018). "Effects of Different Substrates on Rectangular Microstrip Patch Antenna for X-band". In: *Asian Journal of Engineering and Applied Technology* 7.2, pp. 91–95. DOI: 10.51983/ajeat-2018.7.2.1000. URL: https://ojs.trp.org.in/index.php/ajeat/article/view/1000.

Khan, M. U., M. S. Sharawi, and R. Mittra (2015). "Microstrip patch antenna miniaturisation techniques: A review". In: *IET Microwaves, Antennas & Propagation* 9.9, pp. 913–922. DOI: 10.1049/iet-map.2014.0602.

Khandelwal, M. K., B. K. Kanaujia, and S. Kumar (2017). "Defected ground structure: Fundamentals, analysis, and applications in modern wireless trends". In: *International Journal of Antennas and Propagation* 2017, pp. 1–22. DOI: 10.1155/2017/2018527.

Khattak, M. I. et al. (2019). "Elliptical slot circular patch antenna array with dual-band behavior for future 5G mobile communication networks". In: *Progress in Electromagnetics Research C* 89, pp. 133–147.

Kishore, S. and A. R. A. Rajak (2022). "Microstrip patch antenna with C slot for 5G communication at 30 GHz". In: *Emerging Science Journal* 6.6, pp. 1315–1327.

Kraus, J. D. and R. J. Marhefka (2011). *Antennas for all applications*. 4th ed. McGraw-Hill.

Kumar, A. and R. Verma (2017). "Design analysis of different types of feed to microstrip patch antenna". In: *IRE Journals* 1.6, pp. 7–10. URL: https://irejournals.com/formatedpaper/1700115.pdf.

Kumar, A. et al. (2020). "Efficient isolation of a MIMO antenna using defected ground structure". In: *Electronics* 9.8, p. 1265. DOI: 10.3390/electronics9081265.

Kumar, P. et al. (2024). "Design and Performance Analysis of Defected Ground Slotted Patch Antenna for Sub-6 GHz 5G Applications". In: *IEEE Antennas and Wireless Propagation Letters*. URL: https://www.researchgate.net/publication/377024368.

Kumar, V. (2020). "Advanced feeding techniques for 5G antennas". In: *Wireless Technology Review*.

Kumar Dash, Rajib et al. (Jan. 2022). "Design of triangular shaped slotted patch antennas for both wideband and multiband applications". In: *International Journal of Applied Electromagnetics and Mechanics* 68, pp. 1–20. DOI: 10.3233/JAE-210098.

Liu, Qianwen, Lei Zhu, and Wenjun Lu (2025). "Self-decoupled square patch antenna arrays by exciting and using mixed electric/magnetic coupling between adjacent radiators". In: *Chinese Journal of Electronics* 34.2, pp. 483–494. DOI: 10.23919/cje.2023.00.222. URL: https://doi.org/10.23919/cje.2023.00.222.

Mabaso, M. and P. Kumar (2019). "A Microstrip Patch Antenna with Defected Ground Structure for Triple Band Wireless Communications". In: *International Communication Association*. DOI: 10.12720/jcm.14.8.684-688.

Maharjan, J. (2020). "Four-element microstrip patch array antenna with corporate-series feed technique". In: *Scientific Programming*, Article ID 8760297. DOI: 10.1155/2020/8760297. URL: https://doi.org/10.1155/2020/8760297.

Mahmood, A. et al. (2021). "Factory 5G: A review of industrial-centric features and deployment options". In: *TechRxiv*. Preprint. DOI: 10.36227/techrxiv.17089265.v1.

Martínez, L. et al. (2024). "Optimized Design and Performance Evaluation of a High-Gain 4x4 Array Patch Rectenna for 5G Networks". In: *IEEE Transactions on Antennas and Propagation*. URL: https://www.researchgate.net/publication/382920860.

Mehta, A. (2015). "Microstrip antenna". In: *International Journal of Scientific & Technology Research* 4.3.

Moloudian, G. et al. (2023). "Design and fabrication of a Wilkinson power divider with harmonic suppression for LTE and GSM applications". In: *Scientific Reports* 13, p. 36918689.

Nadar, K. P. et al. (2023). "Design and analysis of microstrip patch antenna array and electronic beam steering linear phased antenna array with high directivity for space

applications". In: *ACS Omega* 8.45, pp. 43197–43217. DOI: 10.1021/acsomega.3c06691.

Nafi, Nafis Almas et al. (2024). "A novel theta-shaped slotted patch antenna with a unique DGS for Sub-6 GHz 5G communication". In: *Results in Engineering* 24, p. 103506. ISSN: 2590-1230. DOI: 10.1016/j.rineng.2024.103506. URL: https://doi.org/10.1016/j.rineng.2024.103506.

Naji, Dhirgham, Jabir Aziz, and Raad Fyath (May 2012). "Design and Simulation of RFID Aperture Coupled Fractal Antennas". In: *International Journal of Radio Frequency Identification and Wireless Sensor Networks* 2, pp. 1–14. DOI: 10.5772/51269.

Noor, S. K. et al. (2023). "A Patch Antenna with Enhanced Gain and Bandwidth for Sub-6 GHz and Sub-7 GHz 5G Wireless Applications". In: *Electronics* 12.12, p. 2555. DOI: 10.3390/electronics12122555. URL: https://doi.org/10.3390/electronics12122555.

Padire, M. and J. T J (2025). "Design of 4×4 microstrip patch array antenna for 5G mmWave applications". In: *International Journal of Electronics and Communication Engineering* 12, pp. 104–117. DOI: 10.14445/23488549/IJECE-V12I1P108.

Pan, X. and H. Song (2024). "A broadband microstrip antenna with a strip-slot hybrid structure". In: *Academic Journal of Science and Technology* 9.3, pp. 114–118.

Patil, S. A. et al. (2021). "A review on 5G technology: Evolution, features and challenges". In: *Asian Journal of Science and Applied Technology* 10.2, pp. 15–21. DOI: 10.51983/AJSAT-2021.10.2.3044. URL: https://doi.org/10.51983/AJSAT-2021.10.2.3044.

Patil, V. P. (2024). "Parametrical Analysis of Asymmetrical Double U-Slotted Microstrip Circular Patch Antenna for WLAN and Wi-Fi Applications". In: *Journal of Space Technology* 14.1, pp. 24–29.

Pozar, D. M. (2012). *Microwave engineering*. 4th ed. Wiley.

Rahim, M. K. A. et al. (2008). "Antenna array at 2.4 GHz for wireless LAN system using point to point communication". In: *2007 Asia-Pacific Conference on Applied Electromagnetics (APACE)*. IEEE. Johor, Malaysia. DOI: 10.1109/APACE.2007.4603890.

Rahman, Mahfuz (Jan. 2017). "SMALL SIZE COUPLING FEED AND INDUCTIVE SHORTING ANTENNA FOR WIDE BANDWIDTH, INCREASED GAIN AND EFFICIENCY WITH LOW SPECIFIC ABSORPTION RATE (SAR) OPERATION". PhD thesis. DOI: 10.13140/RG.2.2.18078.02884.

Rahman, S. et al. (2020). "Design and Performance Analysis of a Multiband Microstrip Patch Array Antenna at Ku and K Band". In: *International Journal of RF and Microwave Computer-Aided Engineering*. URL: https://www.researchgate.net/publication/333718113.

Rappaport, T. S. et al. (2019). "Wireless communications and applications above 100 GHz: Opportunities and challenges". In: *IEEE Communications Magazine* 57.12, pp. 140–146. DOI: 10.1109/MCOM.001.1900179.

Rashid, S., C. K. Chakrabarty, and M. A. M. Rani (2019). "Review of feeding techniques for microstrip patch antenna". In: *International Journal of Computer Applications* 178.27, pp. 39–42. DOI: 10.5120/ijca2019919010.

Rathinakumar, P., A. J. Jatly, and S. Akshaya (2024). "Slotted Circular Microstrip Patch Antenna with Defected Ground Structure for Biosensing Applications at 2.9 GHz". In: *Proceedings of the 2025 International Conference on Advanced Research in Electronics and Communication Systems (ICARECS-2025)*. Atlantis Press, pp. 465–479.

Raza, H. et al. (2019). "A compact 4×4 MIMO antenna array for 28 GHz applications". In: *Progress In Electromagnetics Research C* 94, pp. 73–85. DOI: 10.2528/PIERC19020302.

Ren, Q. et al. (2022). "Linear antenna array with large element spacing for wide-angle beam scanning with suppressed grating lobes". In: *IEEE Antennas and Wireless Propagation Letters*, pp. 1–1. DOI: 10.1109/LAWP.2022.3163603.

Reynalda, T., A. Munir, and E. Bharata (2011). "Characterization of 4×4 high gain microstrip array antenna for 3.3 GHz WiMAX application". In: *Proceedings of the 2011 6th International Conference on Telecommunication Systems, Services, and Applications (TSSA)*, pp. 215–218. DOI: 10.1109/TSSA.2011.6095437. URL: https://doi.org/10.1109/TSSA.2011.6095437.

Rowe, Wayne and R.B. Waterhouse (July 2006). "Investigation Into the Performance of Proximity Coupled Stacked Patches". In: *Antennas and Propagation, IEEE Transactions on* 54, pp. 1693–1698. DOI: 10.1109/TAP.2006.875462.

Saeed, M. A. and A. O. Nwajana (2024). "A review of beamforming microstrip patch antenna array for future 5G/6G networks". In: *Frontiers in Mechanical Engineering* 9. DOI: 10.3389/fmech.2023.1288171.

Sahana, K. (2024). "Planar Rectangular Microstrip Patch Antenna Array with Corporate-Feed Network for Gain Enhancement". In: *International Journal for Research in Applied Science and Engineering Technology (IJRASET)*. DOI: 10.22214/ijraset.2024.63863.

Sahu, B. K. and S. K. Behera (2017). "Improved microstrip patch antenna with enhanced bandwidth, efficiency and reduced return loss using DGS". In: *Proceedings of the 2017 International Conference on Wireless Communications, Signal Processing and Networking (WiSPNET)*, pp. 935–939. DOI: 10.1109/WiSPNET.2017.8300204. URL: https://doi.org/10.1109/WiSPNET.2017.8300204.

Salih, A. A. et al. (2020). "Evolution of mobile wireless communication to 5G revolution". In: *Technology Reports of Kansai University* 62.5, pp. 2139–2151.

Shafi, M. et al. (2017). "5G: A tutorial overview of standards, trials, challenges, deployment, and practice". In: *IEEE Journal on Selected Areas in Communications* 35.6, pp. 1201–1221. DOI: 10.1109/JSAC.2017.2692307.

Shamim, S. M. et al. (2021). "Design of efficient 37 GHz millimeter-wave microstrip patch antenna for 5G mobile application". In: *Plasmonics* 16, pp. 1–9. DOI: 10.1007/s11468-021-01412-x.

Sharma, R. and K. Patel (2024). "Advancements in Patch Antenna Design for Sub-6 GHz 5G Smartphone Application: A Comprehensive Review". In: *International Journal of Microwave and Wireless Technologies*. URL: https://www.researchgate.net/publication/382826478.

Shaw, J. (2013). "Radiometry and the Friis transmission equation". In: *American Journal of Physics* 81, pp. 33–37. DOI: 10.1119/1.4755780.

Singh, O. and S. K. Sriwas (2025). "ANN-based design analysis of O-shaped slotted microstrip patch antenna for L band applications". In: *International Journal of Electronics* 112.1, pp. 183–195.

Singh, R. et al. (2011). "Microstrip patch antennas: A comprehensive review". In: *IEEE Antennas and Propagation Magazine*.

Tan, W. et al. (2023). "A Patch Antenna with Enhanced Gain and Bandwidth for Sub-6 GHz and Sub-7 GHz 5G Wireless Applications". In: *IEEE Antennas and Wireless Propagation Letters*. URL: https://www.researchgate.net/publication/371313852.

Thakur, E. et al. (2018). "Mathematical analysis of commonly used feeding techniques in rectangular microstrip patch antenna". In: *Advances in Signal Processing and Communication*. Vol. 526. Lecture Notes in Electrical Engineering. Springer. DOI: 10.1007/978-981-13-2553-3_3.

Tiwari, A., U. Pattapu, and S. Das (2024). "A wideband 1:2 T-junction power divider for antenna array with optimum results". In: *International Conference on Microwave, Optical and Communication Engineering*. IEEE, pp. 1–4.

Tiwari, R., R. Sharma, and R. Dubey (2020). "Microstrip patch antenna array design analysis for 5G communication applications". In: *SMART MOVES Journal IJOSCIENCE* 6.5, pp. 1–5. DOI: 10.24113/ijoscience.v6i5.287.

Uddin, M. N. and S. Choi (2020). "Non-uniformly powered and spaced corporate feeding power divider for high-gain beam with low SLL in millimeter-wave antenna array". In: *Sensors* 20.17, p. 4753. DOI: 10.3390/s20174753.

Van-Thang Nguyen, Jae-Young Chung (2022). "Design of a Planar Antenna Array with Wide Bandwidth and Narrow Beamwidth for IR-UWB Radar Applications". In: *mdpi*. URL: https://www.mdpi.com/1809758.

Venkatachalam, D. and G. Murugesan (2019). "A miniaturized planar antenna with defective ground structure for UWB applications". In: *IEICE Electronics Express*. DOI: 10.1587/ELEX.16.20190242.

Wang, Y. et al. (2017). "A compact and broadband Wilkinson power divider with harmonic suppression". In: *Microwave and Optical Technology Letters* 66.1.

Wilkinson, E. J. (1960). "An N-way hybrid power divider". In: *IRE Transactions on Microwave Theory and Techniques* 8.1, pp. 116–118. DOI: 10.1109/TMTT.1960.1124668. URL: https://doi.org/10.1109/TMTT.1960.1124668.

Wong, K. L. et al. (2016). "Compact 4×4 MIMO antennas for 5G smartphones". In: *IEEE Transactions on Antennas and Propagation* 64.6, pp. 2472–2480. DOI: 10.1109/TAP.2016.2546952.

Zhao, Y. et al. (2023a). "A Novel Theta-Shaped Slotted Patch Antenna with a Unique DGS for Sub-6 GHz 5G Communication". In: *IEEE Transactions on Circuits and Systems II: Express Briefs*. URL: https://www.researchgate.net/publication/386220832.

— (2023b). "Wideband high gain metasurface-based 4T4R MIMO antenna with highly isolated ports for sub-6 GHz 5G". In: *arXiv preprint arXiv:2309.07131*. DOI: 10.48550/arXiv.2309.07131.

Zhou, T. F. (2023). "A miniaturized broadband Wilkinson power divider using micro-strip branch lines". In: *Journal of Computer and Communications* 11, pp. 102–108.

Supervisor's Signature: _____ **Date:** _____